ARTICLE

doi:10.1038/nature19804

Diversity-oriented synthesis yields novel multistage antimalarial inhibitors

Nobutaka Kato[1]*, Eamon Comer[1]*, Tomoyo Sakata-Kato[2], Arvind Sharma[3], Manmohan Sharma[3], Micah Maetani[1,4], Jessica Bastien[1], Nicolas M. Brancucci[2], Joshua A. Bittker[1], Victoria Corey[5], David Clarke[2], Emily R. Derbyshire[1,6,7], Gillian L. Dornan[8], Sandra Duffy[9], Sean Eckley[10], Maurice A. Itoe[2], Karin M. J. Koolen[11], Timothy A. Lewis[1], Ping S. Lui[2], Amanda K. Lukens[1,2], Emily Lund[2], Sandra March[1,12], Elamaran Meibalan[2], Bennett C. Meier[1,4], Jacob A. McPhail[8], Branko Mitasev[10], Eli L. Moss[1], Morgane Sayes[1], Yvonne Van Gessel[10], Mathias J. Wawer[1], Takashi Yoshinaga[13], Anne-Marie Zeeman[14], Vicky M. Avery[9], Sangeeta N. Bhatia[1,12], John E. Burke[8], Flaminia Catteruccia[2], Jon C. Clardy[1,6], Paul A. Clemons[1], Koen J. Dechering[11], Jeremy R. Duvall[1], Michael A. Foley[1], Fabian Gusovsky[10], Clemens H. M. Kocken[14], Matthias Marti[2], Marshall L. Morningstar[1], Benito Munoz[1], Daniel E. Neafsey[1], Amit Sharma[3], Elizabeth A. Winzeler[5], Dyann F. Wirth[1,2], Christina A. Scherer[1] & Stuart L. Schreiber[1,4]

Antimalarial drugs have thus far been chiefly derived from two sources—natural products and synthetic drug-like compounds. Here we investigate whether antimalarial agents with novel mechanisms of action could be discovered using a diverse collection of synthetic compounds that have three-dimensional features reminiscent of natural products and are underrepresented in typical screening collections. We report the identification of such compounds with both previously reported and undescribed mechanisms of action, including a series of bicyclic azetidines that inhibit a new antimalarial target, phenylalanyl-tRNA synthetase. These molecules are curative in mice at a single, low dose and show activity against all parasite life stages in multiple *in vivo* efficacy models. Our findings identify bicyclic azetidines with the potential to both cure and prevent transmission of the disease as well as protect at-risk populations with a single oral dose, highlighting the strength of diversity-oriented synthesis in revealing promising therapeutic targets.

Malaria is a deadly disease caused by protozoan parasites of the genus *Plasmodium*. Effective eradication strategies have been elusive, primarily owing to the complex life cycle of *Plasmodium* and the emergence of drug-resistant strains of *P. falciparum*, the most lethal *Plasmodium* species in humans[1]. The majority of the current antimalarial drugs target the asexual blood stage of *Plasmodium*, in which they parasitize and replicate within erythrocytes[2]. Even though liver- and transmission-stage parasites do not cause malarial symptoms, prophylaxis and transmission-blocking drugs are essential for the proactive prevention of disease epidemics and to protect vulnerable populations[3,4]. Unfortunately, the current antimalarial drugs do not address all of the requirements for the targeting of pan-life-cycle activity. Several recent reports have described next-generation drug candidates that may achieve some of these important goals[2,5–9]. However, eradication will require multiple innovative ways of targeting the parasite[10–12]. The antimalarial pipeline will therefore benefit from compounds with diverse mechanisms of action, features that should help circumvent the many resistance mechanisms that render existing drugs ineffective.

We identified two key features of a successful strategy for overcoming these challenges. The first of these is the application of modern methods of asymmetric organic synthesis to create unique chemical matter; the second is to test the resulting compounds in a series of phenotype-based screens designed to uncover agents that act on targets essential for several stages of the parasite life cycle (that is, multistage activity). We were encouraged by a small-scale pilot experiment that followed this blueprint and yielded the antimalarial agent ML238 (refs 13–15). The experiments described here excluded this earlier pilot set of compounds.

We tested synthetic compounds with structures that were inspired by the structural complexity and diversity of the entire ensemble of natural products, rather than by specific natural products. In this way, we deliberately break the link to natural selection and the limitations it provides in terms of target diversity[16]. A high-throughput *P. falciparum* phenotypic screen of infected erythrocytes was used to detect inhibitors of parasite growth, with counter-screens using parasites that are resistant to approved or developmental drugs, and with liver- and transmission-stage parasites used to facilitate the discovery of compounds that act through novel mechanisms of action and target multiple stages of malarial infection.

Approximately 100,000 compounds, synthesized at the Broad Institute using the build/couple/pair strategy[17,18] of diversity-oriented synthesis (DOS), were screened against a multi-drug-resistant strain (*P. falciparum* strain Dd2) using a phenotypic blood-stage growth-inhibition assay, which models a human blood-stage infection. Compounds scored as positives were counter-screened in parallel

[1]Broad Institute of Harvard and MIT, 415 Main Street, Cambridge, Massachusetts 02142, USA. [2]Harvard T.H. Chan School of Public Health, 665 Huntington Avenue Boston, Massachusetts 02115, USA. [3]Molecular Medicine Group, International Centre for Genetic Engineering and Biotechnology, Aruna Asaf Ali Road, New Delhi 110067, India. [4]Department of Chemistry and Chemical Biology, Harvard University, 12 Oxford Street, Cambridge, Massachusetts 02138, USA. [5]School of Medicine, University of California, San Diego, 9500 Gilman Drive 0760, La Jolla, California 92093, USA. [6]Department of Biological Chemistry and Molecular Pharmacology, Harvard Medical School, 240 Longwood Avenue, Boston, Massachusetts 02115, USA. [7]Department of Chemistry and Department of Molecular Genetics and Microbiology, Duke University, 124 Science Drive, Durham, North Carolina 27708, USA. [8]Department of Biochemistry and Microbiology, University of Victoria, 270 Petch Hall, Victoria, British Colombia V8P 5C2, Canada. [9]Eskitis Institute for Drug Discovery, Griffith University, Nathan Campus, Griffith University, Nathan, Brisbane, Queensland 4111, Australia. [10]Eisai Inc., 4 Corporate Drive, Andover, Massachusetts 01810, USA. [11]TropIQ Health Sciences, Geert Grooteplein 28, Huispost 268, 6525 GA Nijmegen, The Netherlands. [12]Department of Electrical Engineering and Computer Science, Massachusetts Institute of Technology, 500 Main Street, Cambridge, Massachusetts 02142, USA. [13]Eisai Co. Ltd, 5-1-3 Tokodai, Tsukuba, Ibaraki 300-2635, Japan. [14]Department of Parasitology, Biochemical Primate Research Centre, 2280 GH Rijswijk, The Netherlands.
*These authors contributed equally to this work.

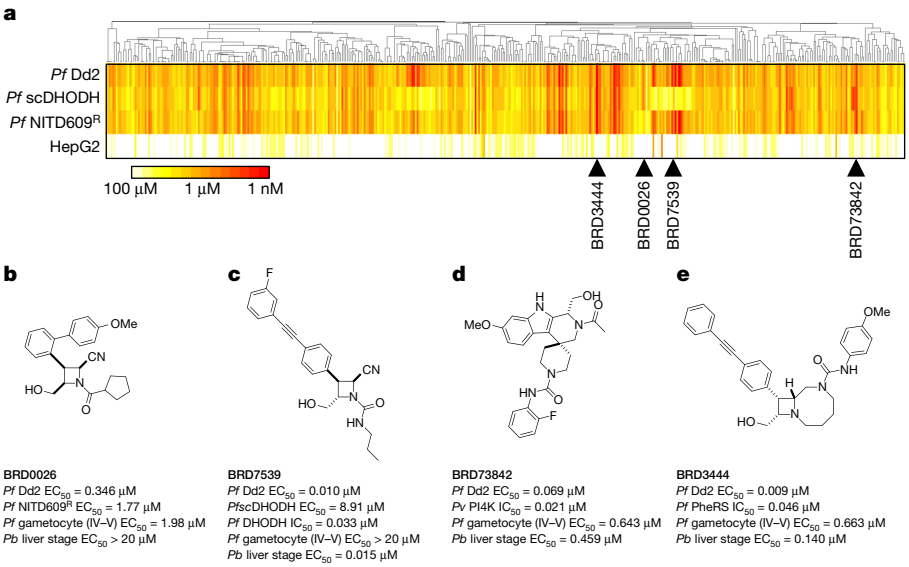

Figure 1 | Cascading triage strategy reveals targets for some of the hit compounds and highlights potential novel mechanisms of action for others. a–e, A total of 468 compounds ('positives' in the growth inhibition primary assay) were tested in dose against *P. falciparum* Dd2, a transgenic *P. falciparum* line expressing *Saccharomyces cerevisiae* DHODH (*Pfsc*DHODH), a *P. falciparum* strain resistant to NITD609 (*Pf* NITD609^R) and a mammalian cell line (HepG2). *P. falciparum* ATPase4 is the presumed molecular target of NITD609 (ref. 9). **a**, Compounds were clustered across the horizontal axis by structural similarity. Colours represent compound potency (EC_{50}). Two compound clusters, exemplified by BRD0026 (**b**) and BRD7539 (**c**), showed selectively reduced potency against the *Pf* NITD609^R and *Pfsc*DHODH strains, respectively, while BRD73842 (**d**) and BRD3444 (**e**) were equipotent across the three *P. falciparum* strains. *Pb*, *P. berghei; Pf*, *P. falciparum*; *Pv*, *P. vivax*; PheRS, phenylalanyl-tRNA synthetase.

against a panel of parasite isolates and diverse drug-resistant clones to deprioritize compounds with previously identified mechanisms of action (Fig. 1a and Supplementary Tables 1, 2). After evaluating results from assays against the liver-stage (*Plasmodium berghei* strain ANKA) and transmission-stage (*P. falciparum* strain 3D7) parasites, four chemical series with additional liver-stage and/or transmission-blocking activities (BRD0026, BRD7539, BRD73842 and BRD3444; Fig. 1b–e, Extended Data Table 1 and Supplementary Tables 1, 2) were selected. This layered screening process also yielded other series not described here that may merit attention in the future (available at the Malaria Therapeutics Response Portal, http://portals.broadinstitute.org/mtrp/). Underlying features of DOS helped to guide the selection and development of the four nominated series. The compound collection includes stereoisomeric families that yield stereochemistry-based structure–activity relationships (SSAR); their inclusion indicated the possibility of selective interactions with targets. The short, modular pathways, entailing inter- and intramolecular coupling reactions, facilitate medicinal chemistry optimization. Three of the four series yielded new compound scaffolds against known targets. These include: (i) disruptors of sodium ion regulation mediated by *P. falciparum* ATPase4 (ref. 9; BRD0026 is active against asexual and late sexual blood stages of parasites, Fig. 1b and Extended Data Fig. 1a–d); (ii) potent and selective inhibitors of *P. falciparum* dihydroorotate dehydrogenase (*pf* DHODH)[19] (BRD7539 is active against liver-stage and asexual blood-stage parasites; Fig. 1c and Extended Data Fig. 1e–h); and (iii) potent and selective inhibitors of *P. falciparum* phosphatidylinositol-4-kinase (*pf* PI4K)[20,21] (BRD73842 is active against liver-stage, asexual and late sexual blood-stage parasites; Fig. 1d, Extended Data Figs 1i–m, 2a and Supplementary Table 3). The fourth series was found to inhibit a previously unknown antimalarial target and is characterized in detail below.

Bicyclic azetidines inhibit cytosolic *Pf* PheRS

The bicyclic azetidine BRD3444 showed multistage activity *in vitro* (*P. falciparum* Dd2, blood stage, half-maximal effective concentration (EC_{50}) = 9 nM; *P. falciparum* 3D7, transmission stage, gametocyte IV–V, EC_{50} = 663 nM; *P. berghei* strain ANKA, liver stage, EC_{50} = 140 nM; Fig. 1e, Extended Data Table 1 and Supplementary Table 1). To elucidate the mechanism of action of the bicyclic azetidine series, three resistant lines were evolved against BRD1095 (Fig. 2a and Extended Data Fig. 2b), a derivative of BRD3444 with increased aqueous solubility, from eight independent cultures ($>8 \times 10^9$ inocula). After more than 3 months of drug pressure, EC_{50} values were increased by 4–84-fold. Two clones were obtained from each culture and genomic DNA from each clone was analysed via whole-genome sequencing (Fig. 3a, b and Supplementary Table 4). Analysis of resistant clones revealed that each had at least one non-synonymous single-nucleotide variant (SNV) in the PF3D7_0109800 locus, which is predicted to encode the alpha subunit of the cytosolic phenylalanyl-tRNA synthetase (*Pf* PheRS)

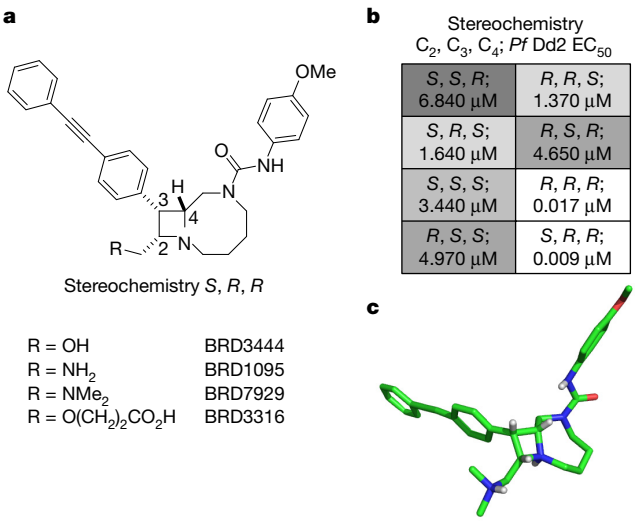

Figure 2 | Structures of key compounds, SSAR study of BRD3444 and X-ray crystal structure of BRD7929. a, Structures of four bicyclic azetidine compounds. **b**, SSAR of BRD3444 showing that stereoisomers at the C_2 position are equipotent, which suggests that this position is not necessary for activity. **c**, X-ray crystal structure of BRD7929 showing 3D conformation (BRD7929 was crystallized as a salt with two equivalents of L-tartaric acid; only the structure of BRD7929 is shown for clarity).

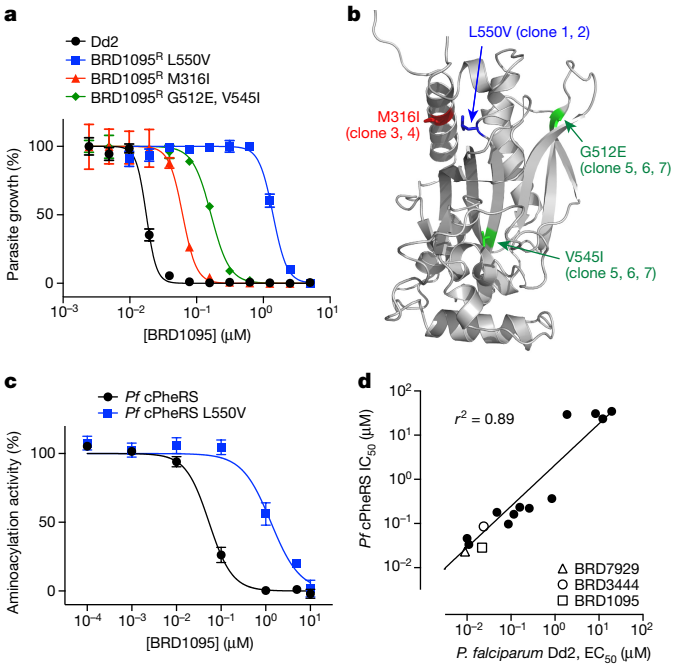

Figure 3 | The bicyclic azetidine series targets the cytoplasmic *Pf* PheRS. a, *P. falciparum* Dd2 clones resistant to BRD1095, a derivative of BRD3444 with increased aqueous solubility, were selected *in vitro* and non-synonymous SNVs were identified via whole-genome sequencing. All clones from three individual flasks contained non-synonymous SNVs within the PF3D7_0109800 locus, which encodes the alpha subunit of the cytoplasmic PheRS. **b**, The non-synonymous SNVs identified in clones from flask 1 (red), flask 2 (blue), and flask 3 (green) are shown overlaid on a homology model based on the human cytoplasmic PheRS (PDB accession 3L4G) generated in PyMol. **c**, BRD1095 was assayed against purified recombinant proteins of wild-type cytosolic *Pf* PheRS and a mutant containing a SNV (giving a L550V substitution), identified from the resistant strain. IC_{50} value of the wild-type PheRS was 0.045 μM, whereas the IC_{50} value for $BRD1095^{L550V}$ was 1.30 μM (data are mean ± s.d. for two biological and two technical replicates). **d**, The bicyclic azetidine series showed a strong correlation between blood-stage growth inhibition and biochemical inhibition of cytosolic *Pf* PheRS activity. We assayed 15 bicyclic azetidine analogues with varying potency against blood-stage parasites (Dd2 strain) against purified recombinant *Pf* PheRS. The biochemically derived IC_{50} values correlate strongly ($r^2 = 0.89$) with the EC_{50} values determined using the blood-stage growth inhibition assay (see Extended Data Table 2 for structure–activity relationship study and chemical structures).

of *P. falciparum* (ref. 22). Examination of more than 100 drug-resistant *P. falciparum* clones failed to reveal even a single SNV in the PF3D7_0109800 locus, indicating that the probability of *Pf* PheRS having three independent mutations by chance is very low. To confirm that cytosolic PheRS is the molecular target of BRD1095, the compound was assayed against purified recombinant proteins. BRD1095 inhibited the aminoacylation activity of recombinant *Pf* PheRS in a concentration-dependent manner (half-maximal inhibitory concentration (IC_{50}) = 46 nM; Fig. 3c). We also reasoned that if the primary antiplasmodial mechanism of the bicyclic azetidine series was via inhibition of *Pf* PheRS activity, then IC_{50} values for the aminoacylation activity of purified recombinant *Pf* PheRS proteins should correlate with EC_{50} values obtained in parasite growth inhibition assays. Indeed, a high correlation between the two parameters ($r^2 = 0.89$) was observed using 16 synthetic analogues of BRD1095 covering a range of activities (Fig. 3d and Extended Data Table 2). This notable correlation, together with the aforementioned genetic evidence, indicates that cytosolic *Pf* PheRS is the relevant molecular target of the bicyclic azetidine series. In addition, supplementation with exogenous L-phenylalanine (but not D-phenylalanine, L-aspartic acid, L-threonine or L-tyrosine) to the *in vitro* culture medium increased the EC_{50} value of BRD1095 in a concentration-dependent manner (Supplementary Table 5).

Owing to its newfound susceptibility to inhibition, *Pf* PheRS joins the aminoacyl-tRNA synthetase class of emerging targets for antimalarial agents[23–29]. Although they share common tRNA esterification catalytic activities, these proteins are structurally diverse and physiologically distinct enzymes. The target described here (*P. falciparum* cytosolic PheRS) is unique as it is the first member of the class in which inhibition, as we will describe, results in elimination of asexual blood-, liver- and transmission-stage parasites, preventing disease transmission, ensuring prophylaxis and providing single-dose cures of the disease in mouse models of malaria.

Optimization of the bicyclic azetidine series

BRD3444 exhibited poor solubility (<1 μM in PBS), high intrinsic clearance in human and mouse microsomes (Cl_{int} = 142 and 248 μl min^{-1} mg^{-1}, respectively) and a high volume of distribution (V_{ss} = 12 l kg^{-1}; all data found in Extended Data Table 3). These results translated to a half-life of 3.7 h in an intravenous pharmacokinetic study in CD-1 mice. Analysis of all eight stereoisomers of BRD3444 included in the primary screen revealed that activity against *P. falciparum* Dd2 parasites was predominantly found among two isomers differing in stereochemistry at the C_2 position (Fig. 2a, b). Therefore, we postulated that the C_2 position could be manipulated without loss of *in vitro* potency and could be used to improve the physicochemical and pharmacokinetic properties of the series. The modular synthetic pathway facilitated the synthesis of advanced analogues that included BRD1095 and BRD7929, in which the hydroxymethyl group at position C_2 is replaced with aminomethyl and dimethylaminomethyl substituents, respectively. These bicyclic azetidines showed improved solubility (25 and 15 μM in PBS, respectively) and greatly improved intrinsic clearance in mouse microsomes (<20 and 21 μl min^{-1} mg^{-1}, respectively), while retaining *in vitro* potency. In an intravenous and oral pharmacokinetic study in mice, both BRD1095 and BRD7929 displayed greatly improved blood clearance relative to BRD3444. BRD7929 also displayed good bioavailability (80%), superior to that of BRD1095 (50%), and improved *in vitro* potency against *P. cynomolgi* and *P. falciparum* liver-stage and *P. falciparum* transmission-stage parasites (Extended Data Table 1). BRD7929 showed a high V_{ss} of 24 l kg^{-1} (Extended Data Table 3), which, together with a low blood clearance, translated to a long half-life (32 h), making this compound suitable for single-dose oral treatments. The synthesis pathway enabled the laboratory preparation of 7.5 g of BRD7929 for further testing.

BRD7929 shows *in vivo* efficacy against all life stages

We evaluated the multistage activity of BRD7929 using mouse malaria models. When BRD7929 activity was evaluated in the blood-stage model with the rodent malaria parasite *P. berghei* using a luciferase reporter, all infected CD-1 mice treated with a single oral 25 mg kg^{-1} or 50 mg kg^{-1} dose became parasite-free and remained so up to the 30-day end-point based on bioluminescent imaging (Extended Data Fig. 3a, b). To evaluate the therapeutic potential of this series, the *in vivo* efficacy of BRD7929 against the human malaria parasite *P. falciparum* was determined. Approximately 48 h after inoculation with the blood-stage *P. falciparum* $3D7^{HLH/BRD}$ (expressing firefly luciferase), non-obese diabetic/severe combined immunodeficiency (NOD/SCID) *Il2rγ*$^{-/-}$ mice engrafted with human erythrocytes (huRBC NSG) were treated with a single dose of BRD7929 and monitored for 30 days (Fig. 4a and Extended Data Fig. 3c). At 25 mg kg^{-1} (area under curve (AUC) = 62.8 μM h) and 50 mg kg^{-1} (AUC = 125.6 μM h), a rapid decrease in parasite-associated bioluminescence was observed, while at 6.25 mg kg^{-1} (AUC = 15.7 μM h) the rate of the loss of bioluminescence was slower. All huRBC NSG mice treated with single oral 12.5 mg kg^{-1} (AUC = 31.4 μM h), 25 mg kg^{-1} or 50 mg kg^{-1} doses were parasite-free for 30 days based on bioluminescent imaging. The AUC in

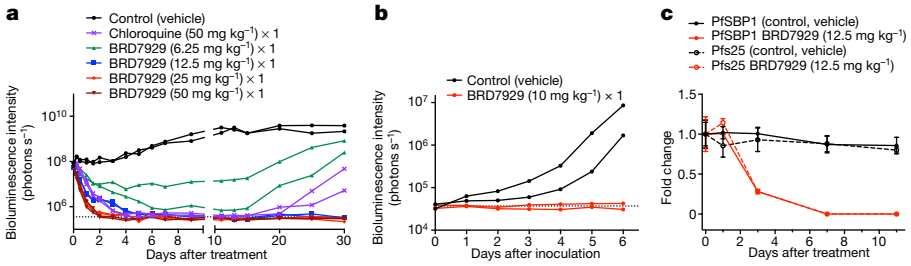

Figure 4 | *In vivo* efficacy studies of BRD7929 using *P. falciparum* and humanized mouse models. a, huRBC NSG mice were inoculated with *P. falciparum* (3D7$^{HLH/BRD}$) blood-stage parasites 48 h before treatment and BRD7929 was administered as a single 50, 25, 12.5 or 6.25 mg kg^{-1} oral dose at 0 h ($n = 2$ for each group, this study was conducted once). Infections were monitored using the *in vivo* imaging system (IVIS). Bioluminescent intensity was quantified from each mouse and plotted against time. The dotted horizontal line represents the mean bioluminescence intensity level obtained from all the animals before the parasite inoculation. No recrudescence was observed as low as a single 25 mg kg^{-1} dose of BRD7929 in the infected animals (see Extended Data Fig. 3b). **b**, huHep FRG-knockout mice were inoculated intravenously with *P. falciparum* (NF54HT-GFP-luc) sporozoites. BRD7929 was administered as a single 10 mg kg^{-1} oral dose 1 day after inoculation, and daily engraftment of human erythrocytes was initiated 5 days after inoculation ($n = 2$ for each group, this study was conducted once). Infections were monitored using IVIS. The dotted horizontal line represents the mean bioluminescence intensity level obtained from all the animals before the sporozoite inoculation. No increase in bioluminescence intensity level was observed from the mice treated with BRD7929 (see Extended Data Fig. 5a). **c**, huRBC NSG mice were infected with blood-stage *P. falciparum* (3D7$^{HLH/BRD}$) parasites for 2 weeks (allowing the gametocytes to mature fully) and were treated with a single oral dose of BRD7929 (12.5 mg kg^{-1}). Blood samples were collected for 11 days and analysed for the presence of the asexual marker SBP1 and the mature gametocyte marker Pfs25 using qRT–PCR ($n = 2$ for each group, this study was conducted once). The transcription of both SBP1 and Pfs25 decreased to undetectable levels 7 days after treatment, strongly suggesting that BRD7929 eliminates both asexual and gametocyte stages and is capable of preventing parasite transmission to the mosquito (data are mean ± s.d. for three technical replicates for each biological sample).

the 25 mg kg^{-1} single-dose cure observed in the model with *P. berghei* is estimated to be 27.5 μM h based on pharmacokinetic studies with CD-1 mice. Thus, single-dose cures were observed in the *P. berghei* CD-1 and *P. falciparum* huRBC NSG mouse models at similar drug exposure levels (AUC = 27.5 and 31.4 μM h, respectively), suggesting that the efficacy against the two *Plasmodium* species is comparable.

In a *P. berghei* liver-stage model, none of the CD-1 mice that were treated with a single dose of 5 or 25 mg kg^{-1} BRD7929 developed blood-stage parasitaemia within a 30-day period following *P. berghei* sporozoite inoculation (Extended Data Fig. 4a, b). Furthermore, mice were treated with a single dose of 10 mg kg^{-1} BRD7929 at various time points before sporozoite inoculation and during liver-stage infection (Extended Data Fig. 4c). All mice treated within the 3 days before inoculation and during liver-stage infection were completely free of blood-stage parasites for the duration of the experiment (32 days), indicating that BRD7929 has potent causal prophylaxis activity. Next, 1 day after inoculation with *P. falciparum* (NF54HT-GFP-luc)[30] sporozoites, FRG knockout (*Fah*$^{-/-}$*Rag2*$^{-/-}$*Il2rg*$^{-/-}$, heavily immunosuppressed) C57BL/6 mice transplanted with human hepatocytes (huHep FRG knockout)[31] were treated with a single oral dose of BRD7929 (10 mg kg^{-1}). Human erythrocytes were intraperitoneally injected daily from 5 to 7 days after inoculation. A gradual increase was detected in parasite liver-stage-associated bioluminescence signals from the lower pectoral and upper abdominal regions of the control (vehicle-treated) mice, whereas no increase in bioluminescence signals was observed from the BRD7929-treated mice (Fig. 4b and Extended Data Fig. 5a). For quantitative reverse transcription PCR (qRT–PCR) analysis[32], blood samples were also collected 7 days after inoculation (the first day of the blood stage)[31] and evaluated for the presence of the blood-stage transcript PF3D7_1120200 (expressing the *P. falciparum* ubiquitin-conjugating enzyme, UCE) (Extended Data Fig. 5b). The presence of the blood-stage marker was not detected in samples from the BRD7929-treated mice, indicating that BRD7929 eliminated the liver-stage parasites.

Finally, to examine whether BRD7929 has activity against mature gametocytes and prevents parasite transmission to mosquitoes *in vivo*, CD-1 mice infected with *P. berghei* were treated with a single oral dose of BRD7929 2 days before exposure to female *Anopheles stephensi* mosquitoes. One week later, the midguts of the blood-fed mosquitoes were dissected and the number of oocysts was counted (Extended Data Fig. 6a–c). No oocysts were detected in midguts dissected from mosquitoes fed on mice treated with 5 or 20 mg kg^{-1} BRD7929, concentrations below those found to be efficacious against asexual blood-stage parasites. To determine whether BRD7929 showed *in vivo* efficacy against *P. falciparum* in humanized mouse models, huRBC NSG mice were infected with blood-stage *P. falciparum* 3D7$^{HLH/BRD}$ parasites for 2 weeks to allow the development of mature gametocytes. Subsequently, mice were treated with a single oral dose of BRD7929 (12.5 mg kg^{-1}, AUC = 31.4 μM h). Blood samples were collected for 11 days after treatment and analysed for the presence of the late-sexual-stage-specific transcript of *Pfs25* (expressing *P. falciparum* 25 kDa ookinete surface-antigen precursor, PF3D7_1031000) using qRT–PCR[32] (Fig. 4c and Extended Data Fig. 6d–f). The transcription of *Pfs25* decreased to undetectable levels 7 days after treatment. Previous literature reports of *in vitro* cellular sensitivity showed that the *Pfs25* marker had a detection limit of 0.02–0.05 gametocytes μl^{-1} (ref. 33), strongly suggesting that BRD7929 has late-stage gametocidal activity and is capable of preventing the transmission of parasites to the mosquito vector at the same level of exposure as that achieves a single-dose cure in the blood stage.

Safety optimization of the bicyclic azetidine series

While no significant cytotoxicity was observed with BRD3444 and BRD3316, moderate cytotoxicity was observed for bicyclic azetidines BRD7929 (half-maximal cytotoxic concentration (CC_{50}) = 9 μM) and BRD1095 (CC_{50} = 16 μM) in the HepG2 cell line (Extended Data Fig. 7a). Both BRD1095 and BRD7929 showed inhibition of I_{Kr} (encoded by *KCNH2*, also known as *hERG*) (IC_{50} = 5.1 and 2.1 μM, respectively; Extended Data Table 3). Medicinal chemistry efforts have shown that mitigation of ion-channel toxicity is possible while maintaining biological activity; for example, BRD3316 shows no significant inhibition of I_{Kr} at >10 μM, indicating that cardiotoxicity is not intrinsically linked to this series. While BRD3444 showed time-dependent inhibition of CYP3A4, BRD7929 showed no inhibition of any of the major human cytochrome P450 (CYP) isoforms (Extended Data Fig. 7a). No phototoxicity was observed with this series in BALB/c 3T3 mouse fibroblasts following exposure to UVA light. BRD7929 and BRD3316 show desirable pharmacokinetic properties, including good oral bioavailability (F = 80 and 63%, respectively). In addition, BRD7929 has a long half-life that enables single-dose treatment. Based on *in vitro* microsomal stability data, BRD7929 and advanced analogues in this series are likely to have a similar profile in

humans, as metabolic clearance was low for both mouse and human species (Extended Data Table 3). BRD7929 was determined to be non-mutagenic using an Ames test in the presence or absence of S9 mix using the *Salmonella typhimurium* strains TA100, TA1535, TA98, TA1537 and *Escherichia coli* strain WP2uvrA (Supplementary Table 6). Histopathological analysis of mice treated at a high dose (100 mg kg^{-1}, estimated C_{max} and AUC are 5.4 μM and 110 μM h, respectively) showed no adverse findings in the limited number of organs examined (Extended Data Fig. 7b). Additional studies involving a wider range of organs, doses and compounds will be needed to assess the toxicity of these and related compounds more thoroughly. In NSG mice the estimated C_{max} and AUC of the single-dose cure are 833 nM and 31.4 μM h, respectively, affording a 6.5-fold safety margin with respect to C_{max}.

Although the emergence of resistance *in vitro* does not necessarily imply that it will happen *in vivo*, it is indicative of any mechanisms of resistance that could arise in the future. To examine the propensity of *de novo* resistance selection, *P. falciparum* Dd2 cultures with initial inocula ranging from 10^5 to 10^9 parasites were maintained in medium supplemented with 20 nM BRD7929 (the EC_{90} of strain Dd2) and monitored for 60 days to identify recrudescent parasitaemia (Extended Data Fig. 7c, d). No recrudescence was observed in Dd2 cultures exposed to a constant pressure of BRD7929, whereas the minimum inoculum of resistance for atovaquone ($EC_{90} = 2$ nM) was 10^7, consistent with previous reports[34].

Discussion

Malaria remains one of the deadliest infectious diseases. Available therapeutic agents are already limited in their efficacy, and drug resistance threatens to diminish our ability to prevent and treat the disease further. Despite a renewed effort to identify compounds with antimalarial activity, the drug discovery and development pipeline lacks target diversity and most malaria drugs are only efficacious during the asexual blood stage of parasite infection.

In these studies, we attempted to identify new antimalarial targets by screening a diverse collection of 100,000 compounds with three-dimensional topographic features derived from stereochemical and skeletal elements that are common in natural products but underrepresented in typical screening collections—compounds now accessible using DOS. The compounds are formed in short, modular syntheses that facilitate chemical optimization and manufacturing[35,36] and have computed physical properties aimed at accelerating drug discovery[37]. We used a primary phenotypic screen to identify a subset of compounds that inhibits parasite growth, counter-screens to prioritize molecules with both novel mechanisms of action and activity at multiple stages of the parasite life cycle, and genetic and biochemical studies to illuminate mechanisms of action. These efforts yielded several series of multiple-stage antimalarial compounds with unique scaffolds that modulate both recently described and established molecular targets.

An earlier pilot study tested key elements of the process above using a distinct 8,000-member DOS library, leading to the discovery of ML238 (refs 13, 14), a molecule that inhibits parasite growth with nanomolar potency by targeting the reductase domain of *P. falciparum* cytochrome *b* (the Q_i site), in contrast to the antimalarial agent atovaquone, which targets the oxidase domain of *P. falciparum* cytochrome *b* (the Q_o site). The study presented here led to many candidate antimalarial agents. We have, thus far, characterized four of these compound series, namely BRD0026 (targeting *P. falciparum* ATPase4), BRD7539 (targeting *P. falciparum* DHODH), BRD73842 (targeting *P. falciparum* PI4K) and BRD3444 (targeting *P. falciparum* cytoplasmic PheRS). These series were prioritized as they showed *in vitro* activity against multiple stages of the *P. falciparum* life cycle, and this was subsequently confirmed *in vivo*. We anticipate that additional compound series uncovered by these experiments, made available via the Malaria Therapeutics Response Portal (http://portals.broadinstitute.org/mtrp/), will target additional proteins that function as multiple-stage vulnerabilities in *Plasmodium* and other Apicomplexa pathogens.

Until now, natural products and synthetic drug-like compounds have served as the primary sources of antimalarial drugs. As parasitic susceptibility to traditional chemotypes decreases, it is becoming increasingly necessary to discover lead compounds that are unaffected by existing mechanisms of resistance. DOS coupled with phenotypic screening offers a systematic means to address this need. The results reported here describe a new target and chemotype—*Pf* PheRS and bicyclic azetidines such as BRD3316 and BRD7929—that have demonstrated the lowest-concentration single-dose cure of three promising next-generation antimalarials in the pipeline[9,38,39] using two mouse models. Single-dose treatments facilitate compliance and overcome cost challenges in resource-deficient regions[40]. The ability of BRD7929 to eliminate blood-stage (both asexual and sexual) and liver-stage parasites suggests bicyclic azetidines have the potential to cure the disease, provide prophylaxis and prevent disease transmission.

Our findings suggest that DOS-derived compound collections, which comprise three-dimensional structures reminiscent of natural products that have yielded many small-molecule probes of diverse mammalian processes[41,42], are also a rich resource for identifying targets and readily optimized chemical scaffolds to supplement the current antimalarial pipeline.

Online Content Methods, along with any additional Extended Data display items and Source Data, are available in the online version of the paper; references unique to these sections appear only in the online paper.

Received 9 October 2015; accepted 31 August 2016.
Published online 7 September 2016.

1. Wells, T. N. Discovering and developing new medicines for malaria control and elimination. *Infect. Disord. Drug Targets* **13,** 292–302 (2013).
2. Flannery, E. L., Chatterjee, A. K. & Winzeler, E. A. Antimalarial drug discovery—approaches and progress towards new medicines. *Nat. Rev. Microbiol.* **11,** 849–862 (2013).
3. Ariey, F. *et al.* A molecular marker of artemisinin-resistant *Plasmodium falciparum* malaria. *Nature* **505,** 50–55 (2014).
4. Campo, B., Vandal, O., Wesche, D. L. & Burrows, J. N. Killing the hypnozoite—drug discovery approaches to prevent relapse in *Plasmodium vivax*. *Pathog. Glob. Health* **109,** 107–122 (2015).
5. Hameed P, S. *et al.* Triaminopyrimidine is a fast-killing and long-acting antimalarial clinical candidate. *Nat. Commun.* **6,** 6715 (2015).
6. Jiménez-Díaz, M. B. *et al.* Improved murine model of malaria using *Plasmodium falciparum* competent strains and non-myelodepleted NOD-*scid* IL2Rγ^{null} mice engrafted with human erythrocytes. *Antimicrob. Agents Chemother.* **53,** 4533–4536 (2009).
7. Phillips, M. A. *et al.* A long-duration dihydroorotate dehydrogenase inhibitor (DSM265) for prevention and treatment of malaria. *Sci. Transl. Med.* **7,** 296ra111 (2015).
8. Roberts, L. & Enserink, M. Malaria. Did they really say ... eradication? *Science* **318,** 1544–1545 (2007).
9. Rottmann, M. *et al.* Spiroindolones, a potent compound class for the treatment of malaria. *Science* **329,** 1175–1180 (2010).
10. Gamo, F.-J. *et al.* Thousands of chemical starting points for antimalarial lead identification. *Nature* **465,** 305–310 (2010).
11. Guiguemde, W. A. *et al.* Chemical genetics of *Plasmodium falciparum*. *Nature* **465,** 311–315 (2010).
12. Meister, S. *et al.* Imaging of *Plasmodium* liver stages to drive next-generation antimalarial drug discovery. *Science* **334,** 1372–1377 (2011).
13. Comer, E. *et al.* Diversity-oriented synthesis-facilitated medicinal chemistry: toward the development of novel antimalarial agents. *J. Med. Chem.* **57,** 8496–8502 (2014).
14. Heidebrecht, R. W. Jr *et al.* Diversity-oriented synthesis yields a novel lead for the treatment of malaria. *ACS Med. Chem. Lett.* **3,** 112–117 (2012).
15. Lukens, A. K. *et al.* Diversity-oriented synthesis probe targets *Plasmodium falciparum* cytochrome *b* ubiquinone reduction site and synergizes with oxidation site inhibitors. *J. Infect. Dis.* **211,** 1097–1103 (2015).
16. Dancík, V., Seiler, K. P., Young, D. W., Schreiber, S. L. & Clemons, P. A. Distinct biological network properties between the targets of natural products and disease genes. *J. Am. Chem. Soc.* **132,** 9259–9261 (2010).
17. Burke, M. D. & Schreiber, S. L. A planning strategy for diversity-oriented synthesis. *Angew. Chem. Int. Edn Engl.* **43,** 46–58 (2004).
18. Marcaurelle, L. A. *et al.* An aldol-based build/couple/pair strategy for the synthesis of medium- and large-sized rings: discovery of macrocyclic histone deacetylase inhibitors. *J. Am. Chem. Soc.* **132,** 16962–16976 (2010).
19. Painter, H. J., Morrisey, J. M., Mather, M. W. & Vaidya, A. B. Specific role of mitochondrial electron transport in blood-stage *Plasmodium falciparum*. *Nature* **446,** 88–91 (2007).
20. McNamara, C. W. *et al.* Targeting *Plasmodium* PI(4)K to eliminate malaria. *Nature* **504,** 248–253 (2013).

21. Ghidelli-Disse, S. *et al.* Identification of *Plasmodium* PI4 kinase as target of MMV390048 by chemoproteomics. *Malar. J.* **13** (suppl. 1), 38 (2014).
22. Sharma, A. & Sharma, A. *Plasmodium falciparum* mitochondria import tRNAs along with an active phenylalanyl-tRNA synthetase. *Biochem. J.* **465,** 459–469 (2015).
23. Pham, J. S. *et al.* Aminoacyl-tRNA synthetases as drug targets in eukaryotic parasites. *Int. J. Parasitol.* **4,** 1–13 (2014).
24. Herman, J. D. *et al.* The cytoplasmic prolyl-tRNA synthetase of the malaria parasite is a dual-stage target of febrifugine and its analogs. *Sci. Transl. Med.* **7,** 288ra77 (2015).
25. Hussain, T., Yogavel, M. & Sharma, A. Inhibition of protein synthesis and malaria parasite development by drug targeting of methionyl-tRNA synthetases. *Antimicrob. Agents Chemother.* **59,** 1856–1867 (2015).
26. Novoa, E. M. *et al.* Analogs of natural aminoacyl-tRNA synthetase inhibitors clear malaria *in vivo*. *Proc. Natl Acad. Sci. USA* **111,** E5508–E5517 (2014).
27. Hoepfner, D. *et al.* Selective and specific inhibition of the *Plasmodium falciparum* lysyl-tRNA synthetase by the fungal secondary metabolite cladosporin. *Cell Host Microbe* **11,** 654–663 (2012).
28. Istvan, E. S. *et al.* Validation of isoleucine utilization targets in *Plasmodium falciparum*. *Proc. Natl Acad. Sci. USA* **108,** 1627–1632 (2011).
29. Bhatt, T. K. *et al.* A genomic glimpse of aminoacyl-tRNA synthetases in malaria parasite *Plasmodium falciparum*. *BMC Genomics* **10,** 644 (2009).
30. Vaughan, A. M. *et al.* A transgenic *Plasmodium falciparum* NF54 strain that expresses GFP-luciferase throughout the parasite life cycle. *Mol. Biochem. Parasitol.* **186,** 143–147 (2012).
31. Vaughan, A. M. *et al. Plasmodium falciparum* genetic crosses in a humanized mouse model. *Nat. Methods* **12,** 631–633 (2015).
32. Chang, H.-H. *et al.* Persistence of *Plasmodium falciparum* parasitemia after artemisinin combination therapy: evidence from a randomized trial in Uganda. *Sci. Rep.* **6,** 26330 (2016).
33. Joice, R. *et al. Plasmodium falciparum* transmission stages accumulate in the human bone marrow. *Sci. Transl. Med.* **6,** 244re5 (2014).
34. Ding, X. C., Ubben, D. & Wells, T. N. A framework for assessing the risk of resistance for anti-malarials in development. *Malar. J.* **11,** 292 (2012).
35. Dandapani, S. & Marcaurelle, L. A. Grand challenge commentary: Accessing new chemical space for 'undruggable' targets. *Nat. Chem. Biol.* **6,** 861–863 (2010).
36. Lovering, F., Bikker, J. & Humblet, C. Escape from flatland: increasing saturation as an approach to improving clinical success. *J. Med. Chem.* **52,** 6752–6756 (2009).
37. Lowe, J. T. *et al.* Synthesis and profiling of a diverse collection of azetidine-based scaffolds for the development of CNS-focused lead-like libraries. *J. Org. Chem.* **77,** 7187–7211 (2012).
38. Baragaña, B. *et al.* A novel multiple-stage antimalarial agent that inhibits protein synthesis. *Nature* **522,** 315–320 (2015).
39. Younis, Y. *et al.* 3,5-Diaryl-2-aminopyridines as a novel class of orally active antimalarials demonstrating single dose cure in mice and clinical candidate potential. *J. Med. Chem.* **55,** 3479–3487 (2012).
40. Burrows, J. N., van Huijsduijnen, R. H., Möhrle, J. J., Oeuvray, C. & Wells, T. N. C. Designing the next generation of medicines for malaria control and eradication. *Malar. J.* **12,** 187 (2013).
41. Ng, P. Y., Tang, Y., Knosp, W. M., Stadler, H. S. & Shaw, J. T. Synthesis of diverse lactam carboxamides leading to the discovery of a new transcription-factor inhibitor. *Angew. Chem. Int. Edn Engl.* **46,** 5352–5355 (2007).
42. Yu, C. *et al.* High-throughput identification of genotype-specific cancer vulnerabilities in mixtures of barcoded tumor cell lines. *Nat. Biotechnol.* **34,** 419–423 (2016).

Supplementary Information is available in the online version of the paper.

Acknowledgements This work was supported in part by the Bill and Melinda Gates Foundation (grant OPP1032518 to S.L.S., grant OPP1054480 to E.A.W. and D.F.W., grant OPP1023607 to S.N.B.), the Global Health Innovative Technology Fund (grant G2014-107 to S.L.S.), Medicines for Malaria Venture and the Wellcome Trust (grant WT078285 to C.H.M.K.), a New Investigator and Open Operating Grant from Canadian Institute of Health Research (grant FRN 142393 to J.E.B.) and Medicines for Malaria Venture (grant 12-2400 to V.M.A.). S.L.S. is an Investigator at the Howard Hughes Medical Institute. Mi.M. was supported by a fellowship from the National Science Foundation (DGE1144152). The authors thank R. Elliott, K. Duncan, and O. Vandal as well as J. Burrows, J. Duffy, F. Escudié and colleagues for discussions and access to invaluable scientific and experimental resources; K. Emmith for assistance with data processing and management; I. Goldowitz for assistance with establishing a gametocyte assay; N. van der Werff for technical assistance with the *P. cynomolgi* assay; J. Kotz and B. Melillo for discussions and assistance with the manuscript; J. Pu, M. Leighty, B. Braibant, S. LeQuement and J. Beaudoin for assistance with compound synthesis; E. Garcia-Rivera for assistance with molecular modelling; A. Hakura for performing the Ames test; Broad Institute Comparative Medicine Platform and Facility for assistance with animal studies; and the Broad Institute Compound Management and analytical teams for assistance with compound access and characterization. We also acknowledge WuXi AppTec and ChemPartner Co., Ltd for *in vitro* and *in vivo* pharmacokinetics assays, and Cyprotek for the phototoxicity analysis. *P. falciparum* scDHODH transgenic strain was a gift from A. B. Vaidya, *P. falciparum* 3D7^{HLH} strain from D. Fidock and *P. falciparum* NF54HT-GFP-luc from S. H. Kappe.

Author Contributions The author contributions are detailed in the Supplementary Information.

Author Information The whole-genome sequencing analysis data in this study have been deposited to the Short Read Archive; accession code SRP064988 and the x-ray crystal structure data for BRD7929 have been deposited to the Cambridge Structural Database: deposition number 1429949. Reprints and permissions information is available at www.nature.com/reprints. The authors declare no competing financial interests. Readers are welcome to comment on the online version of the paper. Correspondence and requests for materials should be addressed to S.L.S. (stuart_schreiber@harvard.edu).

METHODS

***In vitro P. falciparum* blood-stage culture and assay.** Strains of *P. falciparum* (Dd2, 3D7, D6, K1, NF54, V1/3, HB3, 7G8, FCB and TM90C2B) were obtained from the Malaria Research and Reference Reagent Resource Center (MR4). *Pfsc*DHODH, the transgenic *P. falciparum* line expressing *S. cerevisiae* DHODH[19], was a gift from A. B. Vaidya. *P. falciparum* isolates were maintained with O-positive human blood in an atmosphere of 93% N_2, 4% CO_2, 3% O_2 at 37 °C in complete culturing medium (10.4 g l^{-1} RPMI 1640, 5.94 g l^{-1} HEPES, 5 g l^{-1} albumax II, 50 mg l^{-1} hypoxanthine, 2.1 g l^{-1} sodium bicarbonate, 10% human serum and 43 mg l^{-1} gentamicin). Parasites were cultured in medium until parasitaemia reached 3–8%. Parasitaemia was determined by checking at least 500 red blood cells from a Giemsa-stained blood smear. For the compound screening, a parasite dilution at 2.0% parasitaemia and 2.0% haematocrit was created with medium. 25 µl of medium was dispensed into 384-well black, clear-bottom plates and 100 nl of each compound in DMSO was transferred into assay plates along with the control compound (mefloquine). Next, 25 µl of the parasite suspension in medium was dispensed into the assay plates giving a final parasitaemia of 1% and a final haematocrit of 1%. The assay plates were incubated for 72 h at 37 °C. 10 µl of detection reagent consisting of 10× SYBR Green I (Invitrogen; supplied in 10,000× concentration) in lysis buffer (20 mM Tris-HCl, 5 mM EDTA, 0.16% (w/v) Saponin, 1.6% (v/v) Triton X-100) was dispensed into the assay plates. For optimal staining, the assay plates were left at room temperature for 24 h in the dark. The assay plates were read with 505 dichroic mirrors with 485 nm excitation and 530 nm emission settings in an Envision (PerkinElmer).

Chemoinformatics clustering. High-throughput screening hits were hierarchically clustered by structural similarity using average linkage on pairwise Jaccard distances[43] between ECFP4 fingerprints[44]. Pipeline Pilot[45] was used for fingerprint and distance calculation; clustering and heat-map generation was done in R (ref. 46).

***In vitro P. berghei* liver-stage assay.** HepG2 cells (ATCC) were maintained in DMEM, 10% (v/v) FBS (Sigma), and 1% (v/v) antibiotic–antimycotic in a standard tissue culture incubator (37 °C, 5% CO_2). *P. berghei* (ANKA GFP–luc) infected *A. stephensi* mosquitoes were obtained from the New York University Langone Medical Center Insectary. For assays, ~17,500 HepG2 cells per well were added to a 384-well microtitre plate in duplicate. After 18–24 h at 37 °C the media was exchanged and compounds were added. After 1 h, parasites obtained from freshly dissected mosquitoes were added to the plates (4,000 parasites per well), the plates were spun for 10 min at 1,000 r.p.m. and then incubated at 37 °C. The final assay volume was 30 µl. After a 48-h incubation at 37 °C, Bright-Glo (Promega) was added to the parasite plate to measure relative luminescence. The relative signal intensity of each plate was evaluated with an EnVision (PerkinElmer) system.

***In vitro P. falciparum* liver-stage assay.** Micropatterned co-culture (MPCC) is an *in vitro* co-culture system of primary human hepatocytes organized into colonies and surrounded by supportive stromal cells. Hepatocytes in this format maintain a functional phenotype for up to 4–6 weeks without proliferation, as assessed by major liver-specific functions and gene expression[47–49]. In brief, 96-well plates were coated homogenously with rat-tail type I collagen (50 µg ml^{-1}) and subjected to soft-lithographic techniques to pattern the collagen into 500-µm-island microdomains that mediate selective hepatocyte adhesion. To create MPCCs, cryopreserved primary human hepatocytes (BioreclamationIVT) were pelleted by centrifugation at 100*g* for 6 min at 4 °C, assessed for viability using Trypan blue exclusion (typically 70–90%), and seeded on micropatterned collagen plates (each well contained ~10,000 hepatocytes organized into colonies of 500 µM) in serum-free DMEM with 1% penicillin–streptomycin. The cells were washed with serum-free DMEM with 1% penicillin–streptomycin 2–3 h later and replaced with human hepatocyte culture medium[48]. 3T3-J2 mouse embryonic fibroblasts were seeded (7,000 cells per well) 24 h after hepatocyte seeding. 3T3-J2 fibroblasts were courtesy of H. Green[50].

MPCCs were infected with 75,000 sporozoites (NF54) (Johns Hopkins University) 1 day after hepatocytes were seeded[48,49]. After incubation at 37 °C and 5% CO_2 for 3 h, wells were washed once with PBS, and the respective compounds were added. Cultures were dosed daily. Samples were fixed on day 3.5 after infection. For immunofluorescence staining, MPCCs were fixed with −20 °C methanol for 10 min at 4 °C, washed twice with PBS, blocked with 2% BSA in PBS, and incubated with mouse anti-*P. falciparum* Hsp70 antibodies (clone 4C9, 2 µg ml^{-1}) for 1 h at room temperature. Samples were washed with PBS then incubated with Alexa 488-conjugated secondary goat anti-mouse for 1 h at room temperature. Samples were washed with PBS, counterstained with the DNA dye Hoechst 33258 (Invitrogen; 1:1,000), and mounted on glass slides with fluoromount G (Southern Biotech). Images were captured on a Nikon Eclipse Ti fluorescence microscope. Diameters of developing liver stage parasites were measured and used to calculate the corresponding area.

***In vitro P. cynomolgi* liver-stage assay.** All rhesus macaques (*Macaca mulatta*) used in this study were bred in captivity for research purposes, and were housed at the Biomedical Primate Research Centre (BPRC; AAALAC-certified institute) facilities under compliance with the Dutch law on animal experiments, European directive 86/609/EEC and with the 'Standard for Humane Care and Use of Laboratory Animals by Foreign Institutions' identification number A5539-01, provided by the Department of Health and Human Services of the US National Institutes of Health. The local independent ethical committee first approved all protocols. Non-randomized rhesus macaques (male or female; 5—14 years old; one animal per month) were infected with 1×10^6 *P. cynomolgi* (M strain) blood-stage parasites, and bled at peak parasitaemia. Approximately 300 female *A. stephensi* mosquitoes (Sind-Kasur strain, Nijmegen University Medical Centre St Radboud) were fed with this blood as described previously[51].

Rhesus monkey hepatocytes were isolated from liver lobes as described by previously[52]. Sporozoite infections were performed within 3 days of hepatocyte isolation. Sporozoite inoculation of primary rhesus monkey hepatocytes was performed as described previously[53,54]. On day 6, intracellular *P. cynomolgi* malaria parasites were fixed, stained with purified rabbit antiserum reactive against *P. cynomolgi* Hsp70.1 (ref. 53), and visualized with FITC-labelled goat anti-rabbit IgG antibodies. Quantification of small 'hypnozoite' exoerythrocytic forms (1 nucleus, a small round shape, a maximal diameter of 7 µm) or large 'developing parasite' exoerythrocytic forms (more than 1 nucleus, larger than 7 µm and round or irregular shape) was determined for each well using a high-content imaging system (Operetta, PerkinElmer).

***In vitro* transmission-blocking assay (gametocyte IV–V).** *P. falciparum* 3D7 stage IV–V gametocytes were isolated by discontinuous Percoll gradient centrifugation of parasite cultures treated with 50 mM *N*-acetyl-D-glucosamine for 3 days to kill asexual parasites. Gametocytes (1.0×10^5) were seeded in 96-well plates and incubated with compounds for 72 h. *In vitro* anti-gametocyte activity was measured using CellTiter-Glo (Promega).

***In vitro* transmission-blocking imaging assay (early, I–III; and late, IV–V, gametocyte).** A detailed description of the method is published elsewhere[55]. In brief, $NF54^{pfs16\text{-}LUC\text{-}GFP}$ highly synchronous gametocytes were induced from a single intra-erythrocytic asexual replication cycle. On day 0 of gametocyte development, spontaneously generated gametocytes were removed by VarioMACS magnetic column (MAC) technology. Early stage I gametocytes were collected on day 2 of development and late-stage gametocytes (stage IV) on day 8 using MAC columns. Percentage parasitaemia and haematocrit was adjusted to 10 and 0.1, respectively. 45 µl of parasite sample were added to PerkinElmer Cell carrier poly-D-lysine imaging plates containing 5 µl of test compound at 16 doses, including control wells containing 4% DMSO and 50 µM puromycin (0.4% and 5 µM final concentrations, respectively), the plates sealed with a membrane (Breatheasy or 4ti-05 15/ST) and incubated for 72 h in standard incubation conditions of 5% CO_2, 5% O_2, 90% N_2 and 60% humidity at 37 °C. After incubation, 5 µl of 0.07 µg ml^{-1} MitoTracker Red CM-H2XRos (MTR) (Invitrogen) in PBS was added to each well, and plates were resealed with membranes and incubated overnight under standard conditions. The following day, the plates were brought to room temperature for at least one hour before being measured on the Opera QEHS Instrument. Image analysis was performed using an Acapella (PerkinElmer)-based algorithm that identifies gametocytes of the expected morphological shape with respect to degree of elongation and specifically those parasites that are determined as viable by the MitoTracker Red CM-H2XRos fluorescence size and intensity. IC_{50} values were determined using GraphPad Prism 4, using a 4-parameter log dose, nonlinear regression analysis, with sigmoidal dose–response (variable slope) curve fit.

***P. falciparum* standard membrane feeding assay.** *P. falciparum* transmission-blocking activity of BRD7929 was assessed in a standard membrane feeding assay as previously described[56]. In brief, *P. falciparum*$^{NF54\ hsp70\text{-}GFP\text{-}luc}$ reporter parasites were cultured up to stage V gametocytes (day 14). Test compounds were serially diluted in DMSO and subsequently in RPMI medium to reach a final DMSO concentration of 0.1%. Diluted compound was either pre-incubated with stage V gametocytes for 24 h (indirect mode) or directly added to the blood meal (direct mode). Gametocytes were adjusted to 50% haematocrit, 50% human serum and fed to *A. stephensi* mosquitoes. All compound dilutions were tested in duplicate in independent feeders. After 8 days, mosquitoes were collected and the relative decrease in oocysts density in the midgut was determined by measurement of luminescence signals in 24 individual mosquitoes from each cage. For each vehicle (control) cage, an additional 10 mosquitoes were dissected and examined by microscopy to determine the baseline oocyst intensity.

***In vitro* resistance selections.** *In vitro* resistance selections were performed as previously described[15]. In brief, approximately 1×10^9 *P. falciparum* Dd2 parasites were treated with 60 nM ($EC_{99.9}$) or 150 nM ($10 \times EC_{50}$) of BRD1095 in each of four independent flasks for 3–4 days. After the compounds were removed, the cultures were maintained in compound-free complete RPMI growth medium with regular media exchange until healthy parasites reappeared. Once parasitaemia reached

2–4%, compound pressure was repeated and these steps were executed for about 2 months until the initial EC_{50} shift was observed. Three out of four independent selections pressured at 60 nM developed a phenotypic EC_{50} shift. None of the selections pressured at 150 nM resulted in resistant parasites. After an initial shift in the dose–response phenotype was observed, selection at an increased concentration was repeated in the same manner until at least a threefold shift in EC_{50} was observed. Selected parasites were then cloned by limiting dilution.

BRD73842-resistant selections were conducted in a similar manner except that parasites were initially treated at 0.5 μM (10× EC_{50}) for 4 days or 150 nM ($EC_{99.9}$) for 2 days in each of two independent flasks. The Y1356N mutant was derived from a flask pressured at 0.5 μM and the L1418F mutant was developed from one of the flasks exposed to the 150 nM.

Whole-genome sequencing and target identification. DNA libraries were prepared for sequencing using the Illumina Nextera XT kit (Illumina), and quality-checked before sequencing on a Tapestation. Libraries were clustered and run as 100-bp paired-end reads on an Illumina HiSeq 2000 in RapidRun mode, according to the manufacturer's instructions. Samples were analysed by aligning to the *P. falciparum* 3D7 reference genome (PlasmoDB v. 11.1). To identify SNVs and CNVs, a sequencing pipeline developed for *P. falciparum* (*Plasmodium* Type Uncovering Software, Platypus) was used as previously described, with the exception of an increase in the base quality filter from 196.5 to 1,000 (ref. 57).

***P. falciparum* DHODH biochemical assay.** Substrate-dependent inhibition of recombinant *P. falciparum* DHODH protein was assessed in an *in vitro* assay in 384-well clear plates (Corning 3640) as described previously[58]. A 20-point dilution series of inhibitor concentrations were assayed against 2–10 nM protein with 500 μM L-dihydroorotate substrate (excess), 18 μM dodecylubiquinone electron acceptor (~K_m), and 100 μM 2,6-dichloroindophenol indicator dye in assay buffer (100 mM HEPES pH 8.0, 150 mM NaCl, 5% glycerol, 0.5% Triton X-100). Assays were incubated at 25 °C for 20 min and then assessed via OD_{600}. Data were normalized to 1% DMSO and excess inhibitor (25 μM DSM265; ref. 7).

Human DHODH biochemical assay. Substrate-dependent inhibition of recombinant human DHODH protein was assessed in an *in vitro* assay in 384-well clear plates (Corning 3640) as described previously[59]. A 20-point dilution series of inhibitor concentrations was assayed against 13 nM protein with 1 mM L-dihydroorotate substrate (excess), 100 μM dodecylubiquinone electron acceptor, and 60 μM 2,6-dichloroindophenol indicator dye in assay buffer (50 mM Tris HCl pH 8.0, 150 mM KCl, 0.1% Triton X-100). Assays were incubated at 25 °C for 20 min and then assessed via OD_{600}. Data were normalized to 1% DMSO and no enzyme.

***P. vivax* PI4K biochemical assay.** The synthetic gene for full-length *P. vivax* PI4K (PVX_098050) was synthesized from GeneArt (ThermoScientific), and was expressed and purified as previously described[20]. Aliquots of *P. vivax* PI4Kβ were flash-frozen in liquid nitrogen and stored at −80°C. Full-length human PI4KB (uniprot gene Q9UBF8-2) was expressed and purified as previously described[60]. 100 nM extruded lipid vesicles were made to mimic Golgi organelle vesicles (20% phosphatidylinositol, 10% phosphatidylserine, 45% phosphatidylcholine and 25% phosphatidylethanolamine) in lipid buffer (20 mM HEPES pH 7.5 (room temperature), 100 mM KCl, 0.5 mM EDTA). Lipid kinase assays were carried out using the Transcreener ADP^2 FI Assay (BellBrook Labs) following the published protocol as previously described[61]. 4-μl reactions ran at 21 °C for 30 min in a buffer containing 30 mM HEPES pH 7.5, 100 mM NaCl, 50 mM KCl, 5 mM $MgCl_2$, 0.25 mM EDTA, 0.4% (v/v) Triton X-100, 1 mM TCEP, 0.5 mg ml^{-1} Golgi-mimic vesicles and 10 μM ATP. *P. vivax* PI4Kβ was used at 7.5 nM and human PI4KB was used at 200 nM. Fluorescence intensity was measured using a Spectramax M5 plate reader with excitation at 590 nm and emission at 620 nm (20-nm bandwidth). IC_{50} values were calculated from triplicate inhibitor curves using GraphPad Prism software.

PheRS homology modelling. The model was built using the SWISS-MODEL online resource[62–64] and Prime[65] (Schrödinger Release 2015-2: Prime, version 4.0, Schrödinger), with human PheRS (PDB accession 3L4G) as a template for *P. falciparum* PheRS (PlasmoDB Gene ID: PF3D7_0109800). The template was chosen based on highest sequence identity and similarity identified via PSI-BLAST. Target-template alignment was made using ProMod-II and validated with Prime STA. Coordinates from residues that were conserved between the target and the template were copied from the template to the model, and remaining sites were remodelled using segments from known structures. The side chains were then rebuilt, and the model was finally refined using a force field.

***P. falciparum* cytoplasmic PheRS biochemical assay.** Protein sequences of both α- (PF3D7_0109800) and β- (PF3D7_1104000) subunits of cytoplasmic *P. falciparum* PheRS were obtained from PlasmoDB (http://plasmodb.org/plasmo/). Full length α- and β-subunit gene sequences optimized for expression in *E. coli* were cloned into pETM11 (Kanamycin resistance) and pETM20 (ampicillin resistance) expression vectors using Nco1 and Kpn1 sites and co-transformed into *E. coli* B834 cells. Protein expression was induced by addition of 0.5 mM isopropyl β-D-1-thiogalactopyranoside (IPTG) and cells were grown until an OD_{600} of 0.6–0.8 was reached at 37 °C. They were then allowed to grow at 18 °C for 20 h after induction. Cells were separated by centrifugation at 5,000*g* for 20 min and the bacterial pellets were suspended in a buffer consisting of 50 mM Tris–HCl (pH 7.5), 200 mM NaCl, 4 mM β-mercaptoethanol, 15% (v/v) glycerol, 0.1 mg ml^{-1} lysozyme and 1 mM phenylmethylsulfonyl fluoride (PMSF). Cells were lysed by sonication and cleared by centrifugation at 20,000*g* for 1 h. The supernatant was applied on to prepacked NiNTA column (GE Healthcare), and bound proteins were eluted by gradient-mixing with elution buffer (50 mM Tris–HCl (pH 7.5), 80 mM NaCl, 4 mM β-mercaptoethanol, 15% (v/v) glycerol, 1 M imidazole). Pure fractions were pooled and loaded on to heparin column for further purification. Again, bound proteins were eluted using gradient of heparin elution buffer 50 mM Tris–HCl (pH 7.5), 1 M NaCl, 4 mM β-mercaptoethanol, 15% (v/v) glycerol). Pure fractions were again pooled and dialysed overnight into a buffer containing 50 mM Tris–HCl (pH 7.5), 200 mM NaCl, 4 mM β-mercaptoethanol, 1 mM DTT and 0.5 mM EDTA. TEV protease (1:50 ratio of protease:protein) was added to the protein sample and incubated at 20 °C for 24 h to remove the polyhistidine tag. Protein was further purified via gel-filtration chromatography on a GE HiLoad 60/600 Superdex column in 50 mM Tris–HCl (pH 7.5), 200 mM NaCl, 4 mM β-mercaptoethanol, 1 mM $MgCl_2$. The eluted protein (a heterodimer of *P. falciparum* cPheRS) were collected, assessed for purity via SDS–PAGE and stored at −80 °C.

Nuclear encoded $tRNA^{Phe}$ from *P. falciparum* was synthesized using an *in vitro* transcription method as described earlier[22,66]. Aminoacylation and enzyme inhibition assays for *P. falciparum* cytosolic PheRS were performed as described earlier[22,67]. Enzymatic assays were performed in buffer containing 30 mM HEPES (pH 7.5), 150 mM NaCl, 30 mM KCl, 50 mM $MgCl_2$, 1 mM DTT, 100 μM ATP, 100 μM L-phenylalanine, 15 μM *P. falciparum* $tRNA^{Phe}$, 2 U ml^{-1} *E. coli* inorganic pyrophosphatase (NEB) and 500 nM recombinant *P. falciparum* PheRS at 3 °C. Reactions at different time points were stopped by the addition of 40 mM EDTA and subsequent transfer to ice. Recombinant maltose binding protein was used as negative control. The cPheRS inhibition assays were performed using inhibitor concentrations of 0.01 nM, 0.1 nM, 1 nM, 10 nM, 100 nM, 1 μM, 5 μM and 10 μM for strong binders and 1 nM, 10 nM, 100 nM, 1 μM, 10 μM, 100 μM and 500 μM for weaker binders in the assay buffer. Enzymatic and inhibition experiments were performed twice in triplicate.

Mammalian cell cytotoxicity assays. Mammalian cells (HepG2, A549, and HEK293) were obtained from the ATCC and cultured routinely in DMEM with 10% FBS and 1% (v/v) antibiotic–antimycotic. For cytotoxicity assays, 1×10^6 cells were seeded into 384-well plates 1 day before compound treatment. Cells were treated with ascending doses of compound for 72 h, and viability was measured using Cell-Titer Glo (Promega). All cell lines were tested for *Mycoplasma* contamination using Universal mycoplasma Detection Kit (ATCC).

***In vitro* ADME/PK and safety assays.** *In vitro* characterization assays (protein binding, microsomal stability, hepatocyte stability, cytochrome P450 (CYP) inhibition, and aqueous solubility) were performed according to industry-standard techniques. Ion channel inhibition studies were performed using the Q-Patch system using standard techniques.

Animal welfare. All animal experiments were conducted in compliance with institutional policies and appropriate regulations and were approved by the institutional animal care and use committees for each of the study sites (the Broad Institute, 0016-09-14; Harvard School of Public Health, 03228; Eisai, 13-05, 13-07, 14-C-0027). No method of randomization or blinding was used in this study.

***In vivo P. berghei* blood-stage assay.** CD-1 mice ($n = 4$ per experimental group; female; 6–7-week-old; 20–24 g, Charles River) were intravenously inoculated with approximately 1×10^5 *P. berghei* (ANKA GFP-luc) blood-stage parasites 24 h before treatment and compounds were administered orally (at 0 h). Parasitaemia was monitored by the *in vivo* imaging system (IVIS SpectrumCT, PerkinElmer) to acquire the bioluminescence signal (150 mg kg^{-1} of luciferin was intraperitoneally injected approximately 10 min before imaging). In addition, blood smear samples were obtained from each mouse periodically, stained with Giemsa, and viewed under a microscope for visual detection of blood parasitaemia. Animals with parasitaemia exceeding 25% were humanely euthanized.

***In vivo P. berghei* causal prophylaxis assay.** CD-1 mice ($n = 4$ per experimental group; female; 6–7-week-old; 20–24 g, Charles River) were inoculated intravenously with approximately 1×10^5 *P. berghei* (ANKA GFP-luc) sporozoites freshly dissected from *A. stephensi* mosquitoes. Immediately after infection, the mice were treated with single oral doses of BRD7929; infection was monitored as described for the *P. berghei* erythrocytic-stage assay. For time-course experiments, the time of compound treatment (single oral dose of 10 mg kg^{-1}) was varied from 5 days before infection to 2 days after infection.

***In vivo P. berghei* transmission-stage assay.** CD-1 ($n = 3$ per experimental group; female; 6–7-week-old; 21–24 g, Charles River) mice were infected with *P. berghei* (ANKA GFP-luc) for 96 h before treatment with vehicle or BRD7929 (day 0).

On day 2, female *A. stephensi* mosquitoes were allowed to feed on the mice for 20 min. After 1 week (day 9), the midguts of the mosquitoes were dissected out and oocysts were enumerated microscopically (12.5× magnification).

***In vivo P. falciparum* blood-stage assay.** *In vivo* adapted *P. falciparum* (3D7$^{HLH/BRD}$) were selected as described previously[68]. In brief, NSG mice ($n = 2$ per experimental group; female; 4–5-week-old; 19–21 g; The Jackson Laboratory) were intraperitoneally injected with 1 ml of human erythrocytes (O-positive, 50% haematocrit, 50% RPMI 1640 with 5% albumax) daily to generate mice with humanized circulating erythrocytes (huRBC NSG). Approximately 2×10^7 blood-stage *P. falciparum* 3D7$^{HLH/BRD}$ (ref. 69) were intravenously infected to huRBC NSG mice and >1% parasitaemia was achieved 5 weeks after infection. After three *in vivo* passages, the parasites were frozen and used experimentally.

Approximately 48 h after infection with 1×10^7 blood-stage of *P. falciparum* 3D7$^{HLH/BRD}$, the mean parasitaemia was approximately 0.4%. huRBC NSG mice were orally treated with a single dose of compound and parasitaemia was monitored for 30 days by IVIS to acquire the bioluminescence signal (150 mg kg^{-1} of luciferin was intraperitoneally injected approximately 10 min before imaging).

***In vivo P. falciparum* transmission-stage assay.** huRBC NSG mice ($n = 2$ per experimental group; female; 4–5-week-old; 18–20 g; Jackson Laboratory) were infected with blood-stage *P. falciparum* 3D7$^{HLH/BRD}$ for 2 weeks to allow the development of mature gametocytes. Subsequently, the mice were treated with a single oral dose of BRD7929. Blood samples were collected for 11 days. For molecular detection of parasite stages, 40 µl of blood was obtained from control and treated mice. In brief, total RNA was isolated from blood samples using RNeasy Plus Kit with genomic DNA eliminator columns (Qiagen). First-strand cDNA synthesis was performed from extracted RNA using SuperScript III First-Strand Synthesis System (Life Technologies). Parasite stages were quantified using a stage-specific qRT–PCR assay as described previously[33,69]. Primers were designed to measure transcript levels of PF3D7_0501300 (ring stage parasites), PF3D7_1477700 (immature gametocytes) and PF3D7_1031000 (mature gametocytes). Primers for PF3D7_1120200 (*P. falciparum* UCE) transcript were used as a constitutively expressed parasite marker. The assay was performed using cDNA in a total reaction volume of 20 µl, containing primers for each gene at a final concentration of 250 nM. Amplification was performed on a Viia7 qRT–PCR machine (Life Technologies) using SYBR Green Master Mix (Applied Biosystems) with the following reaction conditions: 1 cycle × 10 min at 95 °C and 40 cycles × 1 s at 95 °C and 20 s at 60 °C. Each cDNA sample was run in triplicate and the mean C_t value was used for the analysis. C_t values obtained above the cut-off (negative control) for each marker were considered negative for the presence of specific transcripts. Blood samples from each mouse before parasite inoculation were also tested for 'background noise' using the same primer sets. No amplification was detected from any samples.

***In vivo P. falciparum* liver-stage assay.** FRG knockout on C57BL/6 (human repopulated, >70%) mice (huHep FRG knockout; $n = 2$ per experimental group; female; 5.5–6-month-old; 19–21 g; Yecuris) were inoculated intravenously with approximately 1×10^5 *P. falciparum* (NF54HT-GFP-luc) sporozoites and BRD7929 was administered as a single 10 mg kg^{-1} oral dose one day after inoculation[31]. Infection was monitored daily by IVIS. Daily engraftment of human erythrocytes (0.4 ml, O-positive, 50% haematocrit, 50% RPMI 1640 with 5% albumax) was initiated 5 days after inoculation. For qPCR analysis, blood samples (40 µl) were collected 7 days after inoculation. For molecular detection of the blood-stage parasite, 40 µl of blood was obtained from control and treated mice. In brief, total RNA was isolated from blood samples using RNeasy Plus Kit with genomic DNA eliminator columns (Qiagen). First-strand cDNA synthesis was performed from extracted RNA using SuperScript III First-Strand Synthesis System (Life Technologies). The presence of the blood-stage parasites was quantified using a highly stage-specific qRT–PCR assay as described previously[33,70]. Primers were designed to measure transcript levels of PF3D7_1120200 (*P. falciparum* UCE). The assay was performed using cDNA in a 20 µl total reaction volume containing primers for each gene at a final concentration of 250 nM. Amplification was performed on a Viia7 qRT–PCR machine (Life Technologies) using SYBR Green Master Mix (Applied Biosystems) and the reaction conditions are as follows: 1 cycle × 10 min at 95 °C and 40 cycles × 1 s at 95 °C and 20 s at 60 °C. Each cDNA sample was run in triplicate and the mean C_t value was used for the analysis. C_t values obtained above the cut-off (negative control) for each marker were considered negative for presence of specific transcripts. Blood samples from each mouse were also tested for background noise using the same primer sets before parasite inoculation. No amplification was detected from any samples.

Resistance propensity determination assay. *In vitro* cultures of *P. falciparum* Dd2, with the initial inocula ranging from 10^5 to 10^9 parasites, were maintained in complete medium supplemented with 20 nM of BRD7929 (EC_{90} against Dd2). Media was replaced with fresh compound added daily and cultures monitored for 60 days to identify propensity for recrudescent parasitaemia as described[34]. Atovaquone was used as a control ($EC_{90} = 2$ nM).

Solubility assay. Solubility was determined in PBS pH 7.4 with 1% DMSO. Each compound was prepared in triplicate at 100 µM in both 100% DMSO and PBS with 1% DMSO. Compounds were allowed to equilibrate at room temperature with a 750 r.p.m. vortex shake for 18 h. After equilibration, samples were analysed by UPLC–MS (Waters) with compounds detected by single-ion reaction detection on a single quadrupole mass spectrometer. The DMSO samples were used to create a two-point calibration curve to which the response in PBS was fit.

Plasma protein binding assay. Plasma protein binding was determined by equilibrium dialysis using the Rapid Equilibrium Dialysis (RED) device (Pierce Biotechnology) for both human and mouse plasma. Each compound was prepared in duplicate at 5 µM in plasma (0.95% acetonitrile, 0.05% DMSO) and added to one side of the membrane (200 µl) with PBS pH 7.4 added to the other side (350 µl). Compounds were incubated at 37 °C for 5 h with 350 r.p.m. orbital shaking. After incubation, samples were analysed by UPLC–MS (Waters) with compounds detected by SIR detection on a single quadrupole mass spectrometer.

hERG channel inhibition assay. The required potency to inhibit the hERG channel in expressed cell lines were evaluated using an automated patch-clamp system (QPatch-HTX).

Mouse pharmacokinetics assay. Pharmacokinetics of BRD3444 and BRD1095 were performed by Shanghai ChemPartner Co. Ltd., following single intravenous and oral administrations to female CD-1 mice. BRD3444 and BRD1095 were formulated in 70% PEG400 and 30% aqueous glucose (5% in H_2O) for intravenous and oral dosing. Test compounds were dosed as a bolus solution intravenously at 0.6 mg kg^{-1} (dosing solution; 70% PEG400 and 30% aqueous glucose, 5% in H_2O) or dosed orally by gavage as a solution at 1 mg kg^{-1} (dosing solution; 70% PEG400 and 30% aqueous glucose, 5% in H_2O) to female CD-1 mice ($n = 9$ per dose route). Pharmacokinetic parameters of BRD7929 and BRD3316 were determined in CD-1 mice. BRD7929 and BRD3316 were formulated in 10% ethanol, 4% Tween, 86% saline for both intravenous and oral dosing. Pharmacokinetic parameters were estimated by non-compartmental model using WinNonlin 6.2. Pharmacokinetic parameters for BRD7929 and BRD3316 were estimated by a non-compartmental model using proprietary Eisai software. Pharmacokinetic parameters of BRD7539 and BRD9185 were determined in CD-1 mice. Compounds were formulated in 70% PEG300 and 30% (5% glucose in H_2O) at 0.5 mg ml^{-1} for oral dosing, and 5% DMSO, 10% cremophor, and 85% H_2O at 0.25 mg ml^{-1} for intravenous formulation. Pharmacokinetic parameters were estimated by non-compartmental model using WinNonlin 6.2. Pharmacokinetics of BRD7539 and BRD9185 were performed by WuXi AppTec. The protocol was approved by Eisai IACUC, 13-07, 13, 05, and 14-c-0027.

Metabolic stability assay. Compounds were evaluated *in vitro* to determine their metabolic stability in incubations containing liver microsomes or hepatocytes of mouse and human. In the presence of NADPH, liver microsomes (0.2 mg ml^{-1}) from mouse (CD-1) and human were incubated with compounds (0.5 and 5 µM) for 0, 10 and 90 min. The depletion of compounds in the incubation mixtures, determined using liquid chromatography tandem mass spectromety LC–MS/MS, was used to estimate K_m and V_{max} values and determine half-lives for both mouse and human microsomes.

CYP inhibition assay. Compounds were evaluated *in vitro* for the potential inhibition of human cytochrome P450 (CYP) isoforms using human liver microsomes. Two concentrations (1 and 10 µM) of compound were incubated with pooled liver microsomes (0.2 mg ml^{-1}) and a cocktail mixture of probe substrates for selective CYP isoform. The selective activities tested were CYP1A2-mediated phenacetin *O*-demethylation, CYP2C8-mediated rosiglitazone para-hydroxylation, CYP2C9-mediated tolbutamide 4′-hydroxylation, CYP2C19-mediated (*S*)-mephenytoin 4′-hydroxylation, CYP2D6-mediated (±)-bufuralol 1′-hydroxylation and, CYP3A4/5-mediated midazolam 1′-hydroxylation. The positive controls tested were α-naphthoflavone for CYP1A2, montelukast for CYP2C8, sulfaphenazole for CYP2C9, tranylcypromine for CYP2C19, quinidine for CYP2D6, and ketoconazole for CYP3A4/5. The samples were analysed by LC–MS/MS. IC_{50} values were estimated using nonlinear regression.

Time-dependent inactivation assay. The time-dependent inactivation potential of compounds were assessed in human liver microsomes for CYP2C9, CYP2D6, and CYP3A4/5 by determining K_I and k_{inact} values when appropriate. Two concentrations (6 and 30 µM) of compound were incubated in primary reaction mixtures containing phosphate buffer and 0.2 mg ml^{-1} human liver microsomes for 0, 5, and 30 min in a 37 °C water bath. The reactions were initiated by the addition of NADPH. Phosphate buffer was substituted for NADPH solution for control. At the respective times, 25 µl of primary incubation was diluted tenfold into pre-incubated secondary incubation mixture containing each CYP-selective probe substrate in order to assess residual activity. The second incubation time was 10 min. The probe substrates used for CYP1A, 2C9, CYP2C19, CYP2D6,

and CYP3A4 were phenacetin (50 μM), tolbutamide (500 μM), (*S*)-mephenytoin (20 μM), bufuralol (50 μM), and midazolam (30 μM), respectively. The CYP time-dependent inhibitors used were furafyllin, tienilic acid, ticlopidine, paroxetin and troleandomycin for CYP2C8, CYP2C9, CYP2C19, CYP2D6 and CYP3A, respectively, at two concentrations. The samples were analysed by LC–MS/MS.

Chemical synthesis and analytical data. See Supplementary Methods.

43. Jaccard, P. Lois de distribution florale dans la zone alpine. *Bull. Soc. Vaud. Sci. Nat.* **38,** 69–130 (1902).
44. Rogers, D. & Hahn, M. Extended-connectivity fingerprints. *J. Chem. Inf. Model.* **50,** 742–754 (2010).
45. Pipeline Pilot v. 8.5.0.200; http://cscenter.pbsci.ucsc.edu:9944/ (Accelrys Software Inc., 2011).
46. R Core Development Team. *R: A Language and Environment for Statistical Computing v. 3.0;* http://www.R-project.org/ (R Foundation for Statistical Computing, Vienna, Austria, 2013).
47. Khetani, S. R. & Bhatia, S. N. Microscale culture of human liver cells for drug development. *Nat. Biotechnol.* **26,** 120–126 (2008).
48. March, S. *et al.* A microscale human liver platform that supports the hepatic stages of *Plasmodium falciparum* and *vivax*. *Cell Host Microbe* **14,** 104–115 (2013).
49. March, S. *et al.* Micropatterned coculture of primary human hepatocytes and supportive cells for the study of hepatotropic pathogens. *Nat. Protocols* **10,** 2027–2053 (2015).
50. Rheinwald, J. G. & Green, H. Serial cultivation of strains of human epidermal keratinocytes: the formation of keratinizing colonies from single cells. *Cell* **6,** 331–343 (1975).
51. Ponnudurai, T. *et al.* Infectivity of cultured *Plasmodium falciparum* gametocytes to mosquitoes. *Parasitology* **98,** 165–173 (1989).
52. Guguen-Guillouzo, C. *et al.* High yield preparation of isolated human adult hepatocytes by enzymatic perfusion of the liver. *Cell Biol. Int. Rep.* **6,** 625–628 (1982).
53. Dembele, L. *et al.* Towards an *in vitro* model of *Plasmodium* hypnozoites suitable for drug discovery. *PLoS One* **6,** e18162 (2011).
54. Mazier, D. *et al.* Complete development of hepatic stages of *Plasmodium falciparum in vitro*. *Science* **227,** 440–442 (1985).
55. Duffy, S. & Avery, V. M. Identification of inhibitors of *Plasmodium falciparum* gametocyte development. *Malar. J.* **12,** 408 (2013).
56. Stone, W. J. R. *et al.* A scalable assessment of *Plasmodium falciparum* transmission in the standard membrane-feeding assay, using transgenic parasites expressing green fluorescent protein-luciferase. *J. Infect. Dis.* **210,** 1456–1463 (2014).
57. Manary, M. J. *et al.* Identification of pathogen genomic variants through an integrated pipeline. *BMC Bioinformatics* **15,** 1–14 (2014).
58. Ross, L. S. *et al. In vitro* resistance selections for *Plasmodium falciparum* dihydroorotate dehydrogenase inhibitors give mutants with multiple point mutations in the drug-binding site and altered growth. *J. Biol. Chem.* **289,** 17980–17995 (2014).
59. Hansen, M. *et al.* Inhibitor binding in a class 2 dihydroorotate dehydrogenase causes variations in the membrane-associated N-terminal domain. *Protein Sci.* **13,** 1031–1042 (2004).
60. Burke, J. E. *et al.* Structures of PI4KIIIβ complexes show simultaneous recruitment of Rab11 and its effectors. *Science* **344,** 1035–1038 (2014).
61. Burke, J. E. & Williams, R. L. Dynamic steps in receptor tyrosine kinase mediated activation of class IA phosphoinositide 3-kinases (PI3K) captured by H/D exchange (HDX-MS). *Adv. Biol. Regul.* **53,** 97–110 (2013).
62. Arnold, K., Bordoli, L., Kopp, J. & Schwede, T. The SWISS-MODEL workspace: a web-based environment for protein structure homology modelling. *Bioinformatics* **22,** 195–201 (2006).
63. Benkert, P., Biasini, M. & Schwede, T. Toward the estimation of the absolute quality of individual protein structure models. *Bioinformatics* **27,** 343–350 (2011).
64. Biasini, M. *et al.* SWISS-MODEL: modelling protein tertiary and quaternary structure using evolutionary information. *Nucleic Acids Res.* **42,** W252–W258 (2014).
65. Jacobson, M. P. *et al.* A hierarchical approach to all-atom protein loop prediction. *Proteins* **55,** 351–367 (2004).
66. Sherlin, L. D. *et al.* Chemical and enzymatic synthesis of tRNAs for high-throughput crystallization. *RNA* **7,** 1671–1678 (2001).
67. Cestari, I. & Stuart, K. A spectrophotometric assay for quantitative measurement of aminoacyl-tRNA synthetase activity. *J. Biomol. Screen.* **18,** 490–497 (2013).
68. Angulo-Barturen, I. *et al.* A murine model of *falciparum*-malaria by *in vivo* selection of competent strains in non-myelodepleted mice engrafted with human erythrocytes. *PLoS One* **3,** e2252 (2008).
69. Ekland, E. H., Schneider, J. & Fidock, D. A. Identifying apicoplast-targeting antimalarials using high-throughput compatible approaches. *FASEB J.* **25,** 3583–3593 (2011).
70. Joice, R. *et al.* Inferring developmental stage composition from gene expression in human malaria. *PLOS Comput. Biol.* **9,** e1003392 (2013).
71. Ruecker, A. *et al.* A male and female gametocyte functional viability assay to identify biologically relevant malaria transmission-blocking drugs. *Antimicrob. Agents Chemother.* **58,** 7292–7302 (2014).
72. Zeeman, A.-M. *et al.* KAI407, a potent non-8-aminoquinoline compound that kills *Plasmodium cynomolgi* early dormant liver stage parasites *in vitro*. *Antimicrob. Agents Chemother.* **58,** 1586–1595 (2014).
73. Lukens, A. K. *et al.* Harnessing evolutionary fitness in *Plasmodium falciparum* for drug discovery and suppressing resistance. *Proc. Natl Acad. Sci. USA* **111,** 799–804 (2014).

a

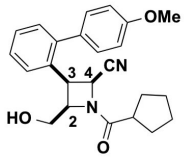

BRD0026
Stereochemistry R, S, S

b

Stereochemistry C_2, C_3, C_4
Pf, Dd2 EC_{50}

S, S, R > 5.00 μM	R, R, S > 5.00 μM
S, R, S > 5.00 μM	R, S, R 0.532 μM
S, S, S 0.867 μM	R, R, R > 5.00 μM
R, S, S 0.346 μM	S, R, R > 5.00 μM

c

Assay (μM)	BRD0026
Pf, Dd2, EC_{50}	0.346
*Pf*NITD609^{R}, EC_{50}	1.77
Pf gametocyte, IV-V, EC_{50}	1.98
Pb liver stage, EC_{50}	> 20
PBS solubility	~20
HepG2, CC_{50}	> 50

d

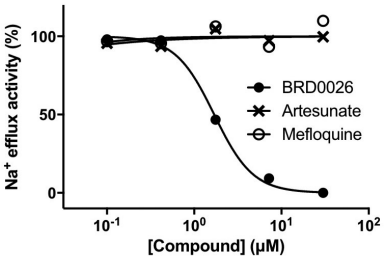

e

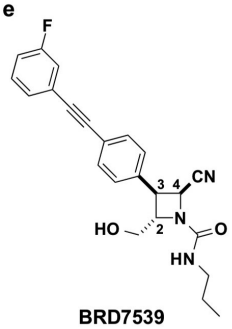

BRD7539
Stereochemistry S, S, S

f

Stereochemistry C_2, C_3, C_4
Pf, Dd2 EC_{50}

R, S, S 0.035 μM	S, R, R > 5.00 μM
R, R, S > 5.00 μM	S, S, R > 5.00 μM
R, S, R > 5.00 μM	S, R, S > 5.00 μM
R, R, R 3.01 μM	S, S, S 0.010 μM

g

Assay (μM)	BRD7539
Pf, Dd2, EC_{50}	0.010
*Pf*scDHODH, EC_{50}	8.910
Pf, TM90C6B*, EC_{50}	0.011
*Pf*CYTb:G33V†, EC_{50}	0.003
*Pf*DHODH:E182D‡, EC_{50}	0.637
*Pf*rDHODH, IC_{50}	0.033
Pf gametocyte, IV-V, EC_{50}	> 20.0
Pb liver stage, EC_{50}	> 15.0
PBS solubility	< 1.0
HepG2, CC_{50}	> 50.0

h

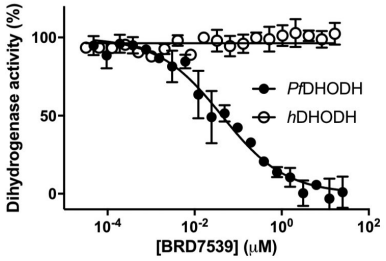

i

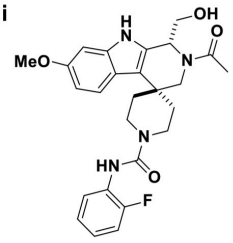

BRD73842
Stereochemistry R

j

Stereochemistry
Pf, Dd2 EC_{50}

R 0.069 μM	S 2.31 μM

k

Assay (μM)	BRD73842
Pf, Dd2, EC_{50}	0.069
Pf gametocyte, IV-V, EC_{50}	0.643
Pb liver stage, EC_{50}	0.459
Pv PI(4)K, IC_{50}	0.021
PBS solubility (μM)	66
HepG2 CC_{50} (μM)	49
hERG IC_{50} (μM)	>10

l

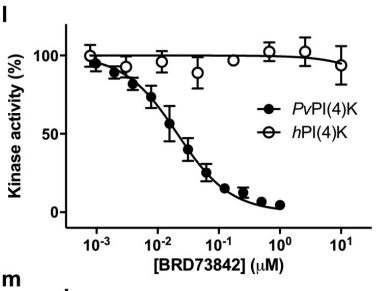

m

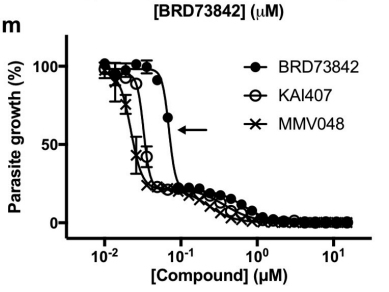

Extended Data Figure 1 | See next page for caption.

Extended Data Figure 1 | Three screening-hit series yield new compound scaffolds against known targets. a–d, BRD0026 exhibits the same mode of action as NITD609 and showed moderate *in vitro* potency against asexual ($EC_{50} = 0.346\,\mu M$) and late-sexual ($EC_{50} = 1.98\,\mu M$) blood stages of the parasites and exhibited reduced potency against *P. falciparum* $NITD609^{R}$ ($EC_{50} = 1.77\,\mu M$), a transgenic strain carrying a point mutation in *P. falciparum* ATPase4 (ref. 9). *P. falciparum* ATPase4 is the presumed molecular target of NITD609 (ref. 9). **a**, **b**, Three of the eight possible stereoisomers (*R*,*S*,*R*; *S*,*S*,*S*; and *R*,*S*,*S*) of BRD0026 have activity. **c**, Initial characterization of BRD0026 showed good solubility in PBS and low cytotoxicity. **d**, Treatment with BRD0026 resulted in a rapid increase in the parasite cytosolic Na^{+} concentration, while artesunate- or mefloquine-treated parasites maintained a constant cytosolic Na^{+} concentration. This result suggests that parasites treated with BRD0026 are not able to counter the influx of Na^{+} by actively extruding the cation, similar to the proposed mechanism for NITD609 (data are mean ± s.d.; two biological and two technical replicates). **e–h**, BRD7539 targets and inhibits *P. falciparum* DHODH. BRD7539 showed excellent *in vitro* potency against liver-stages ($EC_{50} = 0.015\,\mu M$) and asexual blood-stages ($EC_{50} = 0.010\,\mu M$) of the parasite, conferring markedly reduced potency against *Pfsc*DHODH[19]. This strain heterologously expresses the cytosolic *S. cerevisiae* DHODH, which does not require ubiquinone as an electron acceptor. Thus, this transgenic strain is resistant to inhibitors of mitochondrial electron transport chain functions[19]. BRD7539 was tested against three different *P. falciparum* strains with mutations in mitochondrial genes targeted by other antimalarial agents: (i) TM90C6B strain, containing a point mutation in the quinol oxidase domain of *P. falciparum* cytochrome *b* (Q_o site) and resistant to atovaquone[15]; (ii) a *P. falciparum* $CYTb^{G33V}$ mutant strain, selected against IDI5994 and containing a point mutation in the quinone reductase site of *P. falciparum* cytochrome *b* (Q_i site)[15]; and (iii) a *P. falciparum* $DHODH^{E182D}$ mutant strain, selected against Genz-666136 and containing a point mutation in the *P. falciparum* DHODH gene[73]. BRD7539 exhibited an approximately 59-fold shift in potency against the *P. falciparum* $DHODH^{E182D}$ strain, whereas potency was unaffected in the TM90C6B and *P. falciparum* $CYTb^{G33V}$ strains. BRD7539 also inhibits recombinant *P. falciparum* DHODH in an *in vitro* biochemical assay ($IC_{50} = 0.033\,\mu M$) but not the human orthologue. Altogether, these results demonstrate that BRD7539 targets *P. falciparum* DHODH. **e**, **f**, Only two (*S*,*S*,*S* and *R*,*S*,*S*) of eight possible stereoisomers of BRD7539 showed activity. **g**, *In vitro* growth inhibition assays showed no change in activity in *P. falciparum* $CYTb^{G33V}$ and TM90C6B strains but exhibited a tenfold change in potency in *P. falciparum* $DHODH^{E182D}$ strain, indicating that BRD7539 targets *P. falciparum* DHODH but not *P. falciparum* cytochrome bc_1. **h**, BRD7539 inhibited recombinant *P. falciparum* DHODH *in vitro* with an IC_{50} of 33 nM; no inhibition of the human orthologues was observed (data are mean ± s.d. for two biological and two technical replicates). **i–m**, BRD73842 targets and inhibits *P. falciparum* PI4K. BRD73842 showed excellent *in vitro* activity against asexual ($EC_{50} = 0.069\,\mu M$), late-sexual blood-stage ($EC_{50} = 0.643\,\mu M$) and liver-stage ($EC_{50} = 0.459\,\mu M$) parasites. **i**, **j**, The structure of BRD73842 indicates the required stereochemistry for activity (*R* stereoisomer). **k**, Initial characterization of BRD73842 showed good solubility and limited cytotoxicity. To gain insight into the mechanism of action of BRD73842, two resistant *P. falciparum* lines were evolved against BRD73842 from four independent cultures (a total of over 4×10^{9} inocula, see Extended Data Fig. 2a). After more than 3 months of drug pressure, the EC_{50} values increased approximately 10- to 20-fold. Two clones were obtained from each culture. Sequence analyses revealed that all clones contain non-synonymous SNVs in PF3D7_0509800, the locus that encodes *P. falciparum* PI4K (Supplementary Table 3). **l**, To confirm that PI4K is the molecular target of BRD73842, the compound was assayed against purified recombinant *P. vivax* PI4K protein. BRD73842 selectively inhibits the kinase activity of *P. vivax* PI4K ($IC_{50} = 21$ nM), but not human PI4K. *P. falciparum* PI4K has been identified as the molecular target of two recently described antimalarial compounds, KAI407 (ref. 20) and MMV048 (ref. 21).(data are mean ± s.d.; two biological and two technical replicates). **m**, The biphasic dose–response curve is a signature of *P. falciparum* PI4K inhibitors (data are mean ± s.d.; three biological and three technical replicates). The EC_{50} values reported in this study are derived from the first transition of the dose–response curves (indicated by arrow).

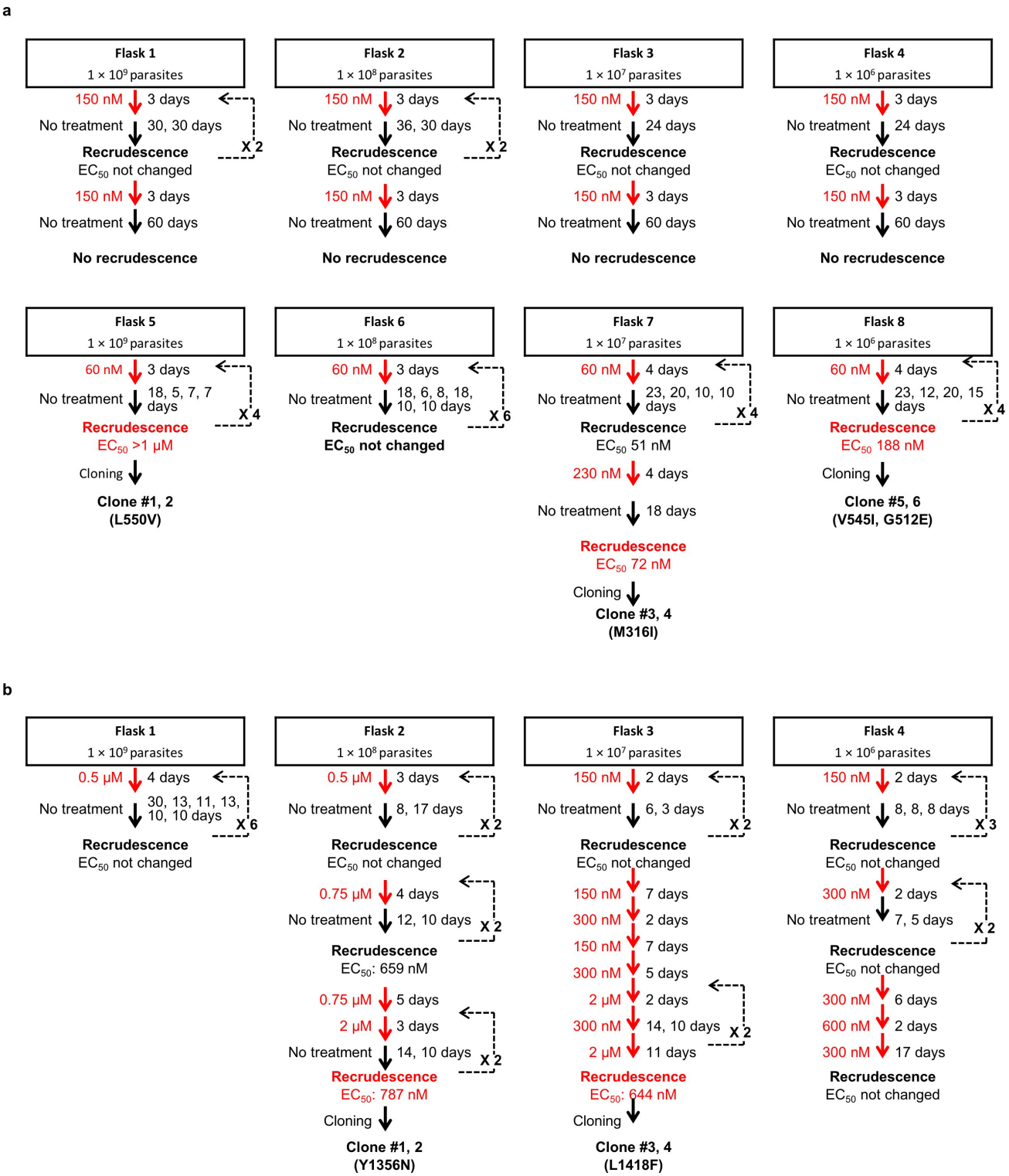

Extended Data Figure 2 | Resistance selection of BRD38427 and BRD1095. a, Over 3 months of intermittent and increasing resistance selection pressure of BRD73842 starting at 150 nM ($EC_{99.9}$) or 0.5 µM (10× EC_{50}) yielded two cultures showing a 13- to 16-fold EC_{50} shift. Two clonal lines from each culture were developed and subjected to whole-genome sequencing. **b**, Over 3 months of intermittent pressure of BRD1095 at 60 nM ($EC_{99.9}$) or 150 nM (10 × EC_{50}) yielded three cultures showing a 3- to 67-fold EC_{50} shift. Two clonal lines from each culture were developed and subjected to whole-genome sequencing.

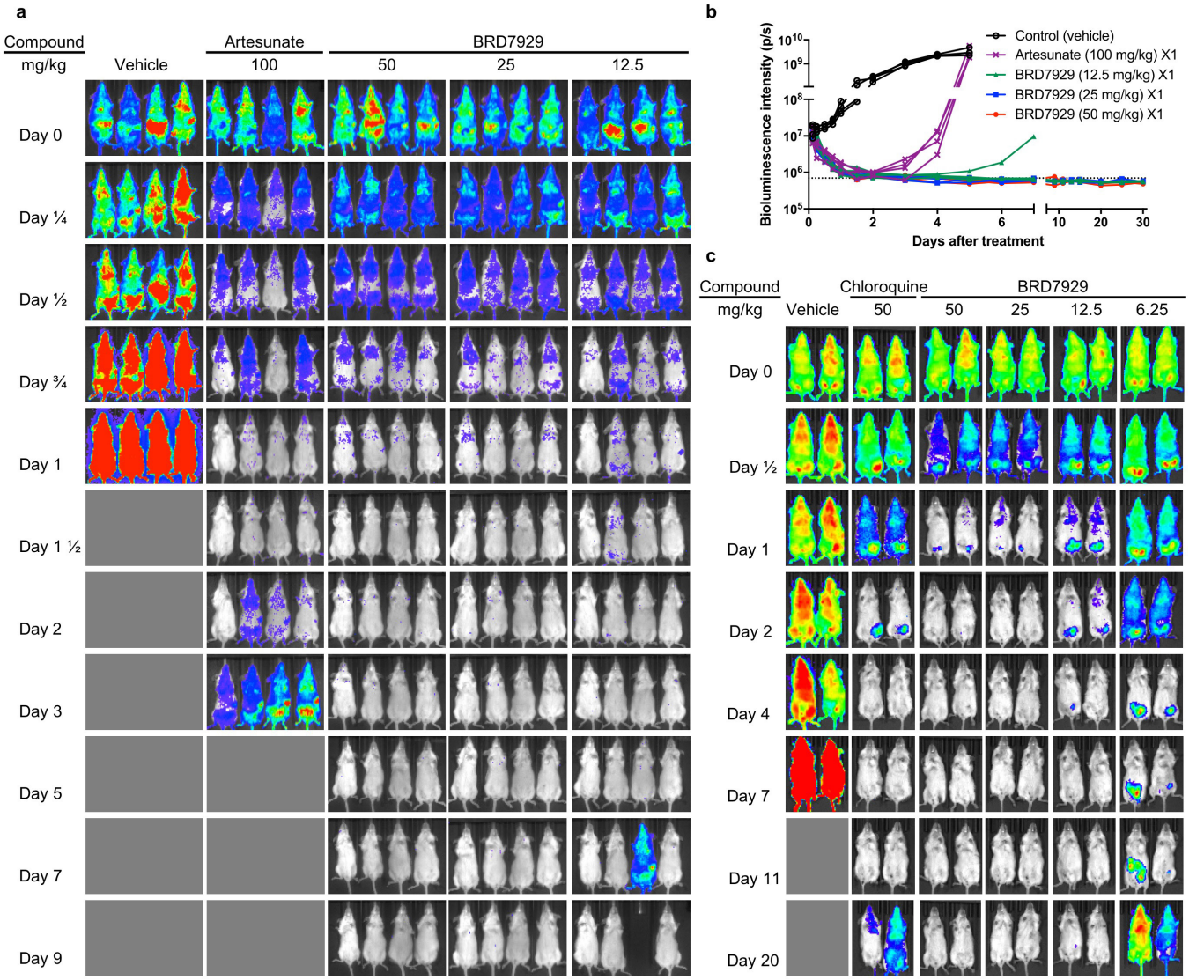

Extended Data Figure 3 | *In vivo* blood-stage efficacy study of BRD7929. a, BRD7929 shows single-dose *in vivo* efficacy in a *P. berghei* model of malaria. CD-1 mice were inoculated intravenously with approximately 2×10^7 *P. berghei* (ANKA GFP-luc) blood-stage parasites intravenously 24 h before treatment and BRD7929 was administered as a single 50, 25, or 12.5 mg kg^{-1} dose orally at 0 h ($n = 4$ for each group, this study was conducted once). Infections were monitored using IVIS. A single 100 mg kg^{-1} dose of artesunate results in rapid suppression of parasites, but owing to its short half-life, the parasites re-emerge very quickly. A single 25 mg kg^{-1} dose of BRD7929 resulted in 100% cure of the infected animals. One in four animals treated with a single oral dose of 12.5 mg kg^{-1} showed recrudescence at 6 days after treatment, but all other animals administered with 12.5 mg kg^{-1} were also completely parasite-free for 30 days. To ensure that no viable parasites remained, approximately 100 µl of combined blood samples from the four animals treated with 25 mg kg^{-1} of BRD7929 was intravenously injected into two naive mice and parasitaemia was monitored for an additional 30 days. No parasites were detected, suggesting that BRD7929 achieved a sterile cure for *P. berghei* with a single oral dose of as low as 25 mg kg^{-1}. The same colour scale is used for the all images; not all time-point images are shown here. **b**, Bioluminescent intensity was quantified from each mouse and plotted against time. The dotted horizontal line represents the mean bioluminescence intensity level obtained from all the animals before the parasite inoculation. **c**, BRD7929 shows single-dose *in vivo* efficacy in a *P. falciparum* huRBC NSG mouse blood-stage model. huRBC NSG mice were inoculated intravenously with approximately 1×10^7 *P. falciparum* 3D7$^{HLH/BRD}$ blood-stage parasites 48 h before treatment and BRD7929 was administered as a single 50, 25, 12.5 or 6.12 mg kg^{-1} dose orally at 0 h ($n = 2$ for each group, this study was conducted once). Infections were monitored using the IVIS. No recrudescence was observed at doses as low as a single 12.5 mg kg^{-1} of BRD7929 in the infected animals. To ensure that no viable parasites remained, approximately 350 µl of combined blood samples from the two animals treated with 12.5 mg kg^{-1} of BRD7929 was cultured *in vitro* and monitored for an additional 30 days. No parasites were detected, suggesting that BRD7929 achieved a sterile cure for *P. falciparum* 3D7$^{HLH/BRD}$ with a single oral dose as low as 12.5 mg kg^{-1} (see Fig. 4a). The same colour scale is used for the all images; not all time point images are shown. Images of mice treated with vehicle on days 11 and 20 are not shown, because the bioluminescent signal was too high to show in the same colour scale as other images.

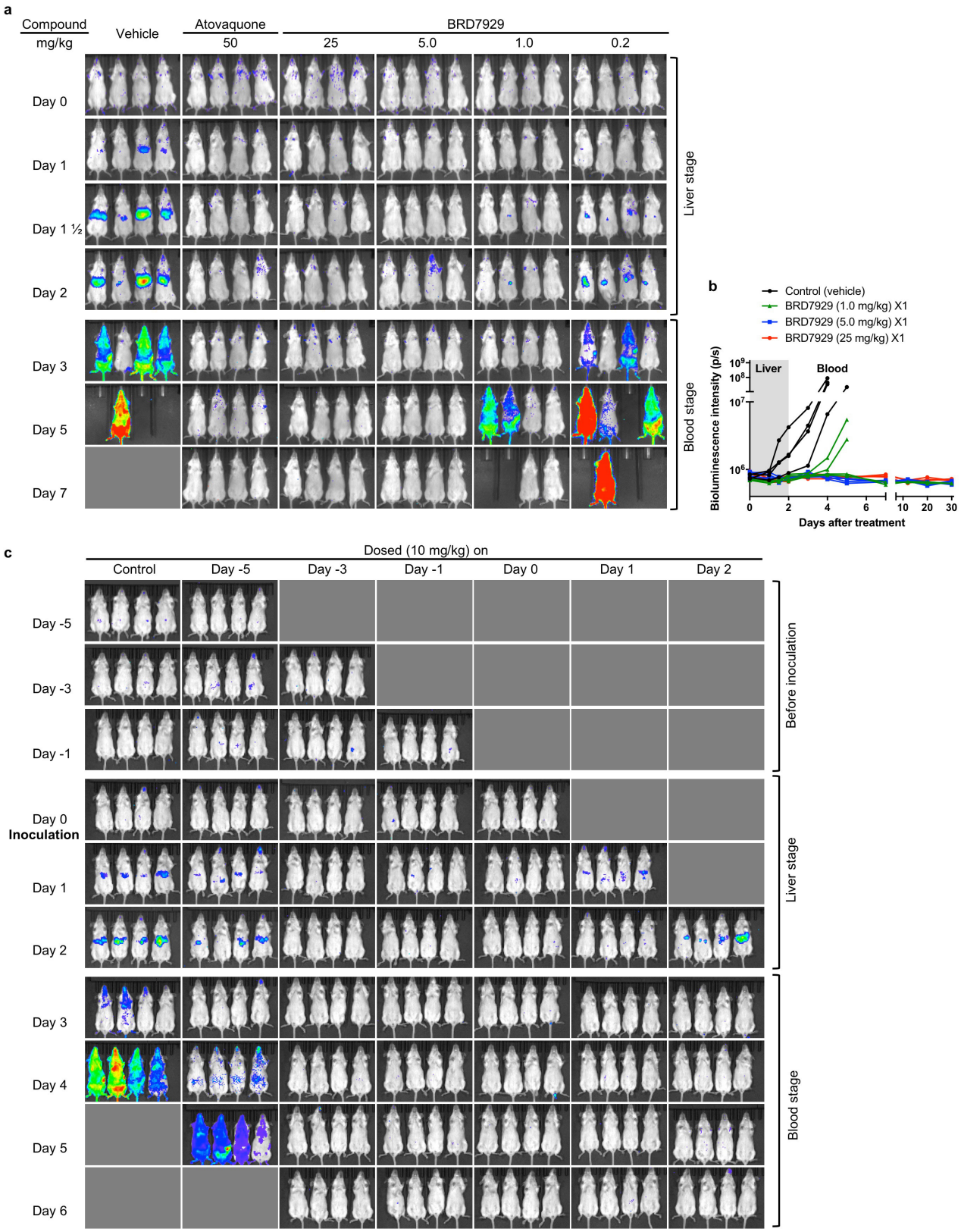

Extended Data Figure 4 | See next page for caption.

Extended Data Figure 4 | *In vivo* liver-stage efficacy study of BRD7929 in a mouse malaria model. a, BRD7929 shows single-dose causal prophylaxis in a *P. berghei* liver-stage model. CD-1 mice were inoculated intravenously with approximately 1×10^5 freshly dissected *P. berghei* ANKA luc-GFP sporozoites freshly dissected from *A. stephensi* salivary glands and immediately treated with a single oral dose of BRD7929 (25, 5, 1 or 0.2 mg kg^{-1}). Infections were monitored using IVIS; mice were monitored until day 30 to ensure complete cure. No recrudescence was observed at doses as low as a single 5 mg kg^{-1} of BRD7929 in the infected animals ($n = 4$ for each group, study conducted once). The same colour scale is used for the all images. Not all time point images are shown. **b**, Bioluminescent intensity was quantified from each mouse and plotted against time. **c**, BRD7929 shows single-dose causal prophylaxis in a *P. berghei* liver-stage model up to 3 days before infection and two days after infection. CD-1 mice were infected with *P. berghei* and infections were monitored as described in **a**. Single oral doses of BRD7929 (10 mg kg^{-1}) were administered at days 5, 3, and 1 before infection (days −5, −3 and −1), on day 0, and on days 1 and 2 after infection ($n = 4$ for each group, this study was conducted once). All dosing regimens except for the day −5 dose offered complete protection from infection for 32 days, indicating that BRD7929 has potent causal prophylaxis activity. The same colour scale is used for all images. Not all time-point images are shown.

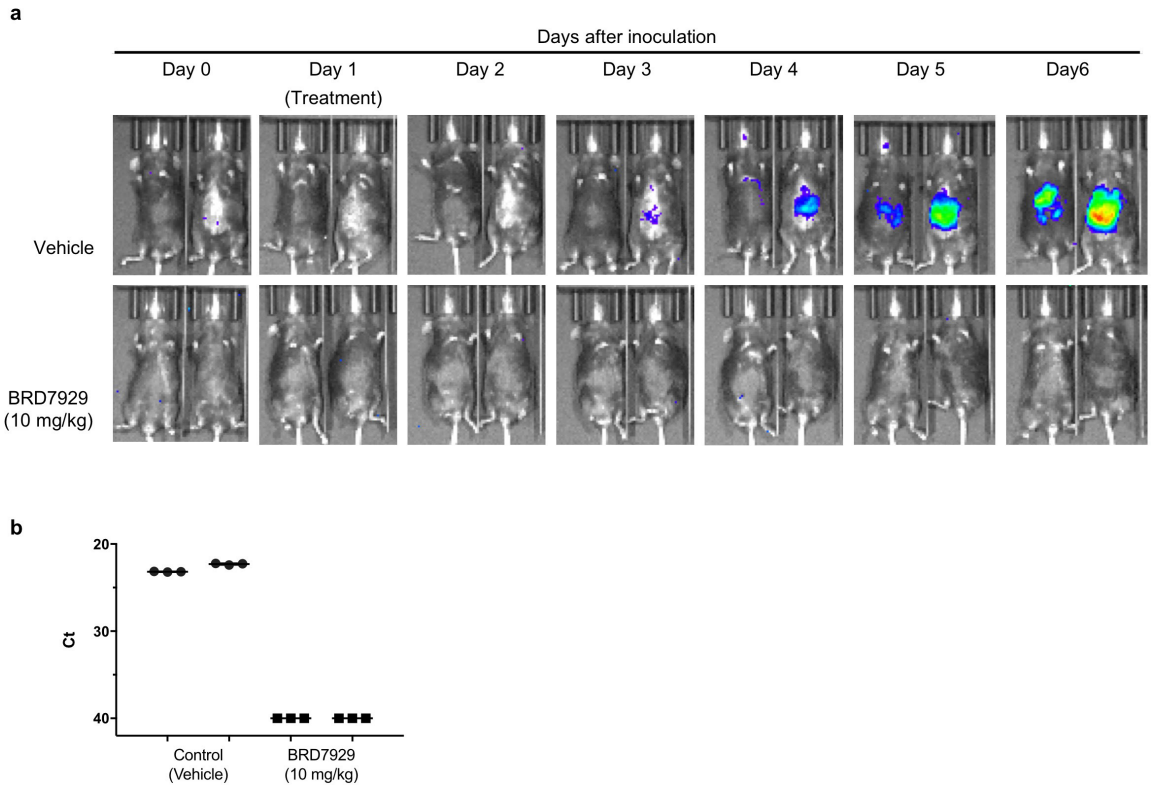

Extended Data Figure 5 | *In vivo* liver-stage efficacy study of BRD7929 in a humanized mouse model. a, BRD7929 shows single-dose *in vivo* efficacy in a *P. falciparum* huHep FRG-knockout mouse liver-stage model. huHep FRG knockout mice were inoculated intravenously with approximately 1×10^5 *P. falciparum* (NF54HT-GFP-luc) sporozoites and BRD7929 was administered as a single 10 mg kg^{-1} oral dose 1 day after inoculation ($n = 2$ for each group, this study was conducted once). Infections were monitored using IVIS. The same colour scale is used for all images. No increase in bioluminescence intensity level was observed from the mice treated with BRD7929 (see Fig. 4b). **b**, Blood samples were also collected from each mouse 7 days after inoculation (the first day of the blood stage) and analysed for the presence of the blood-stage transcripts PF3D7_0812600 (*P. falciparum* UCE) using qRT–PCR[32] (two biological replicates for each group and three technical replicates for each biological sample). Each dot represents a technical replicate of a sample and each horizontal line represents a mean of technical replicates from each mouse. The presence of the blood-stage parasite specific transcripts was detected from the control (vehicle) mice, while no amplification of the marker was detected after 40 amplification cycles (C_t value = 40) from the mice treated with BRD7929. Primer efficiency and sensitivity of the primer pairs for *P. falciparum* UCE have a detection limit ranging between 10 and 100 transcript copies[33]. Approximately 110 μl of combined blood samples from the two treated animals was also cultured *in vitro* and monitored for an additional 30 days but viable parasites were not detected.

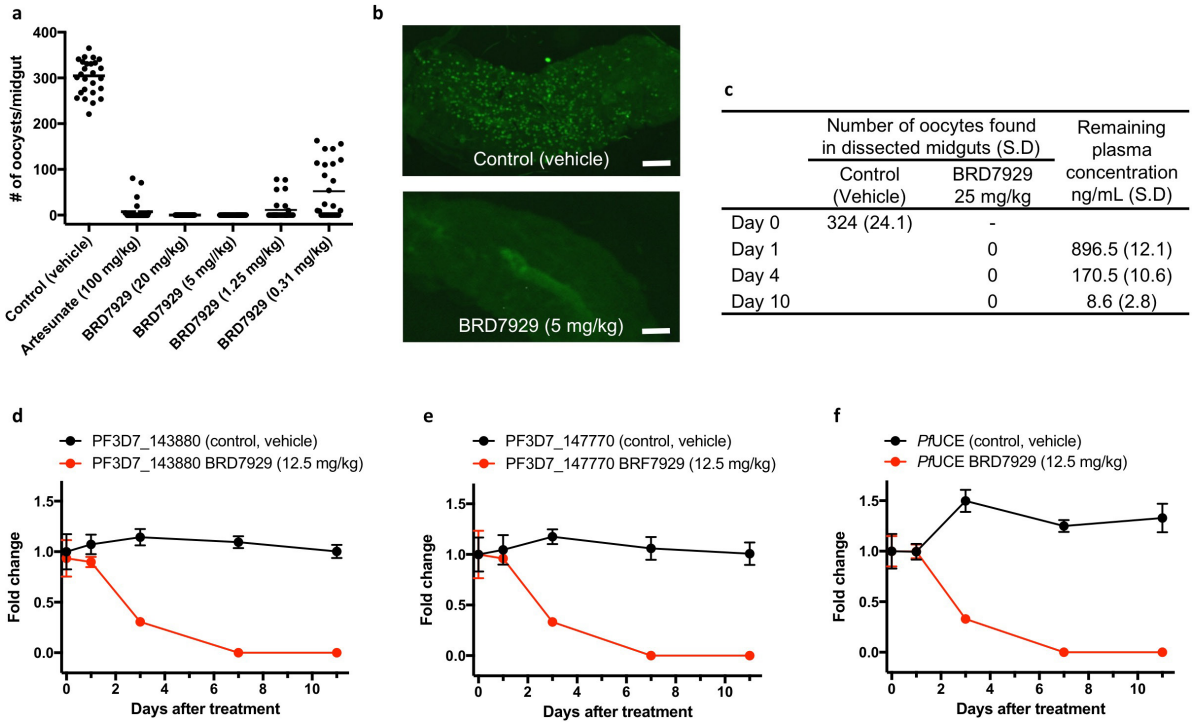

	Number of oocytes found in dissected midguts (S.D)		Remaining plasma concentration ng/mL (S.D)
	Control (Vehicle)	BRD7929 25 mg/kg	
Day 0	324 (24.1)	-	
Day 1		0	896.5 (12.1)
Day 4		0	170.5 (10.6)
Day 10		0	8.6 (2.8)

Extended Data Figure 6 | *In vivo* transmission-stage efficacy study of BRD7929. a, Oral doses of BRD7929 2 days before feeding mosquitoes upon infected mice resulted in complete blocking of transmission at 5 mg kg^{-1}, and reduced transmission activity at 1.25 mg kg^{-1} and 0.31 mg kg^{-1} ($n = 2$ for each group, this study was conducted once). **b**, Mosquitoes fed on vehicle-treated mice showed heavy infection 1 week after feeding, while mosquitoes fed on treated mice showed no or very few oocysts in the midguts. Representative images are shown; scale bars, 100 μm. **c**, To confirm that BRD7929 eliminates mature gametocytes in the host circulation rather than killing gametes, zygotes or ookinetes in the mosquito midgut, CD-1 mice infected with *P. berghei* (parasitaemia between 11 to 19%) were first treated with BRD7929 (oral, 25 mg kg^{-1}). Infected mice were then exposed to female *A. stephensi* mosquitoes for blood feeding 1, 4 or 10 days after the treatment. Blood samples were also obtained before the blood feedings to measure the plasma concentration of remaining BRD7929 ($n = 2$ for each group, this study was conducted once). No oocysts were found in midguts dissected from mosquitoes from all time points, whereas 896.5, 170.5 and 8.6 ng ml^{-1} of the compound remained in the circulation 1, 4 and 10 days after respectively treatment, respectively, suggesting that BRD7929 eliminated mature gametocytes in the mice. **d**–**f**, *In vivo* transmission-stage efficacy study of BRD7929 (humanized mouse model). huRBC NSG mice were infected with the blood-stage *P. falciparum* 3D7$^{HLH/BRD}$ for 2 weeks to allow the gametocytes to mature fully and were treated with a single oral dose of BRD7929 (12.5 mg kg^{-1}). $n = 2$ for each group, this study was conducted once. Blood samples collected from vehicle- and BRD7929-treated mice were tested for the presence of gametocyte-specific transcripts using mature gametocyte marker (PF3D7_1438800; **d**) and immature gametocyte marker (PF3D7_1477700; **e**). PF3D7_1120200 (*P. falciparum* UCE), a constitutively expressed gene, was used as a positive control marker for parasite detection (**f**). Data are mean ± s.d.; three technical replicates for each biological sample.

a

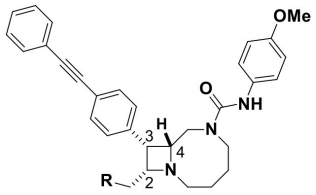

Compound		BRD3444	BRD1095	BRD7929	BRD3316
	R=	OH	NH_2	NMe_2	$O(CH_2)_2CO_2H$
HepG2; CC_{50} (μM)		> 50	16	9	> 50
A549; CC_{50} (μM)		18	10	6	> 50
HEK 293; CC_{50} (μM)		45	16	10	> 50
Phototoxicity 3T3 NRU[a]*		Non-phototoxic		Non-phototoxic	
Reversible CYP inhibition†; IC_{50} (μM)		> 10 (all)	4 (CYP1A)	> 10 (all)	> 10 (all)
Time-dependent CYP inhibition; k_{inact}/KI ($\mu M^{-1}L^{-1}min^{-1}$)‡		0.0158 (CYP3A)	negative (all)	negative (all)	negative (all)

b

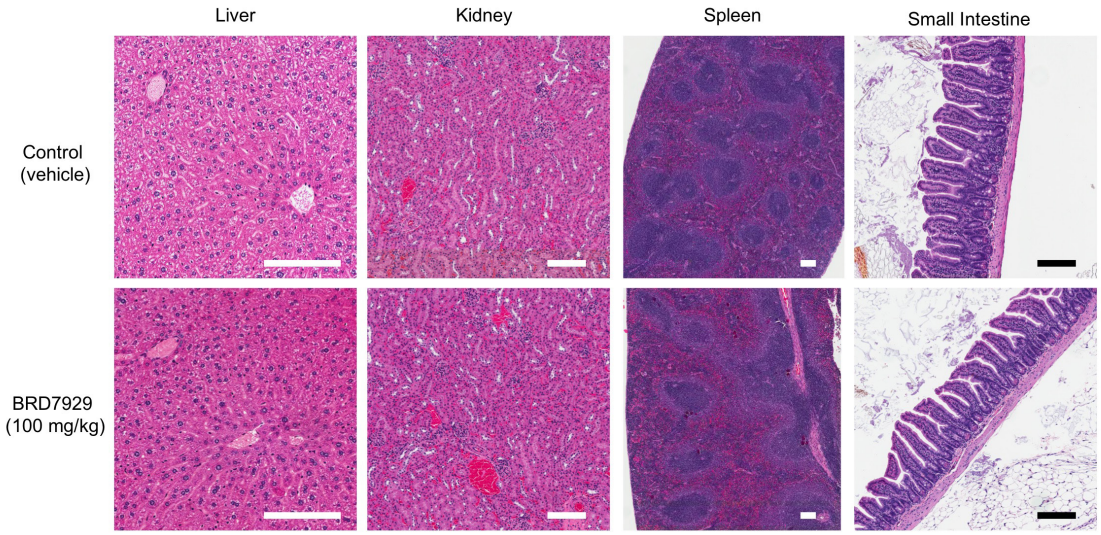

c

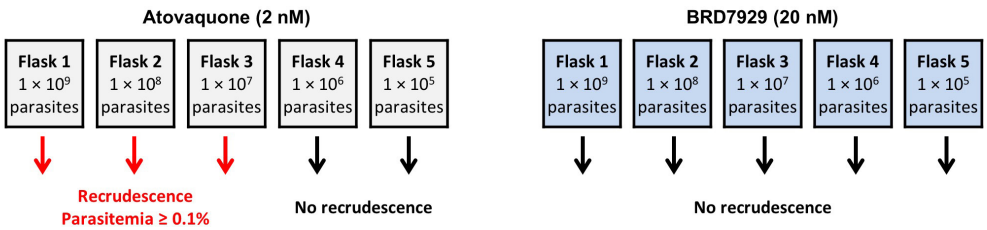

d

	First day for recrudescent parasitemia to reach ≥ 0.1%	
# of inoculum	Atovaquone	BRD7929
1×10^9	31	-
1×10^8	37	-
1×10^7	40	-
1×10^6	-	-
1×10^5	-	-

Extended Data Figure 7 | Safety and resistance propensity profiling of the bicyclic azetidine series. a, Results of *in vitro* cytotoxicity, phototoxicity and CYP inhibition assays. *Phototoxicity was assessed using the NIH 3T3 neutral red assay at Cyprotec; †CYP1A, CYP2C8, CYP2C9, CYP2C19, CYP2D6, CYP3A; ‡CYP1A, CYP2C9, CYP2D6, CYP3A. **b**, Histopathology analysis of mice treated with a high dose (100 mg kg^{-1}) of BRD7929. CD-1 mice were orally treated with 100 mg kg^{-1} BRD7929 and organs were collected 10 days after treatment. No significant tissue damage was detected. Representative images are shown here. Scale bars, 200 μm. **c**, **d**, Measurement of the minimal inoculum for resistance of BRD7929. Cultures containing various numbers of inoculum (1×10^5–1×10^9) were exposed to a constant level of drug pressure (EC_{90}). Parasites developed resistance to atovaquone at the lowest inoculum of 1×10^7 but not to BRD7929.

Extended Data Table 1 | *In vitro* potency of BRD3444, BRD7929 and BRD3316 against multiple parasite stages

Species (strain)	Stage	EC_{50} (μM)		
		BRD3444	BRD7929	BRD3316
P. falciparum (Dd2)	Blood	0.009	0.005	0.019
P. falciparum ($3D7^{HLH/BRD}$)	Blood		0.009	
P. falciparum (3D7)	Gametocyte (IV-V)	0.663	0.160	
P. falciparum (NF54)	Gametocyte (ID / D)*		0.270 / < 10	
P. falciparum (NF54)	Gametocyte (E / L) †	0.282 / 1.44		
P. falciparum (NF54)	Gamete formation (M / F) ‡	~1.00 / 0.804		
P. falciparum (NF54)	Liver	1.31	0.340	
P. berghei (ANKA)	Liver	0.140	0.162	
P. cynomolgi (M)	Liver (SF / LF) ¶	3.34 / 2.86	0.933 / 1.04	

*Data indicate the results of a standard membrane-feeding assay[71]. Indirect (ID) exposure refers to parasites treated with varying drug concentrations for 24 h before mosquito feeding, while direct (D) refers to parasites treated with a single drug concentration (10 μM) immediately before blood feeding.
†Activity against early- (E, stages I–III) and late- (L, stages IV–V) stage gametocytes was assessed according the protocol described previously[55].
‡Activity against male (M) and female (F) stage-V gametocytes was assessed in a dual gamete formation assay as described previously[71]. This assay (a standard membrane-feeding assay) is designed to determine the ability of compounds to either kill the mature *P. falciparum* male and female gametocytes directly or damage them in such a way that they cannot undergo onward development and form gametes in the mosquito midgut.
¶Activity against *P. cynomolgi* in primary rhesus hepatocytes was performed as described previously[72]. This assay measures inhibition of both the small form (SF, hypnozoite-like) and large form (LF, schizont) of intrahepatic *Plasmodium*.

Extended Data Table 2 | Structure–activity relationship study of the bicyclic azetidine series

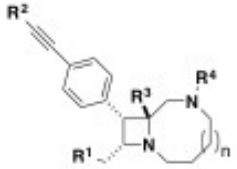

	*Pf*Dd2 EC_{50}(μM)	*Pfc*PheRS IC_{50}(μM)	R¹	R²	R³	R⁴	n
BRD8805	0.003	0.033	-NMe_2	-Ph	-H	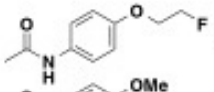	1
BRD7929	0.009	0.023	"	"	"	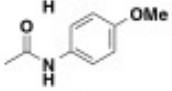	1
BRD1095	0.010	0.046	-NH_2	"	"	"	1
BRD3444	0.011	0.033	-OH	"	"	"	1
BRD3316	0.022	0.029	-$O(CH_2)_2CO_2H$	"	"	"	1
BRD4716	0.024	0.086	-NMe*i*Pr	"	"	"	1
BRD2132	0.048	0.179	-$NMe(CH_2)_2F$	"	"	"	1
BRD0185	0.087	0.097	-OH	"	"	"	2
BRD8493	0.116	0.162		"	"	"	1
BRD6479	0.158	0.233	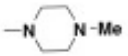	"	"	"	1
BRD4873	0.261	0.221	-OH	-2-CNPh	"	"	1
BRD9599	0.850	0.366	"	-Ph	"	"	0
BRD2936	1.87	29.4	"	"	-CH_2OH	"	1
BRD5349	8.32	30.9	"	"	-H	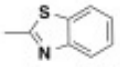	1
BRD5774	12.2	23.4	"		"	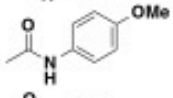	1
BRD8260	19.5	34.6	"	-Ph	"	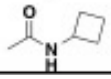	1

The structures of 16 bicyclic azetidine analogues with varying potency against asexual blood-stage parasites (Dd2), along with their corresponding inhibition of the *P. falciparum* PheRS activity in a biochemical assay. Aminoacylation inhibition activities were characterized using purified recombinant PheRS in which a range of inhibitor concentrations was used to determine IC_{50} values. The biochemically derived IC_{50} values correlate extremely well ($r^2 = 0.89$) with the EC_{50} determined using the blood-stage parasite growth-inhibition assay (see Fig. 3d).

Extended Data Table 3 | *In vitro* and *in vivo* pharmacokinetic properties of the bicyclic azetidine series

	BRD3444*	BRD1095*	BRD7929*	BRD7929†	BRD3316*
Pf, Dd2 EC_{50} (nM)	9	10	9		23
PBS solubility (μM)	< 1	25	15		91
Mouse Plasma protein binding (%)	99.9	99.3	99.9		
Mouse Cl_{int} (μL/min/mg)	248	< 20	21		38
Human Cl_{int} (μL/min/mg)	142	< 20	31		34
HepG2 CC_{50} (μM)	> 50	15.6	9		> 50
hERG IC_{50} (μM)	5.2	5.1	2.1		> 10

Route (mg/kg)	IV (3)	PO (10)	IV (3)	PO (10)	IV (2.5)	IV (2.5)‡	PO (10)	PO (3)	PO (9)	IV (3.2)	PO (13)
Cmax (μM)		0.6		0.6			0.54	0.21	0.6		6.8
Tmax (hr)		0.5		4			8	12	12		1
$T_{1/2}$ (hr)	3.7	3.2		28.8	N.C	32				2.3	2.4
$AUC_{0\text{-}t}$ (μM*hr)	1.2¶	4¶	7¶	11.7¶	3.5¶	9#	11¶	6.4¶	19.7¶	13..2¶	33.5¶
$AUC_{0\text{-}inf}$ (μM*hr)	1.4	4	14.9			11.2		7.2	22.6	13.2	33.5
$MRT_{0\text{-}inf}$ (hr)	2.8		39.2		40.5	45		35.4	37.8	3.3	3.9
Vss (L/kg)	12		16		24	19				1.4	
F (%)	86		50				79.5§				63
CL (mL/min/kg)	72		6.7		9.9	7.1				7.1	

BRD3444 and BRD1095 were formulated in 70% PEG400 and 30% aqueous glucose (5% in H_2O) for intravenous and oral dosing and pharmacokinetics were determined in CD-1 mice as described in Methods. Pharmacokinetic studies of BRD3444 and BRD1095 were performed by ChemPartner Co., Ltd and were estimated by a non-compartmental model using WinNonlin 6.2. BRD7929 and BRD3316 were formulated in 10% ethanol, 4% Tween, 86% saline for both intravenous and oral dosing. Pharmacokinetics in *P. falciparum* $3D7^{HLH/BRD}$-infected NSG mice was determined on dried blood spot samples from infected NSG mice using standard methods. Pharmacokinetics parameters for BRD7929 and BRD3316 were estimated by a non-compartmental model using proprietary Eisai software. Cl_{int}, intrinsic clearance; CL, clearance; MRT, mean resistance time; N.C, not calculated owing to insufficient data; V_{ss}, steady-state volume of distribution.

*Pharmacokinetic in CD-1 mice.

†Pharmacokinetic in *P. falciparum* $3D7^{HLH/BRD}$-infected NSG mice.

‡Intravenously determined in a separate assay over 72 h to determine half-life.

¶$t = 24$ h.

#$t = 72$ h.

§Per cent value based on initial intravenous study at 24 h.

doi:10.1038/nature19804

Diversity synthesis yields novel multistage antimalarial inhibitors

Nobutaka Kato[1]*, Eamon Comer[1]*, Tomoyo Sakata-Kato[2], Arvind Sharma[3], Manmohan Sharma[3], Micah Maetani[1,4], Jessica Bastien[1], Nicolas M. Brancucci[2], Joshua A. Bittker[1], Victoria Corey[5], David Clarke[2], Emily R. Derbyshire[1,6,7], Gillian Dornan[8], Sandra Duffy[9], Sean Eckley[10], Maurice A, Itoe[2], Karin MJ Koolen[11], Timothy A. Lewis[1], Ping S. Lui[2], Amanda K. Lukens[1,2], Emily Lund[2], Sandra March[1,12], Elamaran Meibalan[2], Bennett C. Meier[1,4], Jacob McPhail[8], Branko Mitasev[10], Eli L. Moss[1], Morgane Sayes[1], Yvonne VanGessel[10], Mathias J. Wawer[1], Takashi Yoshinaga[13], Anne-Marie Zeeman[14], Vicky M. Avery[9], Sangeeta N. Bhatia[1,12], John E. Burke[8], Flaminia Catteruccia[2], Jon C. Clardy[1,6], Paul A. Clemons[1], Koen J. Dechering[11], Jeremy R. Duvall[1], Michael A. Foley[1], Fabian Gusovsky[10], Clemens H. M. Kocken[14], Matthias Marti[2], Marshall L. Morningstar[1], Benito Munoz[1], Daniel E. Neafsey[1], Amit Sharma[3], Elizabeth A. Winzeler[5], Dyann F. Wirth[1,2], Christina A. Scherer[1], Stuart L. Schreiber[1,4§]

*These authors contributed equally
§Corresponding author

[1]Broad Institute of Harvard and MIT, 415 Main Street, Cambridge, MA 02142, USA
[2]Harvard T.H. Chan School of Public Health, 665 Huntington Avenue Boston, MA 02115, USA
[3]Molecular Medicine Group, International Centre for Genetic Engineering and Biotechnology, Aruna Asaf Ali Road, New Delhi, 110067
[4]Department of Chemistry and Chemical Biology, Harvard University, 12 Oxford Street, Cambridge, MA 02138, USA
[5]School of Medicine, University of California San Diego, 9500 Gilman Drive 0760 La Jolla, CA 92093, USA
[6]Department of Biological Chemistry and Molecular Pharmacology, Harvard Medical School, 240 Longwood Avenue, Boston, MA 02115, USA
[7]Department of Chemistry and Department of Molecular Genetics and Microbiology, Duke University, 124 Science Drive, Durham, NC 27708, USA
[8]Department of Biochemistry and Microbiology, University of Victoria, 270 Petch Hall, Victoria BC, V8P 5C2, Canada
[9]Eskitis Institute for Drug Discovery, Griffith University, Nathan Campus, Griffith University, Queensland 4111, Australia
[10]Eisai Inc., 4 Corporate Drive, Andover, MA 01810, USA
[11]TropIQ Health Sciences, Geert Grooteplein 28, Huispost 268, 6525 GA Nijmegen, The Netherlands
[12]Department of Electrical Engineering and Computer Science, Massachusetts Institute of Technology, 500 Main Street, Cambridge, MA 02142, USA
[13]Eisai Co., Ltd, 5-1-3 Tokodai Tsukuba, Ibaraki 300-2635, Japan
[14]Department of Parasitology, Biochemical Primate Research Centre, 2280 GH Rijswijk, The Netherlands

Author Contributions

Author	Institution	role(S)
Vicky M. Avery	Eskitis Institute for Drug Discovery, Griffith University	*in vitro P. falciparum* gametocyte imaging assays
Jessica Bastien	The Broad Institute of Harvard and MIT	Preparation of analogues
Sangeeta N. Bhatia	Department of Electrical Engineering and Computer Science, Massachusetts Institute of Technology The Broad Institute of Harvard and MIT	supervising *in vitro P. falciparum* liver-stage assay
Joshua A. Bittker	The Broad Institute of Harvard and MIT	designing the Malaria Therapeutics Response Portal
Nicolas M. Brancucci	Department of Immunology and Infectious Diseases, Harvard T. H. Chan School of Public Health	*in vivo P. falciparum* transmission blocking assay analysis
John E. Burke	Department of Biochemistry and Microbiology, University of Victoria	supervising (PI4K) recombinant protein generation, *in vitro* biochemical assays
Flaminia Catteruccia	Department of Immunology and Infectious Diseases, Harvard T. H. Chan School of Public Health	supervising mosquito maintenance, sporozoite generation, midgut dissection
Jon C. Clardy	The Broad Institute of Harvard and MIT Department of biological chemistry and molecular pharmacology, Harvard Medical School	supervising *P. berghei* sporozoite generation
David Clarke	Department of Immunology and Infectious Diseases, Harvard T. H. Chan School of Public Health	mosquito maintenance, *P. berghei* sporozoite generation
Paul A. Clemons	The Broad Institute of Harvard and MIT	cheminformatics analysis and visualization
Eamon Comer	The Broad Institute of Harvard and MIT	lead chemist
Victoria Corey	School of Medicine, University of California San Diego	target identification, whole genome sequencing & analysis
Koen J. Dechering	TropIQ Health Sciences	*P. falciparum* SMFA assay
Emily R. Derbyshire	The Broad Institute of Harvard and MIT Department of biological chemistry and molecular pharmacology, Harvard Medical School Department of Chemistry and Department of Molecular Genetics and Microbiology, Duke University	*P. berghei* sporozoite generation
Gillian Dornan	Department of Biochemistry and Microbiology, University of Victoria	(PI4K) recombinant protein generation, *in vitro* biochemical assays
Sandra Duffy	Eskitis Institute for Drug Discovery, Griffith University	*in vitro P. falciparum* gametocyte imaging assays
Jeremy R. Duvall	The Broad Institute of Harvard and MIT	supervising chemistry at Broad
Sean Eckley	Eisai Inc.	*in vitro* & *in vivo* PK
Michael A. Foley	The Broad Institute of Harvard and MIT	supervising chemistry at Broad
Fabian Gusovsky	Eisai Inc.	project manager
Maurice A. Itoe	Department of Immunology and Infectious Diseases, Harvard T. H. Chan School of Public Health	*P. falciparum* sporozoite generation
Nobutaka Kato	The Broad Institute of Harvard and MIT	lead biologist
Clemens H. Kocken	Department of Parasitology, Biochemical Primate Research Centre	supervising *in vitro P. cynomolgi* assay
Karin MJ Koolen	TropIQ Health Sciences	*P. falciparum* SMFA assay
Timothy A. Lewis	The Broad Institute of Harvard and MIT	Preparation of analogues
Ping S. Lui	Department of Immunology and Infectious Diseases, Harvard T. H. Chan School of Public Health	*P. falciparum* sporozoite generation
Amanda K. Lukens	Department of Immunology and Infectious Diseases, Harvard T. H. Chan School of Public Health	generating resistance strains
Emily Lund	Department of Immunology and Infectious Diseases, Harvard T. H. Chan School of Public Health	mosquito maintenance, *P. berghei* sporozoite generation, midgut dissection
Micah Maetani	The Broad Institute of Harvard and MIT Department of Chemistry and Chemical Biology, Harvard University	*Pf*DHODH biochemical assay
Sandra March	Department of Electrical Engineering and Computer Science, Massachusetts Institute of Technology The Broad Institute of Harvard and MIT	*in vitro P. falciparum* liver-stage assay
Matthias Marti	Department of Immunology and Infectious Diseases, Harvard T. H. Chan School of Public Health	supervising *in vivo P. falciparum* transmission stage assay analysis
Jacob McPhail	Department of Biochemistry and Microbiology, University of Victoria	(PI4K) recombinant protein generation, *in vitro* biochemical assays
Elamaran Meibalan	Department of Immunology and Infectious Diseases, Harvard T. H. Chan School of Public Health	*in vivo P. falciparum* blood-stage *and* transmission blocking assay analysis
Bennett C. Meier	The Broad Institute of Harvard and MIT Department of Chemistry and Chemical Biology, Harvard University	development of the Malaria Therapeutics Response Portal
Branko Mitasev	Eisai Inc.	process chemistry
Marshall L. Morningstar	The Broad Institute of Harvard and MIT	supervising chemistry at Broad
Eli L. Moss	The Broad Institute of Harvard and MIT	target identification, whole genome sequencing & analysis
Benito Munoz	The Broad Institute of Harvard and MIT	supervising chemistry at Broad
Daniel E. Neafsey	The Broad Institute of Harvard and MIT	supervising target identification, whole genome sequencing & analysis
Tomoyo Sakata-Kato	Department of Immunology and Infectious Diseases, Harvard T. H. Chan School of Public Health	target identification, generating resistance strains
Morgane Sayes	The Broad Institute of Harvard and MIT	Preparation of analogues
Christina A. Scherer	The Broad Institute of Harvard and MIT	project manager
Stuart L. Schreiber	The Broad Institute of Harvard and MIT Department of Chemistry and Chemical Biology, Harvard University	principal investigator
Amit Sharma	International Centre for Genetic Engineering and Biotechnology	supervising *Pfc*PheRS recombinant protein generation, in vitro biochemical assays
Arvind Sharma	International Centre for Genetic Engineering and Biotechnology	*Pfc*PheRS recombinant protein generation, in vitro biochemical assays
Manmohan Sharma	International Centre for Genetic Engineering and Biotechnology	*Pfc*PheRS recombinant protein generation, in vitro biochemical assays
Yvonne VanGess	Eisai Inc.	*in vivo* safety profiling
Mathias J. Wawer	The Broad Institute of Harvard and MIT	cheminformatics analysis and visualization
Elizabeth A. Winzeler	School of Medicine, University of California San Diego	supervising target identification, whole genome sequencing & analysis
Dyann F. Wirth	The Broad Institute of Harvard and MIT Department of Immunology and Infectious Diseases, Harvard T. H. Chan School of Public Health	supervising target identification, generating resistance strains
Takashi Yoshinaga	Eisai Inc.	*in vitro* safety profiling
Anne-Marie Zeeman	Department of Parasitology, Biochemical Primate Research Centre	*in vitro P. cynomolgi* assay

Supplementary Methods

Chemical Synthesis and Analytical Data

Abbreviations

DCM	dichloromethane
DMF	dimethylformamide
DMSO	dimethylsulphoxide
EtOAc	ethyl acetate
HPLC	high performance liquid chromatography
MeOH	methanol
PBS	phosphate buffered saline
THF	tetrahydrofuran
TFA	trifluoroacetic acid
TLC	thin layer chromatography
UPLC	ultra performance liquid chromatography
XPhos Pd G3	(2-Dicyclohexylphosphino-2′,4′,6′-triisopropyl-1,1′-biphenyl)[2-(2′-amino-1,1′-biphenyl)]palladium(II) methanesulfonate

Chemical Synthesis of BRD3444, BRD1095, BRD3316 and BRD7929

All compounds screened in this study are derived from a synthetic process performed at the Broad institute based on the principles of diversity-oriented synthesis. The electronic descriptions of these compounds using SMILES descriptors have been deposited in the public database PubChem (https://pubchem.ncbi.nlm.nih.gov/). These include the primary screening hits, which include BRD3444, BRD73842, BRD0026 and BRD7539. All reactions were carried out under N_2 or argon atmosphere. All reagents and solvents were purchased from commercial vendors and used as received, or synthesized according to the footnoted references. NMR spectra were recorded on a Bruker 300 (300 MHz ^{1}H, 75 MHz ^{13}C), Bruker 400 (400 MHz ^{1}H, 100 MHz ^{13}C), and Varian 400 (400 MHz ^{1}H, 100 MHz ^{13}C) spectrometer. Proton chemical shifts are reported in ppm (δ) referenced to the NMR solvent[74]. Data are reported as follows: chemical shifts, multiplicity (br = broad, s = singlet, d = doublet, t = triplet, q = quartet, p = pentet, m = multiplet; coupling constant(s) in Hz; integration). Unless otherwise indicated NMR data were collected at 25°C. Flash chromatography was performed using 40-60 μm Silica Gel (60 Å mesh) on a Teledyne Isco Combiflash Rf. For purity analysis one of two general methods was used. For method one, purity was measured by LC-MS on a Waters 2795 separations module by UV absorbance at 210 nm and identity was determined on a SQ mass spectrometer by positive electrospray ionization. Mobile phase A consisted of 0.01% formic acid in water, while mobile phase B consisted of 0.01% formic acid in acetonitrile. The gradient ran from 5% to 95% mobile phase B over 2.5, 5 or 7.5 minutes at 1.75 mL/min. An Agilent Poroshell 120 EC-C18, 2.7 um, 3.0x30 mm column was used with column temperature maintained at 40°C. For method two, purity was measured by LC-MS on an Agilent 1200 separations module by UV absorbance at 220 nm and identity was determined on a 6120 mass spectrometer by positive electrospray ionization. Mobile phase A consisted of 0.037% trifluoroacetic acid in water, while mobile phase B consisted of 0.018% trifluoroacetic acid in acetonitrile. The gradient ran from 10% to 100% mobile phase B over 4.5 minutes at 0.8 mL/min. A Luna-C18(2), 5 um, 2.0x50 mm column was used with column temperature maintained at 40°C. Analytical TLC was performed on EM Reagent 0.25 mm silica gel 60-F plates. Visualization was accomplished with UV light and aqueous potassium permanganate ($KMnO_4$) stain followed by heating. Accurate mass measurements were obtained on an Agilent 6230 Time-of-Flight mass spectrometer as the $(M+H)^+$. Compound purity and identity were also determined by UPLC-MS. Purity was measured by UV absorbance at 210 nm. Identity was determined on a SQ mass spectrometer by positive and negative electrospray ionization. Mobile phase A consisted of either 0.1% ammonium hydroxide or 0.05% trifluoroacetic acid in water, while

mobile phase B consisted of either 0.1% ammonium hydroxide or 0.06% trifluoroacetic acid in acetonitrile. The gradient ran from 5% to 95% mobile phase B over 2.65 min at 0.9 mL/min. An Acquity BEH C18, 1.7 µm, 2.1x50 mm column was used with column temperature maintained at 65°C. Compounds were dissolved in DMSO at a nominal concentration of 1 mg/mL, and 1.0 uL of this solution was injected. Chiral separations were performed by SFC-MS. A Berger G600 supercritical fluid chromatograph was coupled with a Waters ZQ single quadrupole mass spectrometer operating in positive APCI mode. Using liquefied CO_2 modified with 20% isopropanol, an isocratic separation was performed for 5.0 minutes at 4.0 mL/min on a 4.6x100 mm Chiralpak AD-H column maintained at 40°C. Compounds were dissolved in methanol at a nominal concentration of 1 mg/mL, and 10 µL of this solution was injected.

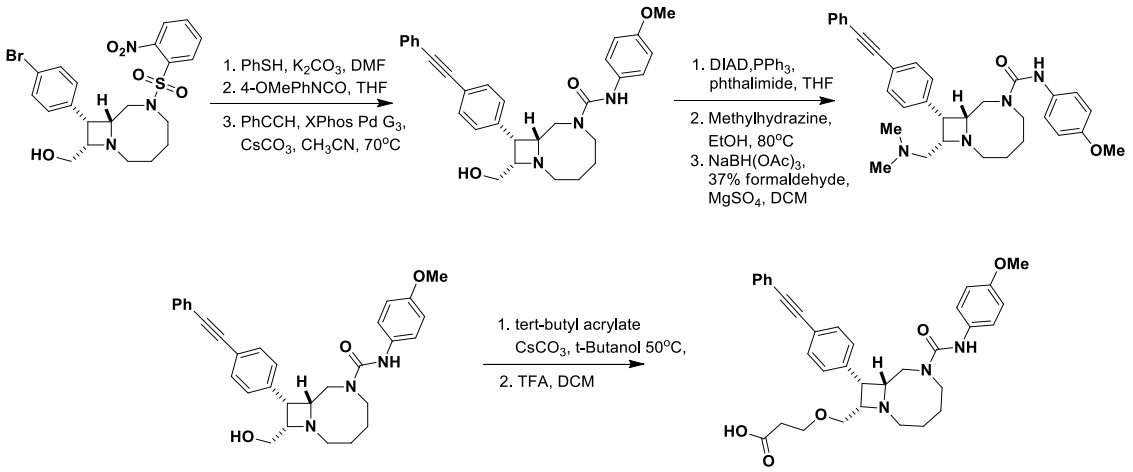

Scheme 1. Synthetic route to BRD3444, BRD1095, BRD3316 and BRD7929

(8R,9R,10S)-9-(4-bromophenyl)-10-(hydroxymethyl)-N-(4-methoxyphenyl)-1,6-diazabicyclo[6.2.0]decane-6-carboxamide

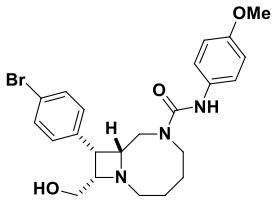

To a solution of ((8R,9R,10S)-9-(4-bromophenyl)-6-((2-nitrophenyl)sulfonyl)-1,6-diazabicyclo[6.2.0]decan-10-yl)methanol (715 mg, 1.401 mmol) (prepared according to the method of Lowe *et al.*[37]) in DMF (7 mL) was added potassium carbonate (1.96 g, 14.01 mmol) and thiophenol (0.721 mL, 7.00 mmol) at room temperature. The reaction was stirred for 16 hours. The reaction was diluted with water and extracted with EtOAc. The organic phase was separated, dried (Na_2SO_4), filtered and concentrated. The crude material was dissolved in DCM and passed over a plug of acidic resin (10 g of 0.76 mmol/g, Si-Tosic acid; Silicycle) and rinsed first with DCM and then with 1M NH_3 in MeOH to afford ((8R,9R,10S)-9-(4-bromophenyl)-1,6-diazabicyclo[6.2.0]decan-10-yl)methanol that was carried onto the subsequent step without further purification. This crude material was dissolved in THF (14 mL). To this solution was added 4-methoxyphenylisocyanate (0.173 mL, 1.332 mmol) in 6 portions over a 2 hours period and the resulting solution was stirred for 16 hours at room temperature. The reaction was concentrated and purified by flash column chromatography and eluting with DCM/MeOH to give the desired compound as a white solid (513 mg, Yield: 77%). ^{1}H NMR (300 MHz, $CDCl_3$) δ 7.46–7.40 (m, 2H), 7.39–7.32 (m, 2H), 7.30–7.20 (m, 2H), 6.90–6.75 (m, 2H), 6.11 (s, 1H), 3.90–3.78 (m, 1H), 3.77 (s, 3H), 3.69–3.54 (m, 5H), 3.54–3.39 (m, 1H), 3.37–3.20 (m, 1H),

3.11–2.93 (m, 1H), 2.91–2.75 (m, 1H), 2.54–2.35 (m, 1H), 1.91–1.71 (m, 2H), 1.72–1.54 (m, 2H). Purity by LCMS (UV Chromatogram, 210nm, 5 min run) 97% by UV, rt = 1.33 min, m/z 474 $(M+H)^+$.

(8R,9R,10S)-10-(hydroxymethyl)-N-(4-methoxyphenyl)-9-(4-(phenylethynyl)phenyl)-1,6-diazabicyclo[6.2.0]decane-6-carboxamide (BRD3444)

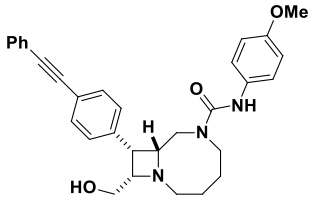

To a solution of (8R,9R,10S)-9-(4-bromophenyl)-10-(hydroxymethyl)-N-(4-methoxyphenyl)-1,6-diazabicyclo[6.2.0]decane-6-carboxamide (326 mg, 0.687 mmol) in degassed acetonitrile (4.6 mL) was added ethynylbenzene (226 µL, 2.062 mmol) and XPhos Pd G3 (58.1 mg, 0.069 mmol). Cesium carbonate (896 mg, 2.75 mmol) was added to the reaction and then heated at 70°C for 1.5 hours. The reaction was cooled to room temperature, diluted with EtOAc and washed with water and brine. The organic phase was separated, dried (Na_2SO_4), filtered and concentrated. The crude material was purified by flash column chromatography eluting with DCM/MeOH to give the desired compound (238 mg, Yield: 78%). ^1H NMR (300 MHz, $CDCl_3$) δ 7.55–7.33 (m, 6H), 7.34–7.22 (m, 3H), 7.22–7.15 (m, 2H), 6.81–6.69 (m, 2H), 6.00 (s, 1H), 3.83–3.73 (m, 1H), 3.70 (s, 3H), 3.65–3.50 (m, 4H), 3.46-3.37 (m, 2H), 3.31 – 3.19 (m, 1H), 3.01–2.91 (m, 1H), 2.88–2.76 (m, 1H), 2.44–2.33 (m, 1H), 1.81–1.68 (m, 3H), 1.64–1.54 (m, 1H). Purity by LCMS (UV Chromatogram, 210nm, 2.5 min run) 99% by UV, rt = 0.87 min, m/z 496 $(M+H)^+$. HRMS (ESI) calcd for $C_{31}H_{33}N_3O_3$ $[M+H]^+$: 496.2600. Found: 496.2604.

tert-butyl 3-(((8R,9R,10S)-6-((4-methoxyphenyl)carbamoyl)-9-(4-(phenylethynyl)phenyl)-1,6-diazabicyclo[6.2.0]decan-10-yl)methoxy)propanoate

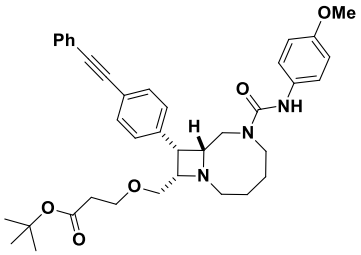

To a solution of (8R,9R,10S)-10-(hydroxymethyl)-N-(4-methoxyphenyl)-9-(4-(phenylethynyl)phenyl)-1,6-diazabicyclo[6.2.0]decane-6-carboxamide (50 mg, 0.101 mmol) in tert-butanol (504 µL) were added tert-butyl acrylate (588 µl, 4.04 mmol) and cesium carbonate (65.7 mg, 0.202 mmol). The solution was stirred at 50°C for 18 hours upon which further cesium carbonate (16 mg, 0.049 mmol) was added. After 23 hours the solution was cooled and extracted with EtOAc and saturated ammonium chloride. The organic layer was dried with $NaSO_4$, filtered and concentrated. The crude material was purified by flash column chromatography eluting with EtOAc/Hexanes to give the desired compound (61 mg, Yield: 97%). ^1H NMR (400 MHz, $CDCl_3$) δ 7.59–7.52 (m, 2H), 7.52–7.44 (m, 3H), 7.41–7.33 (m, 3H), 7.32–7.22 (m, 3H), 6.85 (d, J = 8.4 Hz, 2H), 6.10 (s, 1H), 3.93–3.82 (m, 1H), 3.79 (s, 3H), 3.71–3.38 (m, 7H), 3.37–3.24 (m, 2H), 3.16–3.03 (m, 1H), 2.97–2.85 (m, 1H), 2.44–2.28 (m, 2H), 1.94–1.75 (m, 3H), 1.71–1.59 (m, 2H), 1.44 (s, 9H). Purity by LCMS (UV Chromatogram, 210nm, 2.5 min run) 97% by UV, rt = 1.44 min, m/z 624 $(M+H)^+$.

3-(((8R,9R,10S)-6-((4-methoxyphenyl)carbamoyl)-9-(4-(phenylethynyl)phenyl)-1,6-diazabicyclo[6.2.0]decan-10-yl)methoxy)propanoic acid (BRD3316)

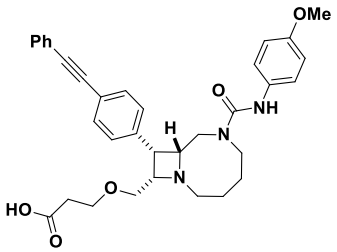

To a solution of tert-butyl 3-(((8R,9R,10S)-6-((4-methoxyphenyl)carbamoyl)-9-(4-(phenylethynyl)phenyl)-1,6-diazabicyclo[6.2.0]decan-10-yl)methoxy)propanoate (31mg, 0.050 mmol) in DCM (1988 µL) was added trifluoroacetic acid (153 µl, 1.988 mmol). The reaction was stirred at room temperature for 19 hours. The reaction was concentrated and the crude material was purified by flash column chromatography eluting with DCM/MeOH to give the desired compound (28 mg, Yield: 99%). ^{1}H NMR (400 MHz, $CDCl_3$) δ 7.72–7.47 (m, 4H), 7.43–7.33 (m, 2H), 7.31–7.20 (m, 5H), 6.85 (d, J = 8.6 Hz, 2H), 6.39 (s, 1H), 4.56–4.35 (m, 1H), 4.36–4.21 (m, 1H), 4.23–4.07 (m, 1H), 4.03–3.82 (m, 3H), 3.79 (s, 3H), 3.71–3.44 (m, 5H), 3.41–3.27 (m, 1H), 3.02–2.80 (m, 1H), 2.78–2.59 (m, 1H), 2.59–2.40 (m, 1H), 2.24–2.10 (m, 1H), 2.10–1.97 (m, 1H), 1.97–1.85 (m, 1H), 1.85–1.68 (m, 1H). Purity by LCMS (UV Chromatogram, 210nm, 7 min run) 99% by UV, rt = 2.65 min, m/z 568 $(M+H)^+$. HRMS (ESI) calcd for $C_{34}H_{37}N_3O_5$ $[M+H]^+$: 568.2811. Found: 568.2818.

(8R,9S,10S)-10-((1,3-dioxoisoindolin-2-yl)methyl)-N-(4-methoxyphenyl)-9-(4-(phenylethynyl)phenyl)-1,6-diazabicyclo[6.2.0]decane-6-carboxamide

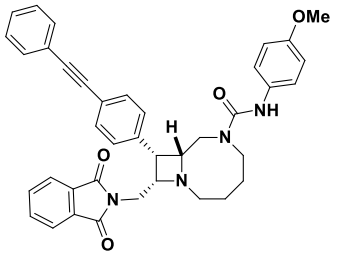

To a solution of triphenylphosphine (772 mg, 2.94 mmol) in THF (14.7 mL) at 0°C was slowly added (E)-diisopropyl diazene-1,2-dicarboxylate (572 µl, 2.94 mmol) under argon. After 10 minutes the mixture became milky yellow. Then 3.98 mL of this prepared mixture (0.796 mmol) was added to a flask containing (8R,9R,10S)-10-(hydroxymethyl)-N-(4-methoxyphenyl)-9-(4-(phenylethynyl)phenyl)-1,6-diazabicyclo[6.2.0]decane-6-carboxamide (112 mg, 0.226 mmol) and phthalimide (49.9 mg, 0.339 mmol) in THF (500 mL) at 0°C. The mixture was stirred at room temperature for 1.5 hours. The reaction was diluted with EtOAc and washed with water and brine. The organic phase was separated, dried (Na_2SO_4), filtered and concentrated. The crude material was purified by flash column chromatography eluting with EtOAc/Hexanes to give the desired compound (103 mg, Yield: 73%). ^{1}H NMR (400 MHz, $CDCl_3$) δ 7.81–7.66 (m, 2H), 7.66–7.58 (m, 2H), 7.55–7.42 (m, 4H), 7.42–7.33 (m, 1H), 7.33–7.21 (m, 3H), 7.23–7.12 (m, 3H), 6.79–6.68 (m, 2H), 6.00 (s, 1H), 3.91–3.72 (m, 2H), 3.69 (s, 3H), 3.65–3.55 (m, 2H), 3.54–3.41 (m, 3H), 3.33–3.19 (m, 1H), 2.91–2.77 (m, 2H), 2.29–2.19 (m, 1H), 1.77–1.61 (m, 3H), 1.60–1.47 (m, 1H). Purity by LCMS (UV Chromatogram, 210nm, 2.5 min run) 91% by UV, rt = 1.63 min, m/z 625 $(M+H)^+$.

(8R,9S,10S)-10-(aminomethyl)-N-(4-methoxyphenyl)-9-(4-(phenylethynyl)phenyl)-1,6-diazabicyclo[6.2.0]decane-6-carboxamide (BRD1095)

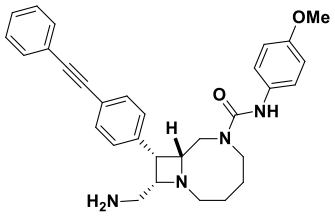

(8R,9S,10S)-10-((1,3-dioxoisoindolin-2-yl)methyl)-N-(4-methoxyphenyl)-9-(4-(phenylethynyl)phenyl)-1,6-diazabicyclo[6.2.0]decane-6-carboxamide (103 mg, 0.165 mmol) was dissolved in ethanol (1649 µL) and to this was added methylhydrazine (87 µl, 1.649 mmol) and the reaction mixture was stirred at 80°C for 3 hours. The reaction mixture was concentrated. The crude material was purified by flash column chromatography eluting with DCM/MeOH to give the desired compound (44mg, Yield: 54%). ^{1}H NMR (400 MHz, $CDCl_3$) δ 7.51–7.34 (m, 6H), 7.32–7.22 (m, 3H), 7.21–7.12 (m, 2H), 6.78–6.72 (m, 2H), 6.05 (s, 1H), 3.83–3.72 (m, 1H), 3.69 (s, 3H), 3.63–3.52 (m, 2H), 3.52–3.42 (m, 1H), 3.41–3.33 (m, 1H), 3.28–3.14 (m, 2H), 2.99–2.87 (m, 1H), 2.88–2.76 (m, 1H), 2.74–2.65 (m, 1H), 2.36–2.25 (m, 1H), 1.81 –1.63 (m, 3H), 1.64–1.46 (m, 1H). ^{13}C NMR NMR (101 MHz, $CDCl_3$) δ 155.78, 154.85, 136.56, 132.10, 131.60, 131.23, 130.83, 128.35, 128.28, 123.28, 122.15, 121.80, 114.09, 89.66, 89.17, 69.84, 65.63, 58.61, 55.54, 50.50, 48.69, 42.59, 40.74, 27.84, 27.07. Purity by LCMS (UV Chromatogram, 210nm, 7 min run) 99% by UV, rt = 2.61 min, m/z 495 $(M+H)^+$. HRMS (ESI) calcd for $C_{31}H_{34}N_4O_2$ $[M+H]^+$: 495.276. Found: 495.2764.

(8R,9S,10S)-10-((dimethylamino)methyl)-N-(4-methoxyphenyl)-9-(4-(phenylethynyl)phenyl)-1,6-diazabicyclo[6.2.0]decane-6-carboxamide (BRD7929)

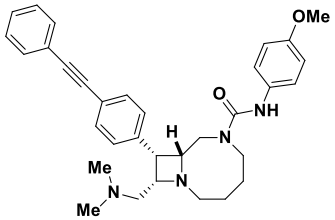

(8R,9S,10S)-10-(aminomethyl)-N-(4-methoxyphenyl)-9-(4-(phenylethynyl)phenyl)-1,6-diazabicyclo[6.2.0]decane-6-carboxamide (39 mg, 0.079 mmol) was dissolved in DCM (1,314 µL) and to this was added magnesium sulfate (95 mg, 0.788 mmol) followed by a solution of 37 wt.% formaldehyde in water (35.2 µL, 0.473 mmol). To this suspension was added anhydrous sodium triacetoxyhydroborate (234 mg, 1.104 mmol). The reaction was stirred for 2 hours upon which saturated sodium bicarbonate solution was added and the mixture was stirred for 15 minutes. The organic components were extracted with DCM and washed with water and brine. The organic phase was separated, dried (Na_2SO_4), filtered and concentrated. The crude material was purified by flash column chromatography eluting with DCM/Methanol to give the desired compound (28 mg, Yield: 67%). ^{1}H NMR (400 MHz, $CDCl_3$) δ 7.60–7.45 (m, 6H), 7.41–7.34 (m, 3H), 7.31–7.24 (m, 2H), 6.88–6.82 (m, 2H), 6.08 (s, 1H), 3.94–3.82 (m, 1H), 3.80 (s, 3H), 3.71–3.50 (m, 4H), 3.34–3.20 (m, 1H), 3.14–3.04 (m, 1H), 2.94–2.84 (m, 1H), 2.58–2.43 (m, 2H), 2.43–2.32 (m, 1H), 2.08 (s, 6H), 1.93–1.58 (m, 4H). ^{13}C NMR (100 MHz, $CDCl_3$) δ 155.71, 154.84, 137.22, 132.19, 131.57, 131.10, 131.05, 128.34, 128.22, 123.29, 122.17, 121.49, 114.03 89.51, 89.32, 66.97, 66.71, 57.89, 57.75, 55.50, 50.63, 48.78,

45.85, 44.82, 27.94, 27.46. Purity by LCMS (UV Chromatogram, 210nm, 7 min run) 99% by UV, rt = 2.58 min, m/z 523 $(M+H)^+$. HRMS (ESI) calcd for $C_{33}H_{38}N_4O_2$ $[M + H]^+$: 523.3073. Found: 523.3074.

Chemical Synthesis of BRD0026

The synthesis of BRD0026 was performed by adapting the synthetic methods reported by Lowe *et al.*[37] Purity by LCMS (UV Chromatogram, 210nm, 1.2 min run) 78% by UV, rt = 0.76 min, m/z 391 $(M+H)^+$.

Chemical Synthesis of BRD73842

The synthesis of BRD73842 was performed by adapting the synthetic methods reported by Klausen *et al.*[75]

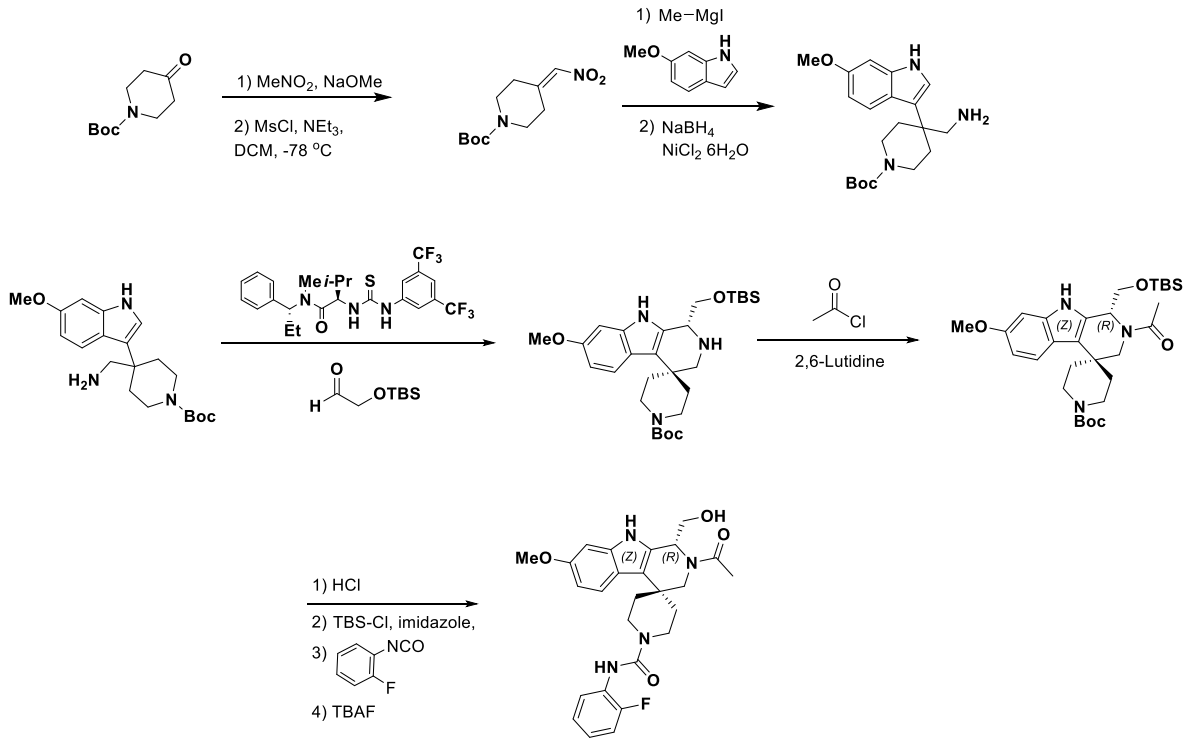

Scheme 2. Synthetic route to BRD73842

tert-butyl 4-(nitromethylene)piperidine-1-carboxylate

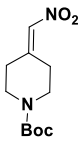

To a solution of 1-Boc-4-piperidinone (15 g, 75 mmol) in MeOH (151 mL) was added nitromethane (41 mL, 753 mmol) and sodium methanolate (2.034 g, 37.6 mmol) at room temperature. The reaction was stirred for 16 hours, then saturated $NaHCO_3$ was added and the mixture was extracted with ethyl acetate. The organic phase was separated, dried (Na_2SO_4), filtered and concentrated to afford crude tert-butyl 4-hydroxy-4-(nitromethyl)piperidine-1-carboxylate that was used directly in the subsequent step. To a solution of this crude material in DCM at -78°C was added triethylamine (46

mL, 331 mmol) and methanesulfonyl chloride (18.73 mL, 241 mmol). The reaction mixture was allowed to stir at -78°C for 30 minutes. The temperature was then increased to -20°C for 4 hours upon which TLC analysis indicated complete reaction. The mixture was carefully poured into a cold ammonium chloride solution and extracted with DCM. The organic phase was separated, dried (Na_2SO_4), filtered and concentrated. The crude material was purified by flash column chromatography eluting with EtOAc/Hexanes to give the desired compound (10 g, Yield: 55%). ^{1}H NMR (300 MHz, $CDCl_3$) δ 7.02 (s, 1H), 3.58 (m, 4H), 3.01 (m, 2H), 2.39–2.29 (m, 2H), 1.50 (s, 9H). Purity by LCMS (UV Chromatogram, 210nm, 2.5 min run) 99% by UV, rt = 1.29 min, m/z 241 $(M-H)^-$.

tert-butyl 4-(6-methoxy-1H-indol-3-yl)-4-(nitromethyl)piperidine-1-carboxylate

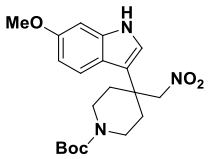

To a solution of 6-methoxy-1H-indole (3.39 g, 23.03 mmol) in THF (57.6 ml) was added methylmagnesium iodide (3.0 M in Et_2O, 8.83 mL, 26.5 mmol) dropwise. The mixture was stirred at room temperature for 20 minutes and then cooled to 0°C. tert-butyl 4-(nitromethylene)piperidine-1-carboxylate (5.58 g, 23.03 mmol) in THF (173 mL) was then added at 0°C dropwise. The reaction mixture was warmed slowly to room temperature and stirred for 16 hours. Saturated ammonium chloride solution was then added was and the reaction was stirred at room temperature for 30 minutes. The organic components were extracted with EtOAc and washed with water and brine. The crude material was purified by flash column chromatography eluting with EtOAc/Hexanes to give the desired product (6.91 g, Yield: 77%). ^{1}H NMR (300 MHz, $CDCl_3$) δ 8.27 (s, 1H), 7.54 (d, J = 8.8 Hz, 1H), 6.85 (m, 3H), 4.71 (s, 2H), 3.85 (m, 5H), 3.13 (m, 2H), 2.45 (m, 2H), 1.95 (ddd, J = 13.7, 11.0, 4.2 Hz, 2H), 1.47 (s, 9H). Purity by LCMS (UV Chromatogram, 210nm, 2.5 min run) 96% by UV, rt = 1.46 min, m/z 390 $(M+H)^+$.

tert-butyl 4-(aminomethyl)-4-(6-methoxy-1H-indol-3-yl)piperidine-1-carboxylate

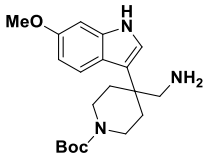

To a solution of tert-butyl 4-(6-methoxy-1H-indol-3-yl)-4-(nitromethyl)piperidine-1-carboxylate (7.7 g, 19.77 mmol) in THF (316 mL) at room temperature was added $NiCl_2.6H_2O$ (4.70 g, 19.77 mmol) and $NaBH_4$ (2.99 g, 79 mmol). The reaction was cooled to 0°C and then MeOH (79 mL) was added very slowly (caution, vigorous reaction). The reaction was warmed to room temperature and after 3 hours, diethylenetriamine (29.9 mL, 277 mmol) was added. After a further 1 hour the reaction mixture was concentrated. A saturated sodium bicarbonate solution was added and the organic components were extracted with EtOAc. The organic phase was separated, dried (Na_2SO_4), filtered and concentrated. The crude material was purified by flash column chromatography eluting with EtOAc/Hexanes to give the desired compound (6.37 g, Yield: 90%). ^{1}H NMR (300 MHz, $CDCl_3$) δ 8.29 (s, 1H), 7.59 (d, J = 8.8 Hz, 1H), 6.90 (dd, J = 6.2, 2.3 Hz, 2H), 6.77 (dd, J = 8.8, 2.4 Hz, 1H), 3.86 (s, 3H), 3.84 – 3.65 (m, 2H), 3.20 – 3.11 (m, 2H), 2.97 (s, 2H), 2.30 – 2.20 (m, 2H), 1.77 – 1.68 (m, 2H), 1.46 (s, 9H). Purity by LCMS (UV Chromatogram, 210nm, 2.5 min run) 97% by UV, rt = 1.28 min, m/z 360 $(M+H)^+$.

(R)-tert-butyl 1'-(((tert-butyldimethylsilyl)oxy)methyl)-7'-methoxy-1',2',3',9'-tetrahydrospiro[piperidine-4,4'-pyrido[3,4-b]indole]-1-carboxylate.

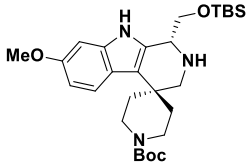

To a solution of tert-butyl 4-(aminomethyl)-4-(6-methoxy-1H-indol-3-yl)piperidine-1-carboxylate (2.61 g, 7.26 mmol) in toluene (132 mL) was added (R)-2-(3-(3,5-bis(trifluoromethyl)phenyl)thioureido)-N,3-dimethyl-N-((R)-1-phenylpropyl)butanamide (0.566 g, 1.089 mmol) at -20°C. The mixture was stirred for 10 minutes before 2-(tert-butyldimethylsilyloxy)acetaldehyde (1.519 g, 8.71 mmol) (freshly distilled) in toluene (1801 µL) was added. The above mixture was allowed to stir at -20°C while it was monitored by LCMS. After 89 hours further (R)-2-(3-(3,5-bis(trifluoromethyl)phenyl)thioureido)-N,3-dimethyl-N-((R)-1-phenylpropyl)butanamide 0.283 g, 0.545 mmol was added. After 135 hours saturated $NaHCO_3$ was added to the reaction mixture. The reaction was warmed to room temperature and extracted with EtOAc. The organic phase was separated, dried (Na_2SO_4), filtered and concentrated. The crude material was purified by flash column chromatography eluting with EtOAc/Hexanes to give the desired compound (2.9 g, Yield: 77%). ^{1}H NMR (300 MHz, $CDCl_3$) δ 8.34 (s, 1H), 7.40 (d, J = 8.7 Hz, 1H), 7.13 (s, 1H), 6.67 (d, J = 2.3 Hz, 1H), 6.60 (dd, J = 8.7, 2.4 Hz, 1H), 4.05 – 3.84 (m, 3H), 3.76 (dd, J = 9.3, 5.0 Hz, 1H), 3.70 (s, 3H), 3.54 (m, 1H), 3.34 (d, J = 12.7 Hz, 1H), 2.93 – 2.61 (m, 3H), 2.40 (m, 1H), 2.07 (m, 1H), 1.67 – 1.48 (m, 2H), 1.38 (s, 9H), 0.83 (s, 9H), -0.00 (s, 3H) -0.01 (s, 3H). (mixture of rotamers by ^{1}HNMR, the major rotamer is quoted). Purity by LCMS (UV Chromatogram, 210nm, 2.5 min run) 98% by UV, rt = 1.39 min, m/z 516 $(M+H)^+$.

An ee of 91% was determined by chiral SFC analysis upon converting this material to the alloc-protected material (R)-2'-allyl 1-tert-butyl 1'-(((tert-butyldimethylsilyl)oxy)methyl)-7'-methoxy-3',9'-dihydrospiro[piperidine-4,4'-pyrido[3,4-b]indole]-1,2'(1'H)-dicarboxylate using the chiral SFC method detailed above.

(R)-tert-butyl 2'-acetyl-1'-(((tert-butyldimethylsilyl)oxy)methyl)-7'-methoxy-1',2',3',9'-tetrahydrospiro[piperidine-4,4'-pyrido[3,4-b]indole]-1-carboxylate

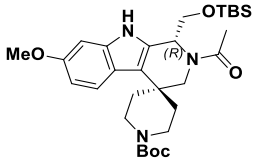

To a solution of (R)-tert-butyl 1'-(((tert-butyldimethylsilyl)oxy)methyl)-7'-methoxy-1',2',3',9'-tetrahydrospiro[piperidine-4,4'-pyrido[3,4-b]indole]-1-carboxylate (1 g, 1.939 mmol) in DCM (19.39 mL) was added N-ethyl-N-isopropylpropan-2-amine (1.693 mL, 9.69 mmol), and the reaction mixture was cooled to 0°C. Then acetyl chloride (0.207 mL, 2.91 mmol) was added dropwise and the reaction was allowed to warm to room temperature and stirred for 1.5 hours. At this point saturated sodium bicarbonate was added and the mixture was extracted with DCM. The organic phase was separated, dried (Na_2SO_4), filtered and concentrated. The crude material was purified by flash column chromatography eluting with EtOAc/Hexanes to give the desired compound. (1.07 g, Yield: 99%). ^{1}H NMR (400 MHz, $CDCl_3$) δ 8.22 (s, 1H), 7.49–7.38 (m, 1H), 6.75–6.69 (m, 1H), 6.69–6.60 (m, 1H), 5.45 (dd, J = 8.8, 4.6 Hz, 1H), 5.27 – 5.16 (m, 1H), 4.92 – 4.81 (m, 1H), 4.23 – 4.01 (m, 1H), 3.98 – 3.80 (m, 2H), 3.73 (s, 3H), 3.68 – 3.61 (m, 1H), 3.23 – 3.05 (m, 1H), 2.98 – 2.77 (m, 1H), 2.73 – 2.54 (m,

1H), 2.52 – 2.45 (m, 1H), 2.15 (s, 3H), 2.0 – 1.9 (m, 1H), 1.85 – 1.75 (m, 1H), 1.43 (s, 9H), 0.84 (s, 9H), 0.00 (s, 3H), -0.01 (s, 3H). (mixture of rotamers by ^{1}HNMR, the major rotamer is quoted). Purity by LCMS (UV Chromatogram, 210nm, 7 min run) 99% by UV, rt = 1.83 min, m/z 558 $(M+H)^+$.

(R)-1-(1'-(((tert-butyldimethylsilyl)oxy)methyl)-7'-methoxyspiro[piperidine-4,4'-pyrido[3,4-b]indol]-2'(1'H,3'H,9'H)-yl)ethanone

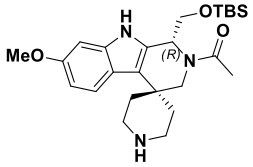

To a solution of (R)-tert-butyl 2'-acetyl-1'-(((tert-butyldimethylsilyl)oxy)methyl)-7'-methoxy-1',2',3',9'-tetrahydrospiro[piperidine-4,4'-pyrido[3,4-b]indole]-1-carboxylate (1.082 g, 1.940 mmol) in DCM (24 mL) was added HCl (2.91 mL, 11.64 mmol, 4M dioxane) and the mixture was stirred at room temperature for 16 hours. The reaction material was concentrated and used directly in the next step. The crude material was dissolved in DMF (12.9 mL) and to this was added tert-butylchlorodimethylsilane (438 mg, 2.91 mmol) and imidazole (264 mg, 3.88 mmol). The reaction was stirred at 0°C for 2 hours. Then saturated ammonium chloride was added and the mixture extracted with DCM. The organic phase was separated, dried (Na_2SO_4), filtered and concentrated. The crude material was purified by flash column chromatography eluting with DCM/MeOH to give the desired compound. (1.08 g, Yield: 93%). ^{1}H NMR (300 MHz, $CDCl_3$) δ 8.31 (s, 1H), 7.82 (d, J = 8.5 Hz, 1H), 7.68 (d, minor rotamer), 7.62 (s, minor rotamer), 7.18 (s, 1H), 7.02 (s, 1H), 6.76 – 6.64 (m, 1H), 5.46 (dd, J = 8.7, 4.9 Hz, 1H), 5.25 – 5.09 (m, 1H), 4.96 – 4.81 (m, 1H), 4.30 – 4.17 (m, 1H), 3.93 – 3.77 (m, 2H), 3.72 (s, 3H), 3.37 – 3.24 (m, 1H), 3.24 – 2.98 (m, 2H), 2.94 – 2.81 (m, 1H), 2.58 – 2.47 (m, 1H), 2.15 (s, 3H), 1.67 – 1.37 (m, 2H), 0.84 (s, 9H), 0.00 (s, 3H), -0.01 (s, 3H). (mixture of rotamers by ^{1}H NMR, the major rotamer is quoted). Purity by LCMS (UV Chromatogram, 210nm, 2.5 min run) 99% by UV, rt = 1.21 min, m/z 458 $(M+H)^+$.

(R)-2'-acetyl-1'-(((tert-butyldimethylsilyl)oxy)methyl)-N-(2-fluorophenyl)-7'-methoxy-1',2',3',9'-tetrahydrospiro[piperidine-4,4'-pyrido[3,4-b]indole]-1-carboxamide

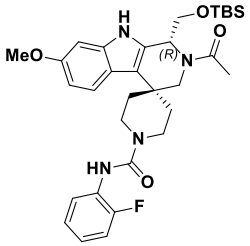

A solution of (R)-1-(1'-((tert-butyldimethylsilyloxy)methyl)-7'-methoxyspiro[piperidine-4,4'-pyrido[3,4-b]indole]-2'(1'H,3'H,9'H)-yl)ethanone (450 mg, 0.983 mmol) in DCM (18 mL) was treated with 1-fluoro-2-isocyanatobenzene (0.121 mL, 1.082 mmol) at 0°C and the reaction was stirred for 3 hours. The reaction was then concentrated under reduced pressure and purified by column chromatography eluting with EtOAc/Hexanes to give the desired compound (509 mg, Yield: 87%). ^{1}H NMR (300 MHz, DMSO-d_6) δ 7.49 – 7.32 (m, 2H), 7.21 – 7.02 (m, 3H), 6.78 (s, 1H), 6.58 (m, 1H), 5.17 – 4.98 (m, 1H), 4.11 – 3.83 (m, 4H), 3.70 (s, 3H), 3.40 – 2.98 (m, 2H), 2.74 – 2.40 (m, 2H), 2.13 (s, 3H), 1.52 – 0.93 (m, 4H), 0.84 (s, 9H), 0.05 (s 3H), 0.00 (s, 3H). (mixture of rotamers by ^{1}HNMR, the major rotamer is quoted). Purity by LCMS (UV Chromatogram, 210nm, 7 min run) 98% by UV, rt = 4.27 min, m/z 595 $(M+H)^+$.

(R)-2'-acetyl-N-(2-fluorophenyl)-1'-(hydroxymethyl)-7'-methoxy-1',2',3',9'-tetrahydrospiro[piperidine-4,4'-pyrido[3,4-b]indole]-1-carboxamide (BRD73842)

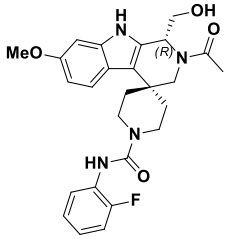

To a solution of (R)-2'-acetyl-1'-(((tert-butyldimethylsilyl)oxy)methyl)-N-(2-fluorophenyl)-7'-methoxy-1',2',3',9'-tetrahydrospiro[piperidine-4,4'-pyrido[3,4-b]indole]-1-carboxamide (496 mg, 0.834 mmol) in THF (8,339 µL) was added tetrabutylammonium fluoride (1M in THF, 2085 µl, 2.085 mmol). After 1 hour saturated ammonium chloride was added and the mixture was extracted with EtOAc. The organic phase was separated, dried (Na_2SO_4), filtered and concentrated. The crude material was purified by flash column chromatography eluting with DCM/MeOH to give the desired compound (407 mg, Yield: 99%). ^{1}H NMR (300 MHz, DMSO-d_6) δ 10.78 (s, 1H), 8.39 (s, 1H), 7.52 – 7.33 (m, 2H), 7.30 – 7.10 (m, 3H), 6.91-6.77 (m, 1H), 6.69-6.55 (m, 1H), 5.50 – 5.30 (m, 1H), 5.19 – 5.07 (m, 1H), 5.03 – 4.91 (m, 1H), 4.16 – 3.90 (m, 2H), 3.74 (s, 4H), 3.39 – 3.28 (m, 1H), 3.29 – 2.97 (m, 3H), 2.77 – 2.54 (m, 1H), 2.18 (s, 3H), 1.56 – 1.20 (m, 2H). (mixture of rotamers by ^{1}H NMR, the major rotamer is quoted). ^{13}C NMR (101 MHz, DMSO) δ 169.92, 169.29, 157.18, 155.91, 155.86, 155.55, 155.42, 154.75, 137.75, 137.55, 131.44, 130.33, 130.18, 128.42, 128.31, 126.68, 126.56, 125.30, 124.48, 124.45, 119.99, 119.76, 119.11, 115.05, 108.72, 108.49, 95.58, 95.45, 62.52, 56.27, 55.68, 50.81, 48.47, 41.82, 41.59, 40.96, 35.49, 35.30, 34.63, 34.14, 32.80, 32.17, 32.15, 22.23. (Mixture of rotamers by ^{13}C NMR). Purity by LCMS (UV Chromatogram, 210nm, 7 min run) 99% by UV, rt = 2.46 min, m/z 481 $(M+H)^+$. HRMS (ESI) calcd for $C_{26}H_{29}FN_4O_4$ $[M+H]^+$: 481.2251. Found: 481.2255.

Chemical Synthesis of BRD7539

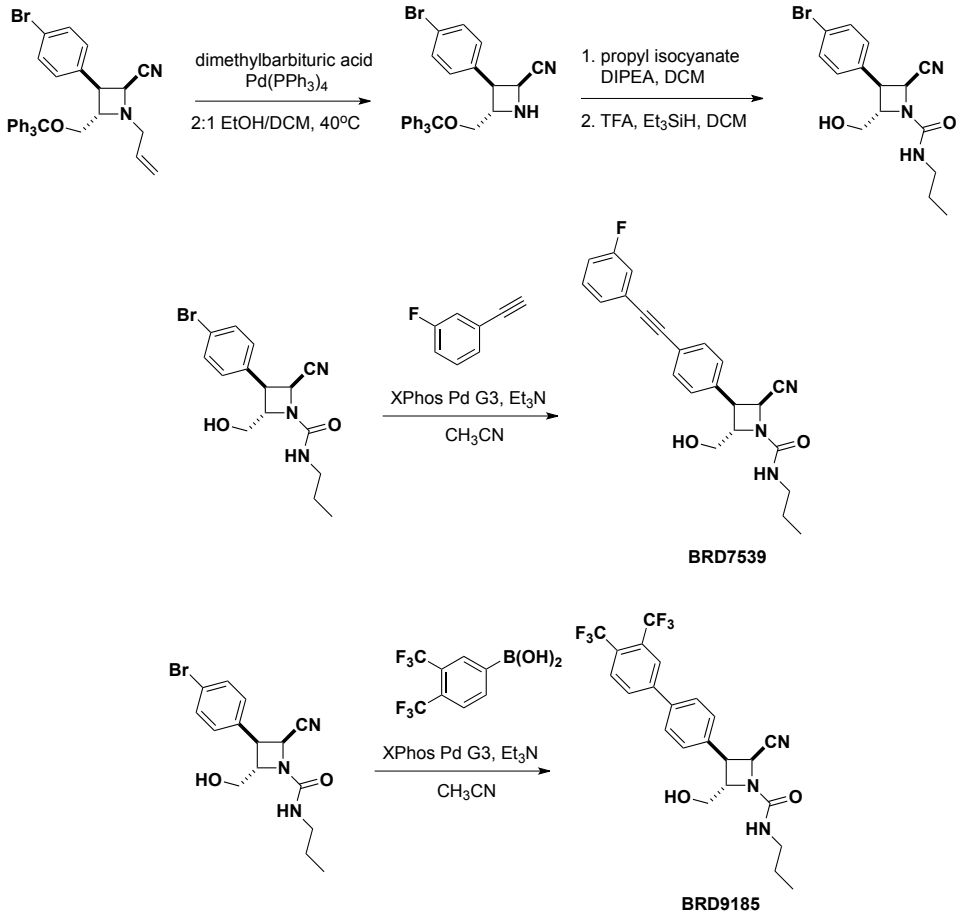

Scheme 3. Synthetic route to BRD7539 and BRD9185.

(2S,3S,4S)-3-(4-bromophenyl)-4-((trityloxy)methyl)azetidine-2-carbonitrile.

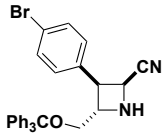

(2S,3S,4S)-1-allyl-3-(4-bromophenyl)-4-((trityloxy)methyl)azetidine-2-carbonitrile (1.04 g, 1.845 mmol) (prepared according to the method of Lowe *et al*[37] was dissolved in 2:1 EtOH (12.3 mL) and DCM (6.15 mL). Dimethylbarbituric acid (432 mg, 2.77 mmol) and $Pd(PPh_3)_4$ (213 mg, 0.185 mmol) were then added, and the mixture was heated to 40°C. After 2 hours, the solvent was removed *in vacuo*, and the resulting residue was purified by flash column chromatography (hexanes/EtOAc) to afford the product as a light yellow foaming solid. (900 mg, 96%). ^{1}H NMR (400 MHz, $CDCl_3$) δ 7.58 – 7.51 (m, 2H), 7.45 – 7.40 (m, 6H), 7.35 – 7.26 (m, 12H), 4.73 (d, *J* = 8.5 Hz, 1H), 4.33 (dt, *J* = 7.1, 4.9 Hz, 1H), 3.89 (dd, *J* = 8.4, 7.2 Hz, 1H), 3.40 (dd, *J* = 10.2, 5.1 Hz, 1H), 3.36 – 3.29 (m, 2H), 2.30 (s, 1H). Purity by LCMS (UV Chromatogram, 210nm, 7.5 min run) 99% by UV, rt = 5.06 min, m/z 557 $(M+HCOOH)^+$.

(2S,3S,4S)-3-(4-bromophenyl)-2-cyano-N-propyl-4-((trityloxy)methyl)azetidine-1-carboxamide.

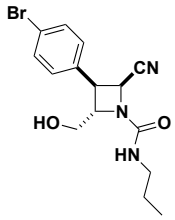

(2S,3S,4S)-3-(4-bromophenyl)-4-((trityloxy)methyl)azetidine-2-carbonitrile (415 mg, 0.815 mmol) was dissolved in DCM (8.2 mL), followed by the dropwise addition of *N,N*-diisopropylethylamine (0.6 mL, 4.08 mmol) and propyl isocyanate (115 mL, 1.222 mmol). After 30 minutes, the reaction was quenched by the addition of methanol (1 mL) and stirred for 15 minutes, after which point the solvent was removed *in vacuo*. The resulting residue was redissolved in DCM (8.2 mL), and trifluoroacetic acid (624 µL, 8.15 mmol) and triethylsilane (195 µL, 1.222 mmol) were added dropwise. The mixture was allowed to stir for 30 minutes before the solvent was once again removed *in vacuo* and resulting residue purified via flash column chromatography (MeOH/DCM) to afford the product as white foaming solid (185 mg, 65%). ^{1}H NMR (400 MHz, $CDCl_3$) δ 7.51 (d, *J* = 7.8 Hz, 2H), 7.20 (d, *J* = 7.7 Hz, 2H), 6.54 (s, 1H), 4.97 (d, *J* = 8.4 Hz, 1H), 4.89 – 4.70 (m, 1H), 4.70 – 4.61 (m, 1H), 3.96 – 3.62 (m, 3H), 3.13 (m, 2H), 1.57 – 1.40 (m, 2H), 0.90 (t, *J* = 7.4 Hz, 3H). Purity by LCMS (UV Chromatogram, 210nm, 7.5 min run) 99% by UV, rt = 5.06 min, m/z 353 $(M+H)^+$.

(2S,3S,4S)-2-cyano-3-(4-((3-fluorophenyl)ethynyl)phenyl)-4-(hydroxymethyl)-N-propylazetidine-1-carboxamide (BRD7539).

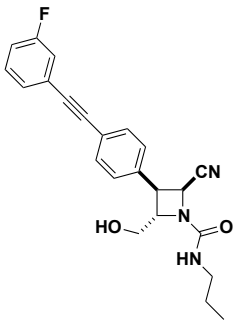

(2S,3S,4S)-3-(4-bromophenyl)-2-cyano-N-propyl-4-((trityloxy)methyl)azetidine-1-carboxamide (105 mg, 0.298 mmol) was dissolved in degassed CH_3CN (3 mL), followed by the addition of 1-ethynyl-3-fluorobenzene (172 µL, 1.491 mmol) and XPhos Pd G3 (38 mg, 0.045 mmol). Finally, Et_3N (1.04 mL, 7.45 mmol) was added, and the reaction was heated at 70°C for 2 hours. The reaction was cooled to room temperature, diluted with pH 7 buffer, and extracted 3x with EtOAc. The organic layer was dried over Na_2SO_4, filtered, and removed *in vacuo*. The resulting mixture was purified by flash column chromatography (MeOH/DCM) to afford the product as a pale yellow powder/solid (106 mg, 91%). ^{1}H NMR (400 MHz, $CDCl_3$) δ 7.56 (d, *J* = 7.7 Hz, 2H), 7.38 – 7.28 (m, 4H), 7.21 (dd, *J* = 9.5, 3.0 Hz, 1H), 7.04 (dq, *J* = 7.8, 3.7 Hz, 1H), 6.27 (s, 1H), 5.01 (d, *J* = 8.4 Hz, 1H), 4.74 (t, *J* = 7.8 Hz, 1H), 4.02 (s, 1H), 3.92 (d, *J* = 10.9 Hz, 1H), 3.88 – 3.80 (m, 1H), 3.74 (t, *J* = 8.1 Hz, 1H), 3.18 (m, 2H), 1.51 (d, *J* = 7.2 Hz, 2H), 0.92 (t, *J* = 7.3 Hz, 3H). ^{13}C NMR (101 MHz, $CDCl_3$) δ 163.73, 161.28, 158.06, 134.35, 132.25, 130.10 (d, *J* = 8.6 Hz), 129.48, 128.51, 127.66 (d, *J* = 3.0 Hz), 124.92 (d, *J* = 9.5 Hz), 123.45, 118.62, 118.39, 116.05, 115.79 (d, *J* = 10.1 Hz), 89.59, 89.29 (d, *J* = 3.4 Hz), 68.12, 65.81, 52.73, 42.29, 39.54, 29.82, 23.27, 11.46. Purity by LCMS (UV Chromatogram, 210nm, 7.5 min run) 99% by UV, rt = 3.49 min, m/z 392 $(M+H)^+$. HRMS (ESI) calcd for $C_{23}H_{22}FN_3O_2$ $[M+H]^+$: 392.1774. Found: 392.1781.

(2S,3S,4S)-3-(3',4'-bis(trifluoromethyl)-[1,1'-biphenyl]-4-yl)-2-cyano-4-(hydroxymethyl)-N-propylazetidine-1-carboxamide.

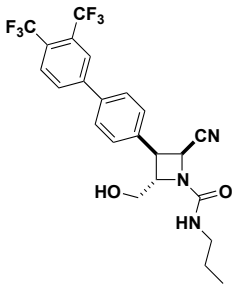

(2S,3S,4S)-3-(4-bromophenyl)-2-cyano-N-propyl-4-((trityloxy)methyl)azetidine-1-carboxamide (7.5 mg, 0.021 mmol) was dissolved in degassed 2:1 THF (300 µL) and 0.5 M K_3PO_4 (150 µL). Finally, XPhos Pd G3 was added, and the reaction was stirred at room temperature for 2.5 hours. The mixture was quenched with pH 7 buffer and extracted 3x with EtOAc. The organic layer was dried over Na_2SO_4, filtered, and removed *in vacuo*. The resulting mixture was purified by flash column chromatography (MeOH/DCM) to afford the product as a white solid (5.5 mg, 53%). ^{1}H NMR (400 MHz, DCM-d_2) δ 7.98 (d, *J* = 1.9 Hz, 2H), 7.81 (s, 1H), 7.65 – 7.60 (m, 2H), 7.47 – 7.42 (m, 2H), 6.01 (d, *J* = 5.9 Hz, 1H), 4.97 (d, *J* = 8.6 Hz, 1H), 4.71 (td, *J* = 8.1, 2.3 Hz, 1H), 3.92 – 3.70 (m, 3H), 3.11 (m, 2H), 1.46 (m, 2H), 0.85 (t, *J* = 7.4 Hz, 3H). ^{13}C NMR (101 MHz, DCM-d_2) δ 157.72, 142.39, 138.36, 135.04 (d, *J* = 7.3 Hz), 132.12, 131.79, 130.79, 129.31, 127.44 (d, *J* = 26.5 Hz), 124.78, 122.07, 121.66 – 121.08 (m), 115.75, 67.89, 65.81, 53.33, 53.13, 52.86, 52.55, 42.11, 39.13, 23.21, 11.07. Purity by LCMS (UV Chromatogram, 210nm, 7.5 min run) 99% by UV, rt = 3.92 min, m/z 486 $(M+H)^+$. HRMS (ESI) calcd for $C_{23}H_{21}F_6N_3O_2$ $[M+H]^+$: 486.1608. Found: 486.1618.

Analytical data for compounds in Extended Data Table 2

The synthesis of these tool compounds were performed using the general synthetic methods outlined in Lowe *et al*.[37] and above for BRD7929

(8R,9S,10S)-10-((dimethylamino)methyl)-N-(4-(2-fluoroethoxy)phenyl)-9-(4-(phenylethynyl)phenyl)-1,6-diazabicyclo[6.2.0]decane-6-carboxamide (Formic acid salt) (BRD8805)

^{1}H NMR (400 MHz, $CDCl_3$) δ 7.49 – 7.41 (m, 4H), 7.41 – 7.33 (m, 2H), 7.32 – 7.23 (m, 3H), 7.23 – 7.14 (m, 2H), 6.83 – 6.71 (m, 2H), 6.05 (s, 1H), 4.76 – 4.68 (m, 1H), 4.63 – 4.54 (m, 1H), 4.18 – 4.10 (m, 1H), 4.10 – 4.02 (m, 1H), 3.86 – 3.72 (m, 1H), 3.63 – 3.46 (m, 4H), 3.21 – 3.10 (m, 1H), 3.05 – 2.92 (m, 1H), 2.84 – 2.73 (m, 1H), 2.64 – 2.52 (m, 2H), 2.33 – 2.23 (m, 1H), 2.08 (s, 6H), 1.84 – 1.64 (m, 3H), 1.64 – 1.47 (m, 1H). Purity by LCMS (UV Chromatogram, 210nm, 4.5 min run) 95% by UV, rt = 2.64 min, m/z 555 $(M+H)^+$.

(8R,9S,10S)-10-((isopropyl(methyl)amino)methyl)-N-(4-methoxyphenyl)-9-(4-(phenylethynyl)phenyl)-1,6-diazabicyclo[6.2.0]decane-6-carboxamide (HCl salt) (BRD4716)

^{1}H NMR (400 MHz, $CDCl_3$) δ 7.51 – 7.36 (m, 6H), 7.33 – 7.23 (m, 3H), 7.24 – 7.10 (m, 2H), 6.80 – 6.69 (m, 2H), 5.99 (s, 1H), 3.84 – 3.73 (m, 1H), 3.70 (s, 3H), 3.66 – 3.47 (m, 4H), 3.20 – 3.10 (m, 1H), 3.10 – 2.98 (m, 1H), 2.89 – 2.76 (m, 1H), 2.43 – 2.29 (m, 2H), 2.12 – 1.93 (m, 2H), 1.85 – 1.67 (br s, 3H), 1.18 (s, 6H), 1.09 – 0.84 (m, 2H), 0.82 – 0.67 (m, 2H). Purity by LCMS (UV Chromatogram, 210nm, 4.5 min run) 96% by UV, rt = 2.29 min, m/z 551 $(M+H)^+$.

(8R,9S,10S)-10-(((2-fluoroethyl)(methyl)amino)methyl)-N-(4-methoxyphenyl)-9-(4-(phenylethynyl)phenyl)-1,6-diazabicyclo[6.2.0]decane-6-carboxamide (HCl salt) (BRD2132)
^{1}H NMR (400 MHz, CH_3OD) δ 7.79 – 7.67 (m, 2H), 7.67 – 7.56 (m, 2H), 7.55 – 7.43 (m, 2H), 7.42 – 7.29 (m, 3H), 7.24 – 7.16 (m, 2H), 6.87 – 6.76 (m, 2H), 4.76 – 4.68 (m, 1H), 4.65 – 4.53 (m, 1H), 4.49 – 4.33 (m, 1H), 4.25 – 4.15 (m, 1H), 4.10 – 3.98 (m, 1H), 3.89 – 3.77 (m, 1H), 3.74 (s, 3H), 3.67 – 4.60 (m, 1H), 3.54 – 3.32 (m, 4H), 3.30 – 3.19 (m, 3H), 3.08 – 2.92 (m, 1H), 2.72 (s, 3H), 1.97 – 1.85 (m, 4H). Purity by LCMS (UV Chromatogram, 210nm, 4.5 min run) 99.5% by UV, rt = 2.25 min, m/z 555 $(M+H)^+$.

(9R,10R,11S)-11-(hydroxymethyl)-N-(4-methoxyphenyl)-10-(4-(phenylethynyl)phenyl)-1,7-diazabicyclo[7.2.0]undecane-7-carboxamide (BRD0185)
^{1}H NMR (300 MHz, $CDCl_3$) δ 7.88 – 7.68 (m, 1H), 7.63 – 7.46 (m, 3H), 7.41 – 7.31 (m, 3H), 7.33 – 7.20 (m, 4H), 6.93 – 6.79 (m, 2H), 6.38 – 6.18 (m, 1H), 5.11 – 4.82 (m, 1H), 4.52 – 4.29 (m, 1H), 4.22 – 3.87 (m, 2H), 3.76 (s, 3H), 3.72 – 3.58 (m, 1H), 3.48 – 3.29 (m, 2H), 3.18 – 2.80 (m, 2H), 2.57 – 2.28 (m, 2H), 1.97 – 1.64 (m, 6H). Purity by LCMS (UV Chromatogram, 210nm, 7 min run) 96% by UV, rt = 2.97 min, m/z 510 $(M+H)^+$.

(8R,9S,10S)-10-(azetidin-1-ylmethyl)-N-(4-methoxyphenyl)-9-(4-(phenylethynyl)phenyl)-1,6-diazabicyclo[6.2.0]decane-6-carboxamide (BRD8493)
^{1}H NMR (400 MHz, CH_3OD) δ 7.56 – 7.46 (m, 6H), 7.41 – 7.30 (m, 3H), 7.25 – 7.14 (m, 2H), 6.88 – 6.76 (m, 2H), 3.91 – 3.78 (m, 1H), 3.75 (s, 3H), 3.60 – 3.47 (m, 2H), 3.46 – 3.33 (m, 2H), 3.26 – 3.17 (m, 3H), 3.25 – 3.21 (m, 1H), 3.19 – 2.96 (m, 5H), 2.90 – 2.80 (m, 1H), 2.75 – 2.53 (m, 2H), 2.07 – 1.89 (m, 2H), 1.81 – 1.63 (m, 2H). Purity by LCMS (UV Chromatogram, 210nm, 4.5 min run) 94% by UV, rt = 2.04 min, m/z 535 $(M+H)^+$.

(8R,9S,10S)-N-(4-methoxyphenyl)-10-((4-methylpiperazin-1-yl)methyl)-9-(4-(phenylethynyl)phenyl)-1,6-diazabicyclo[6.2.0]decane-6-carboxamide (BRD6479)
^{1}H NMR (300 MHz, $CDCl_3$) δ 7.52-7.55 (m, 2H), 7.45 (d, J = 8.3 Hz, 2H), 7.40 – 7.31 (m, 4H), 7.24-7.27 (m, 3H), 6.83 (d, J = 8.9 Hz, 2H), 6.11 (s, 1H), 3.78 (s, 3H), 3.67 (bd s, 1H), 3.65 – 3.55 (m, 2H), 3.49 – 3.36 (m, 2H), 3.18 – 3.00 (m, 2H), 2.98 (d, J = 6.1 Hz, 1H), 2.92 (d, J = 8.7 Hz, 1H), 2.90 – 2.75 (m, 2H), 2.36 – 2.18 (m, 8H), 2.15 (s, 3H), 1.93 – 1.76 (m, 4H). Purity by LCMS (UV Chromatogram, 210nm, 7 min run) 94% by UV, rt = 2.91 min, m/z 578 $(M+H)^+$.

(8R,9R,10S)-9-(4-((2-cyanophenyl)ethynyl)phenyl)-10-(hydroxymethyl)-N-(4-methoxyphenyl)-1,6-diazabicyclo[6.2.0]decane-6-carboxamide (BRD4873)
^{1}H NMR (400 MHz, CH_3OD) δ 7.84 – 7.77 (m, 1H), 7.77 – 7.65 (m, 2H), 7.66 – 7.50 (m, 5H), 7.28 – 7.18 (m, 2H), 6.90 – 6.81 (m, 2H), 4.06 – 4.08 (m, 1H), 3.80-3.73 (m, 4H), 3.69 – 3.62 (m, 1H), 3.62 – 3.42 (m, 4H), 3.27 – 3.14 (m, 2H), 3.08 – 3.00 (m, 1H), 2.48 – 2.39 (m, 1H), 1.89 – 1.64 (m, 4H). Purity by LCMS (UV Chromatogram, 210nm, 4.5 min run) 98.5 % by UV, rt = 2.47 min, m/z 521 $(M+H)^+$.

(7R,8R,9S)-9-(hydroxymethyl)-N-(4-methoxyphenyl)-8-(4-(phenylethynyl)phenyl)-1,5-diazabicyclo[5.2.0]nonane-5-carboxamide (BRD9599)
^{1}H NMR (300 MHz, $CDCl_3$) δ 7.59 – 7.44 (m, 5H), 7.40 – 7.30 (m, 3H), 7.29 – 7.17 (m, 3H), 6.86 – 6.76 (m, 2H), 6.05 (s, 1H), 4.20 – 4.04 (m, 1H), 3.81 – 3.73 (m, 3H), 3.71 – 3.41 (m, 6H), 3.24 – 3.13 (m, 1H), 3.12 – 2.94 (m, 2H), 2.32 – 2.17 (m, 1H), 1.97 – 1.72 (m, 2H). Purity by LCMS (UV Chromatogram, 210nm, 7 min run) 96 % by UV, rt = 2.32 min, m/z 483 $(M+H)^+$.

(8R,9S,10S)-8,10-bis(hydroxymethyl)-N-(4-methoxyphenyl)-9-(4-(phenylethynyl)phenyl)-1,6-diazabicyclo[6.2.0]decane-6-carboxamide (BRD2936)

^{1}H NMR (400 MHz, $CDCl_3$) δ 7.62 – 7.47 (m, 4H), 7.41 – 7.33 (m, 2H), 7.30 – 7.27 (m, 5H), 6.91 – 6.82 (m, 2H), 4.11 – 4.02 (m, 1H), 4.02 – 3.90 (m, 3H), 3.86 – 3.66 (m, 7H), 3.48 – 3.31 (m, 1H), 2.98 – 2.79 (m, 2H), 2.68 – 2.55 (m, 1H), 1.86 – 1.49 (m, 4H). Purity by LCMS (UV Chromatogram, 210nm, 7 min run) 97 % by UV, rt = 3.68 min, m/z 527 $(M+H)^+$.

((8R,9R,10S)-6-(benzo[d]thiazol-2-yl)-9-(4-(phenylethynyl)phenyl)-1,6-diazabicyclo[6.2.0]decan-10-yl)methanol (BRD5349)

^{1}H NMR (400 MHz, CH_3OD) δ 7.68 – 7.59 (m, 4H), 7.61 – 7.48 (m, 4H), 7.49 – 7.44 (m, 1H), 7.42 – 7.37 (m, 2H), 7.31 – 7.23 (m, 1H), 7.14 – 6.99 (m, 1H), 4.08 – 3.93 (m, 1H), 3.87 – 3.71 (m, 1H), 3.70 – 3.57 (m, 3H), 3.59 – 3.38 (m, 4H), 3.23 – 3.09 (m, 1H), 2.42 – 2.31 (m, 1H), 2.01 – 1.65 (m, 4H). Purity by LCMS (UV Chromatogram, 210nm, 4.5 min run) 98.7% by UV, rt = 2.81 min, m/z 480 $(M+H)^+$.

(8R,9R,10S)-9-(4-(cyclopropylethynyl)phenyl)-10-(hydroxymethyl)-N-(4-methoxyphenyl)-1,6-diazabicyclo[6.2.0]decane-6-carboxamide (BRD5774)

^{1}H NMR (400 MHz, CH_3OD) δ 7.47 – 7.36 (m, 2H), 7.31 – 7.23 (m, 2H), 7.22 – 7.11 (m, 2H), 6.88 – 6.73 (m, 2H), 4.06 – 3.92 (m, 1H), 3.75 (s, 3H), 3.68 – 3.56 (m, 2H), 3.55 – 3.33 (m, 4H), 3.23 – 3.06 (m, 2H), 3.03 – 2.91 (m, 1H), 2.44 – 2.33 (m, 1H), 1.85 – 1.59 (m, 4H), 1.50 – 1.37 (m, 1H), 0.92 – 0.79 (m, 2H), 0.77 – 0.66 (m, 2H). Purity by LCMS (UV Chromatogram, 210nm, 4.5 min run) 96% by UV, rt = 2.35 min, m/z 460 $(M+H)^+$.

(8R,9R,10S)-N-cyclobutyl-10-(hydroxymethyl)-9-(4-(phenylethynyl)phenyl)-1,6-diazabicyclo[6.2.0]decane-6-carboxamide (BRD8260)

^{1}H NMR (400 MHz, CH_3OD) δ 7.59 – 7.45 (m, 6H), 7.45 – 7.32 (m, 3H), 4.28 – 4.16 (m, 1H), 3.94 – 3.84 (m, 1H), 3.75 – 3.58 (m, 2H), 3.51 – 3.39 (m, 4H), 3.19 – 3.02 (m, 2H), 2.97 – 2.85 (m, 1H), 2.43 – 2.31 (m, 1H), 2.31 – 2.14 (m, 2H), 2.04 – 1.89 (m, 2H), 1.84 – 1.54 (m, 6H). Purity by LCMS (UV Chromatogram, 210nm, 4.5 min run) 99 % by UV, rt = 2.48 min, m/z 444 $(M+H)^+$.

X-ray crystal structure of BRD7929

BRD7929 was crystallized as a salt with two equivalents of L-tartaric acid. Crystallographic studies were preformed Crystallographic Resources, inc. Dewitt, MI, 48820. The crystallographic data has been deposited in the Cambridge Structural Database (http://www.ccdc.cam.ac.uk) and the data has been assigned the deposition number CCDC 1429949.

Supplementary Figure 4 | Chemical and X-ray crystal structures of BRD7929.

Supplementary Tables

Assay	EC_{50} (nM)				
	BRD0026	BRD7539	BRD73842	BRD3444	Common antimalarial [drug]
Pf, Dd2 [CQ, QN, PY, SDX]	1,010.6 (34.4)*	10.8 (5.1)*	80.1 (2.8)*	9.2 (0.7)*	148.7 (32.3)* [CQ]
*Pfsc*DHODH	368	8,917	26	3	-
*Pf*NITD609^{R}	1,778	6	16	3	-
HepG2	> 26,000	> 26,000	> 26,000	> 26,000	-
Pf, TM90C6B [CQ, PY, MQ, ATV]	-	11	-	-	18,800 [PY]
*Pf*CYTb:G33V [IDI5994]	-	3	-	-	-
*Pf*DHODH:E182D [Genz-666136]	-	637	-	-	-
*Pf*DHODH (enzyme)	-	33	-	-	-
*Pf*PI(4)K (enzyme)	-	-	21	-	-
*Pfc*PheRS (enzyme)	-	-	-	21	-
Pf, 3D7 [SDX]	1,004.7 (82.9)*	10.2 (2.9)*	100.1 (4.6)*	12.3 (1.5)*	-
Pf, D6 [MQ]	1,414.3 (156.4)*	7.1 (3.0)*	68.2 (3.2)*	11.5 (3.2)*	18.8 (4.5)* [MQ]
Pf, K1 [CQ, SDX, PY, CYC]	937.9 (76.2)*	10.3 (3.6)*	58.9 (8.7)*	13.2 (1.2)*	12,100* [PY]
Pf, NF54	1,213.3 (40.3)*	5.4 (1.3)*	53.4 (5.0)*	9.4 (1.4)*	16.2 (1.1)* [MQ]
Pf, V1/3 [CQ, SDX, PY, CYC]	1,560.7 (107.9)*	20.7 (7.6)*	67.7 (4.2)*	16.2 (2.2)*	19,200* [PY]
Pf, HB3 [PY]	889.2 (204.2)*	5.3 (1.6)*	56.8 (4.3)*	11.5 (2.2)*	2,250 (489)* [PY]
Pf, 7G8 [CQ, PY, CYC]	1,330.7 (118.3)*	10.6 (4.0)*	79.4 (0.0)*	13.1 (4.0)*	9,810* [PY]
Pf, FCB [CQ, CYC]	787.0 (181.0)*	13.0 (4.3)*	93.8 (12.2)*	10.4 (2.0)*	174.0 (52.7)* [CQ]
Pf gametocyte (stage IV-V)	-	-	643	663	-
Pb hepatic stage	-	-	459	339	-
Pc hepatic (small form)	-	-	344	3,300	-
Pc hepatic (large form)	-	-	832	2,860	-

CQ, chloroquine; PY, pyrimethamine; MQ, mefloquine; ATV, atovaquone; SDX, sulphadoxine; CYC, cycloguanil.
*Values shown are the mean of three technical and three biological replicates (standard deviations shown in parentheses). Slight differences in values from those reported in the main text reflect measurements made in different experiments.

Supplementary Table 1 | Summary table of four screening hit compounds. For strains harboring drug resistance (Dd2, 3D7, D6, K1, NF54, V1/3, HB3, 7G8, and FCB), the appropriate controls are indicated on the right, including the resistance drug and activity of that drug against a non-resistant control strain.

Strain name	Original strain name	Generated by	Parental strain	Resistant against	Resistant gene	Mutation	Reference (PMID)
*Pf*scDHODH	D10+ DHOD-GFP	Transgenic	D10	ECT inhibitors	*scdhodh*	-	17330044
*Pf*NITD609^{R}	*Pf*Cam-D1247Y	Transgenic	Dd2	NITD609	*pfatp4*	D1247Y	20813948
TM90C6B	TM90C6B	Field isolate	-	Atovaquone	*pfcytb*-Qo site	Y268S	22430961
*Pf*CYTb:G33V	*Pf*CYTb:G33V	Selection	Dd2	IDI 5994	*pfcytb*-Qi site	G33V	25336726
*Pf*DHODH:E182D	3D7: E182D	Selection	3D7	Genz-666136	*pfdhodh*	E182D	24381157
*Pf*BRD73842^{R}-A	-	Selection	Dd2	BRD73842	*pfpi4k*	Y1356N	-
*Pf*BRD73842^{R}-B	-	Selection	Dd2	BRD73842	*pfpi4k*	L1418F	-
*Pf*KAI407^{R}	*Pf*PI(4)K mutant	Transgenic	Dd2	KAI407	*pfpi4k*	H1484Y	24284631
*Pf*MMV048^{R}	-	Transgenic	Dd2	MMV048	*Pfpfpi4k*	-	-

Supplementary Table 2 | Genotypes of *Plasmodium* strains used to characterize phenotypic responses of screening hits.

	Flask 2*		Flask 3*	
EC_{50} (nM) / fold Δ	Clone #1	Clone #2	Clone #3	Clone #4
	1,500 / 21	817 / 11	511 / 7	560 / 7.7
Genome coverage (x)	68	108	90	72
% covered by 15 or more reads	85.3	94.4	89.5	87.2
SNVs identified				
Raw†	76064	84633	80109	76128
Quality‡	4713	7852	6364	5603
Unique prior to IGV¶	157	151	175	169
Unique post IGV¶	8	9	3	5
Intergenic	1	2	1	1
Intronic	0	2	0	1
Synonymous	0	0	1	2
Total nonsynonymous	7	5	1	1
Genes mutated in all samples				
Locus	PF3D7_0509800	PF3D7_0509800	PF3D7_0509800	PF3D7_0509800
Annotation	PI(4)K	PI(4)K	PI(4)K	PI(4)K
Mutation	Y1356N	Y1356N	L1418F	L1418F

*See Supplementary Information for methods.
†After alignment to *P. falciparum* 3D7 reference genome.
‡Quality filters based on parameters defined in Methods.
¶Compared to Dd2 parent.

Supplementary Table 3 | BRD73842 targets *Pf*PI(4)K. Two independent BRD73842-resistant strains were selected and assessed via whole-genome sequencing. Both lines (two clones each) contained mutations within PF3D7_0509800, which encodes the *Pf*PI(4)K. EC_{50} values and fold change (compared to wild type Dd2) are indicated underneath clone IDs.

EC_{50} (nM) / fold Δ	Flask 5*		Flask 7*		Flask 8*		
	Clone #1	Clone #2	Clone #3	Clone #4	Clone #5	Clone #6	Clone #7
	1,200 / 84	1,200 / 84	65 / 4	59 / 4	376 / 25	138 / 9	168 / 11
Genome coverage (x)	77.37	81.92	76.14	73.36	76.15	88.76	61.79
% covered by 15 or more reads	91.2	91.6	91.6	91.7	89.8	90.5	90
SNVs identified							
Raw†	70316	70509	69781	69653	69369	73042	72068
Quality‡	8628	8857	8640	8720	8418	8591	6795
Unique prior to IGV¶	285	324	281	290	269	252	181
Unique post IGV¶	4	5	6	5	4	6	2
Intergenic	0	2	1	1	0	3	0
Intronic	0	0	1	0	1	0	0
Synonymous	1	1	2	2	1	1	0
Total nonsynonymous	3	2	2	2	2	2	2
Genes mutated in all samples							
Locus	PF3D7_0109800	PF3D7_0109800	PF3D7_0109800	PF3D7_0109800	PF3D7_0109800	PF3D7_0109800	PF3D7_0109800
Annotation	PheRSα	PheRSα	PheRSα	PheRSα	PheRSα	PheRSα	PheRSα
Mutation	L550V	L550V	M316I	M316I	G512E; V545I	G512E; V545I	G512E; V545I

*See Supplementary Information for methods.
†After alignment to *P. falciparum* 3D7 reference genome.
‡Quality filters based on parameters defined in Methods.
¶Compared to Dd2 parent.

Supplementary Table 4 | BRD1095 targets *Pf*PheRS. Whole-genome sequencing of BRD1095-resistant clones reveals mutations within the putative cytoplasmic *pfpheRS*. Three independent BRD1095-resistant strains were selected and assessed via whole-genome sequencing. EC_{50} values and fold change (compared to wild type Dd2) are indicated underneath clone IDs. All three lines contained mutations within PF3D7_0109800, which is annotated as encoding the alpha subunit of cytoplasmic PheRS. The resistant clones isolated from two of the flasks contained single SNV, while the clones from the third flask contained two SNVs.

Supplemented amino acid		Average EC_{50} (nM) ± SD				
		BRD1095	BRD7929	Atovaquone	Mefloquine	Dihydro-artemisinin
Control	-	16.4 (2.4)	10.2 (2.0)	0.30 (0.08)	17.2 (3.3)	8.6 (2.3)
L-Phenylalanine	10x	135.6 (5.8)	101.1 (7.7)	0.32 (0.05)	33.9 (0.6)	2.8 (0.5)
	20x	270.4 (4.9)	220.4 (15.1)	0.26 (0.01)	35.1 (0.2)	2.4 (0.1)
	50x	677.1 (73.6)	477.7 (21.6)	0.26 (0.02)	30.2 (0.8)	2.2 (0.1)
D- Phenylalanine	10x	20.8 (2.6)	15.1 (0.3)	0.27 (0.02)	34.9 (0.8)	2.3 (0.1)
	20x	19.1 (1.5)	14.5 (0.9)	0.36 (0.04)	34.3 (0.4)	2.9 (0.2)
	50x	18.6 (1.8)	15.1 (0.7)	0.20 (0.02)	28.9 (0.4)	2.7 (0.4)
L-Aspartic acid	10x	16.9 (2.9)	8.5 (1.7)	0.43 (0.02)	23.7 (1.0)	13.0 (0.4)
	20x	13.7 (2.2)	7.5 (0.6)	0.42 (0.05)	23.7 (3.5)	12.6 (0.4)
	50x	19.1 (2.5)	10.3 (0.6)	0.38 (0.02)	13.9 (6.1)	11.1 (0.6)
L-Threonine	2x	19.2 (5.1)	6.3 (1.1)	0.37 (0.07)	20.0 (2.1)	12.5 (1.2)
	4x	15.0 (1.3)	10.1 (2.3)	0.45 (0.05)	19.0 (0.7)	9.4 (2.3)
	10x	20.3 (3.1)	9.0 (1.5)	0.32 (0.03)	15.4 (1.1)	10.0 (1.7)
L-Tyrosine	10x	16.4 (0.8)	10.7 (1.9)	0.33 (0.02)	17.4 (4.2)	7.1 (0.8)
	20x	17.6 (4.1)	8.6 (0.6)	0.47 (0.13)	15.7 (3.4)	11.0 (1.0)
	50x	17.2 (1.8)	10.1 (2.5)	0.43 (0.10)	21.5 (0.1)	11.3 (1.0)

Supplementary Table 5 | Supplementation with exogenous amino acids to the *in vitro* culture medium increased the EC_{50} values. *In vitro* potency of BRD1095, BRD7929 and other antimalarials were determined by growth inhibition assay with the presence of 5 different amino acids at 3 doses. The activity of BRD1095 and BRD7929 could be effectively reduced by the addition of exogenous L-phenylalanine to the growth medium (RPMI) but exogenous D-phenylalanine L-aspartic acid, L-threonine and L-tyrosine had no effect on the activity of BRD1095 and BRD7929. Values shown are the average of three technical and three biological replicates (standard deviations shown in parentheses).

		Dose (μg/plate)	Number of revertants per plate, Mean (individual data)									
			TA100		TA1535		TA98		TA1537		WP2uvrA	
Without S9 mix	DMSO	0	127 (141, 112)		10 (12, 8)		26 (20, 31)		28 (26, 30)		28 (24, 31)	
	ER-0011 84635-000	6.86	139 (135, 142)		11 (14, 8)		36 (24, 47)		24 (20, 28)		40 (45, 34)	
		20.6	125 (131, 118)		9 (11, 6)		23 (21, 24)		18 (18, 17)		38 (37, 39)	
		61.7	91 (94, 87)	T	2 (2, 1)	T	22 (23, 20)	T	1 (1, 0)	T	41 (33, 48)	T
		185	0 (0, 0)	T	0 (0, 0)	T	0 (0, 0)	T	0 (0, 0)	T	29 (33, 25)	T
		556	0 (0, 0)	T	0 (0, 0)	T	0 (0, 0)	T	0 (0, 0)	T	15 (12, 17)	T
		1667	0 (0, 0)	P,T	0 (0, 0)	P,T	0 (0, 0)	P,T	0 (0, 0)	P,T	0 (0, 0)	P,T
		5000	0 (0, 0)	P,T	0 (0, 0)	P,T	0 (0, 0)	P,T	0 (0, 0)	P,T	0 (0, 0)	P,T
	AF2	0.01	476 (466, 486)		NT		NT		NT		135 (125, 144)	
		0.1	NT		NT		435 (419, 451)		NT		NT	
	9AA	80	NT		NT		NT		377 (342, 411)		NT	
	SA	0.5	NT		559 (568, 550)		NT		NT		NT	
With S9 mix	DMSO	0	136 (131, 140)		11 (10, 11)		41 (37, 44)		20 (13, 26)		40 (48, 32)	
	ER-0011 84635-000	6.86	153 (161, 145)		10 (11, 8)		45 (40, 50)		29 (30, 28)		38 (30, 45)	
		20.6	175 (174, 176)		12 (13, 11)		51 (40, 62)		31 (35, 26)		41 (37, 45)	
		61.7	114 (105, 123)	T	9 (12, 6)	T	32 (34, 30)		9 (10, 8)	T	36 (43, 29)	
		185	0 (0, 0)	T	0 (0, 0)	T	0 (0, 0)	T	0 (0, 0)	T	31 (32, 30)	
		556	0 (0, 0)	T	0 (0, 0)	T	0 (0, 0)	T	0 (0, 0)	T	11 (10, 11)	T
		1667	0 (0, 0)	P,T	0 (0, 0)	P,T	0 (0, 0)	P,T	0 (0, 0)	P,T	0 (0, 0)	P,T
		5000	0 (0, 0)	P,T	0 (0, 0)	P,T	0 (0, 0)	P,T	0 (0, 0)	P,T	0 (0, 0)	P,T
	2AA	0.5	NT		NT		581 (605, 556)		NT		NT	
		1	1144 (1137, 1150)		NT		NT		NT		NT	
		2	NT		278 (278, 277)		NT		108 (92, 124)		NT	
		10	NT		NT		NT		NT		602 (613, 591)	

NT, Not tested; T, Toxic (growth inhibition); P, Precipitation; 9AA, 9-aminoacridine hydrochloride monohydrate; 2AA, 2-aminoanthracene; DMSO, dimethyl sulfoxide; AF2, 2-(2-furyl)-3-(5-nitro-2-furyl)acrylamide; SA, sodium azide.

Supplementary Table 6 | Reverse mutation assay in bacteria with BRD7929. BRD7929 was tested for mutagenicity. The Ames test, with preincubation at 37°C for 20 minutes, was conducted in duplicate in the presence or absence of S9 mix using bacterial strains of *Salmonella typhimurium* TA100, TA1535, TA98, TA1537, and *Escherichia coli* WP2uvrA. The S9 mix included cofactors and S9 fraction from liver homogenate of male Sprague Dawley rats treated with phenobarbital and 5,6-benzoflavone. Dimethyl sulfoxide was used as a vehicle. BRD7929 is judged to be negative in the reverse mutation assay in bacteria under the experimental conditions employed in this study.

Supplementary References

74. Gottlieb, H. E., Kotlyar, V. & Nudelman, A. NMR Chemical Shifts of Common Laboratory Solvents as Trace Impurities. *J Org Chem* **62,** 7512–7515 (1997).
75. Klausen, R. S. & Jacobsen, E. N. Weak Brønsted Acid–Thiourea Co-catalysis: Enantioselective, Catalytic Protio-Pictet–Spengler Reactions. *Org. Lett.* **11,** 887–890 (2009).